ELUCIDATING THE CONTRIBUTIONS OF GENETIC VARIANTS ASSOCIATED WITH ADDICTION PHENOTYPES

by

EILEEN N. ONI

A Dissertation submitted to the

Graduate School-New Brunswick

Rutgers, The State University of New Jersey

And

The Graduate School of Biomedical Sciences

In partial fulfillment of the requirements

For the degree of

Doctor of Philosophy

Graduate Program in Cell and Developmental Biology

Written under the direction of

Ronald P. Hart

And approved by

_____

_____

_____

_____

New Brunswick, New Jersey

OCTOBER, 2016

ABSTRACT OF THE DISSERTATION

ELUCIDATING THE CONTRIBUTIONS OF GENETIC VARIANTS ASSOCIATED WITH ADDICTION PHENOTYPES

By EILEEN N. ONI

Dissertation Director:

Ronald P. Hart

Genome-wide association studies have identified several loci with variant sequences that are correlated with the risk of nicotine addiction and alcohol use disorders (AUD), however, little is known about the cellular mechanisms underlying these genetic variants. Drugs such as nicotine mediate addiction behaviors via the activation of nicotinic acetylcholine receptors (nAChR). We first prepared subject-specific induced pluripotent stem cells (iPSC) from donors homozygous for either the major (D398) or the minor (N398) allele of the nonsynonymous single nucleotide polymorphism (SNP), rs16969968, in the CHRNA5 gene encoding the nAChR α5 subunit . To understand the impact of the N398 variant in human derived cells, we differentiated iPSCs to midbrain-like dopamine (DA) or glutamatergic neurons and then tested their functional properties and response to nicotine. Neurons from both variants demonstrated physiological and biochemical properties consistent with mature neuronal function. Results show that N398 variant midbrain-like DA neurons differentially express genes associated with ligand receptor interaction and synaptic function. The N398 neuronal population responded

more actively with an increased excitatory postsynaptic current response upon the application of nicotine in both midbrain–like DA and glutamatergic neurons. Glutamatergic N398 neurons responded to lower nicotine doses (0.1 μM, concentrations of nicotine similar to those of heavy smokers) with greater frequency and amplitude and rapid desensitization, consistent with previous analyses of N398-associated nicotinic receptor function. Additionally, to understand the impact of AUD variants in humans, we prepared iPSCs from four subjects diagnosed with AUD and carrying three SNPs within the KCNJ6 gene (minor alleles of rs702859, rs702860, and rs2835872) encoding the potassium inward rectifying GIRK2 channel. We differentiated iPSCs into neural stem cells (NSCs) and all were positive for NSC markers (SOX2, Nestin, and Musashi). To model acute alcohol exposure, we exposed NSCs to medium containing 75 mM ethanol. To test whether this concentration would alter NSC growth dynamics, we assessed the cell viability, size, and doubling time over 72 hrs of exposure to which there was no detectable change. From RNAseq gene expression experiments following a 24 hr treatment with or without ethanol, we have identified differential gene enrichment in genes involved in neural differentiation as well as predicted alternative splicing variants in the KCNJ6 gene. We have also begun to assess the neuronal activity using two sources of basal culture medium (BrainPhys [Stem Cell Technologies] and Neurobasal [Gibco]) following Neurogenin 2 lentiviral differentiation of iPSCs. We detected substantial calcium spiking in BrainPhys medium in comparison to Neurobasal medium though calcium imaging analysis. This suggests that BrainPhys medium provides a more sustainable culture environment for future experiments. Planned studies will utilize cultures grown in BrainPhys based medium to assess specific changes in neuronal

activity for each genotype during ethanol exposure. Overall, the results of this work offer a proof-of-principle for utilizing human derived neurons to study gene variants contributing to addiction.

ACKNOWLEDGEMENTS AND DEDICATION

This thesis would not have been possible without the support, encouragement and cooperation of multiple people throughout my graduate career. I would first like to thank my family and friends for the encouragement and support they have given me throughout my time in graduate school. I truly would not have made it through this process without them. I would like to dedicate this thesis to my parents Joseph and Angela Oni and brother Brian Oni for always believing in me and supporting me throughout my graduate career.

I cannot express how invaluable the support I received from my advisor and the Hart laboratory was towards completing my thesis. I would first like to thank my advisor and mentor Dr. Ronald Hart. I will be eternally grateful for the opportunity that Dr. Hart gave me to take this scientific endeavor under his mentorship. I would probably not have succeeded in completing my graduate studies if we're not for Dr. Hart's great patience and support. I would like to extend my thanks to the members of my thesis committee for whose advice and expertise helped to refine my scientific mind. I would especially like to thank Mavis Swerdel, Alana Toro-Ramos, Dr. Jennifer Moore and Dr. Azadeh Jadali Dr. Kristina Hernandez for their guidance and advice. I would also like to extend many thanks to my undergraduate mentor Dr. Cristina Iftode, for introducing me to the world of scientific research and encouraging me to get a PhD. As fellow women in science, you are truly role models for me. I would like give a very special thanks to Apoorva Halikere, for whom I have had the distinct pleasure to collaborate with. I am grateful for your contribution on the many aspects of this project. I wish you well in your future endeavors for which I am sure you will be highly successful. Thank you to our current and former

undergraduates, Lucy Lin, Kunal Garg, Micheal Lazaropalos, Sri Patel for their hard work and dedication.

I would also like to thank the directors of the Initiative to Maximize Student Diversity (IMSD) and Interdisciplinary Job Opportunities for Biomedical Scientists (IJOBS) programs Drs. Jerome Langer, Beatrice Haimovich, Janet Alder, James Millonig and Evelin Erenrich if it were not for your support, I would not be as prepared to take the next steps in my career. Many thanks to the many students and post docs that I have had the pleasure of meeting during time here at Rutgers, specifically Christina Ramirez, Melvili Cintron. This experience would not have been the same without you all. My best memories from graduate school are with all of you and I am confident we will be lifelong friends. Finally, I would like to thank my National Institute of Health funding sources; Initiative to Maximize Student Diversity (IMSD) and National Institute on Alcohol Abuse and Alcoholism minority health, health disparities and diversity training grants.

TABLE OF CONTENTS

LIST OF TABLES

LIST OF FIGURES

INTRODUCTION

Addiction disorders are a major burden to society with the total cost of substance abuse in the U.S. exceeding $600 billion annually (NIDA). Symptoms of addiction disorders are defined by the U.S. Surgeon General, Diagnostic and Statistical Manual of Mental Disorders (DSM-IV)[7], the International Classification of Diseases (ICD-10)[8], as repeated and compulsive self-administration; highly motivated drug seeking behavior despite known harmful consequences, regulation of emotions, greater value from use of the drug over other activities, many repeated unsuccessful attempts to stop and the manifestation of withdrawal or tolerance[9]. Drugs that mediate addiction behavior range from plant based compounds such as cannabinoids and tobacco to manufactured pharmaceuticals (morphine, oxycodone, etc.) originally intended to mediate pain. There are several factors that can contribute to addiction behaviors, including socioeconomic status, levels of access to drugs of abuse, perceptions of use and identified within the past 10 years, genetic variants[10]. Some studies have suggested that these genetic variants may contribute to the risk of relapse and/or risk of addiction phenotypes[11,12]. This work will focus on genetic variants associated with the co-morbid addiction disorders that use nicotine and alcohol.

Alcohol and nicotine addiction behaviors are co-morbid since people with alcohol use disorders (AUDs) are three times more likely to be nicotine dependent[13]. Nicotine addiction is the largest preventable cause of mortality in the U.S., leading to more than 465,000 deaths in 2010[14]. Additionally, AUDs are the third leading cause of death in the U.S., contributing to about 1 in 10 deaths a year, and are estimated to cost 223.5 billion annually in lost productivity and cost of treatment[15-17]. In addition to behavioral

therapies[18], the most common pharmaceutical treatments for nicotine and alcohol addiction include drugs such as varenicline, bupropion and naltrexone[19,20]. These drugs act as either antagonists for nicotine receptors or inhibitors of μ-opioid receptor. Although these treatments have resulted in a 19.8% decrease of smoking within the past 10 years[21] , addiction behaviors using these drugs continue to be a leading health priority, as the risk of relapse remains high. Similarly, outcomes of individual treatment for AUDs are quite variable, to which some have suggested that genetic variants are a contributing factor[22]. It then becomes important to understand specific neuronal, synaptic and cellular biological mechanisms that underlie the contributions of genetic variants addiction behaviors for the development of more effective treatments[23,24].

Synaptic systems involved in addiction

Addiction phenotypes are influenced by internal and external cues, where the success of receiving a reward (from drugs such as alcohol or nicotine) increases the probability of behaviors that provide reward; this also known as positive reinforcement [25]. One of the primary synaptic systems that contribute to the positive reinforcing physiological effects of behaviors seen with drugs such as nicotine and alcohol is within the mesolimbic system, the ventral tegmental area (VTA). Within the VTA, activity is mediated by two major neuronal subtypes; The largest population (around 60%) [26] is midbrain dopamine (DA) and γ-aminobutyric acid (GABAergic) neurons (25%)[27], with a small percentage of VTA neurons that express neuronal features of glutamate-releasing neurons. This small population of neurons was identified by vesicular glutamate receptor ($VGluT2^{+}$) staining of midbrain DA neurons[28,29]. Many if not most DA neurons within

the VTA are inhibited by GABAergic neurons [30]. GABAergic neurons in the VTA serve as the bridge to the lateral habenula controlling dopamine release and are found exclusively in the interpeduncular nucleus (IP), which is innervated by the medial habenula [31-33]. VTA neurons project and release dopamine into multiple regions as diagrammed by Juarez et al.[4] (Figure 1), including the nucleus accumbens, dorsal striatum, amygdala, and cortical forebrain glutamatergic neurons[24,34]. Synaptic inputs to the VTA include the rostral medial tegmental nucleus (RMTg)[35], striatum[36], lateral habenula, pedunculopontine tegmental nucleus, nucleus accumbens, prefrontal cortex PFC and the amygdala as diagrammed in Figure 1. These sites are the primary source of addiction phenotypes mediating motor behaviors, fear response and are mediated by dopamine.

During a reward stimulus such as nicotine or alcohol, DA neurons undergo a shift from tonic to burst firing mode, increasing the amount of extracellular dopamine in the brain. The downstream effect of dopamine release is mediated by variations in VTA neuronal firing patterns[37]. DA neurons in the VTA have two firing patterns: phasic firing, which consists of rapid multi-spiked activity (15-30 Hz), and single slow spiking activity known as tonic firing (2-4 Hz)[38,39]. This change in firing pattern was observed through cyclic voltammetry experiments in cocaine self administered rats[40]. In these experiments, the initial cocaine seeking behavior led to the rapid increase of extracellular dopamine in the nucleus accumbens. This suggests that drugs of abuse can potentially mediate the firing frequencies, altering the release of extracellular dopamine, which can influence motor behaviors.

Upon the release of dopamine, postsynaptic dopamine-specific, G-protein coupled receptors (GPCRs) are activated. These dopamine receptors are divided into D1 and D2 sub-groups, where intracellular cyclic adenosine monophosphate (cAMP) is increased and decreased, respectively[41]. The D1 subgroup, consisting of D1 and D5, are found in the nucleus accumbens, amygdala and frontal cortex and are activated by G-protein Gγαs, increasing cAMP levels, mediating further downstream signaling pathways. They are almost always found post-synaptically[42]. The D2 sub-group, consisting of D2, D3 and D4, is found in the nucleus accumbens, amygdala and frontal cortex and is activated by G-protein Gι, decreasing cAMP levels modulating potassium currents[43]. One example of dopamine release influencing drug seeking behavior came from a cocaine seeking rat model by Phillips et al.[40] From this study cocaine-seeking behavior was increased following electrically stimulated phasic firing of dopamine neurons, which was directly caused by an increased extracellular dopamine. This example illustrates of how changes in extracellular dopamine levels can mediate reward-learning signals causing drug seeking reward behavior [40,44,45].

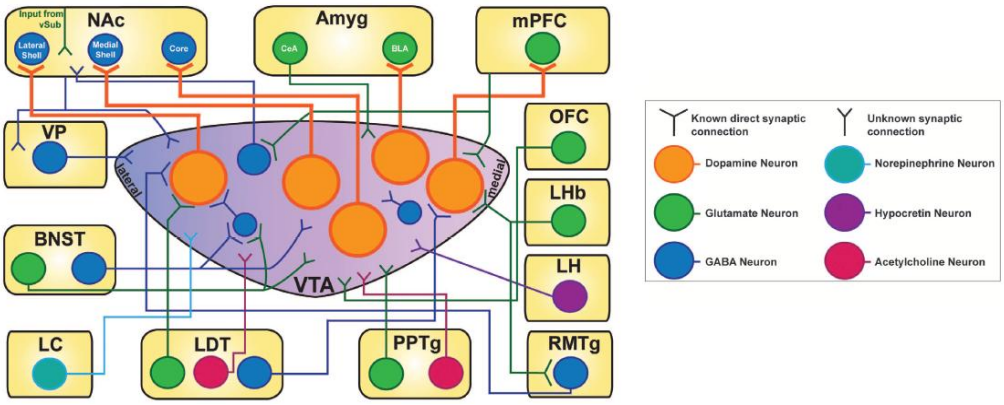

Figure 1 VTA structure including synaptic inputs and outputs as diagrammed by Juarez et al.[4]
VTA Dopamine neurons (orange) project to glutamatergic and GABAergic neurons within the NAc, Amyg, and mPFC and are targets of VTA GABAergic, LDT and mPFC excitatory neurons, among others. VTA GABAergic neurons (blue) project to VTA dopamine neurons and are targets of an array of glutamatergic, acetylcholine, and GABAergic neurons from the PPTg, LDT, and mPFC among others.

Mediators in the neurological response to nicotine: nAChRs

VTA neurons mediate the reinforcement of drugs of abuse by increasing the amount of dopamine within output areas, mediating positive reinforcement and motivation of addiction behaviors. Drugs of abuse such as nicotine mediate the activity of VTA neurons via the nicotinic acetylcholine receptors (nAChR)[46-48]. NAChRs are permeable to potassium and calcium ions and are able to modulate synaptic activity[49]. The five-subunit, transmembrane, ligand-gated nAChRs contain two distinct classes of subunits consisting of variations of nine alpha subunits (α2-α10), and three beta subunits (β2-β4)[50-53]. The structures of functional hetero or homo oligomeric nAChRs, individual subunit structures and ligand binding sites are diagrammed by Zoli et al.[1] (Figure 2). The two ligand binding domains each contain a principal component comprised of the cysteine loop (C-loop) binding pair provided by the α–subunit. The complementary

component is supported by three mainly hydrophobic aromatic amino acids from the β-subunit located at the interface of the binding pocket[52,54].

A

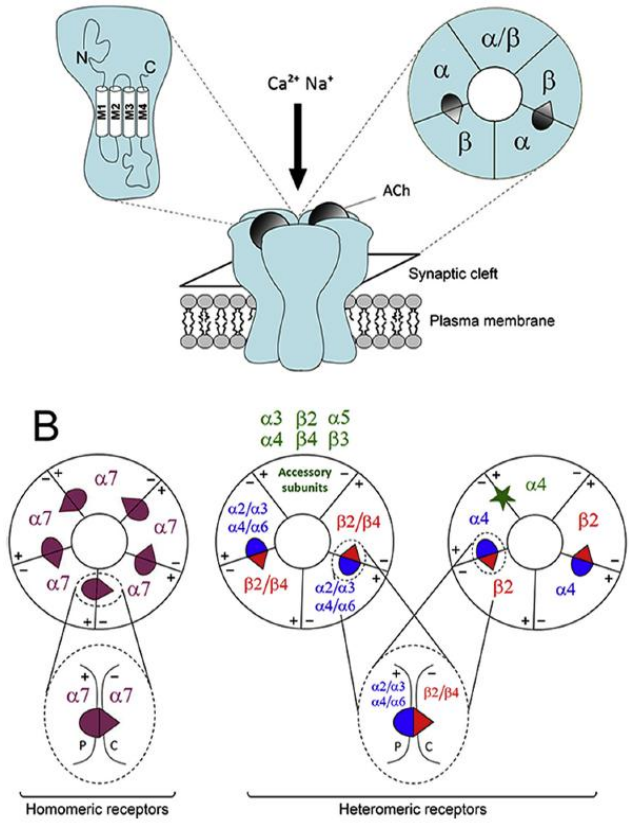

Figure 2 Structure of nAChR subunits as diagrammed by Zoli et al.[1]
A) Example diagram of individual nAChR subunits displaying four trans membrane domains (M1-M-4), ligand binding sites and α and β subunit configuration. B) Possible combinations of homomeric (α7) and heteromeric nAChR subunit configurations, including accessory subunits

The most commonly expressed nicotinic subunits in the brain are α3-α6, and β3 and β4, with two of the most common nAChR configurations being α4β2 and α2β4. The α4β2 configuration is the most directly affected by chronic exposure to nicotine and is involved in regulating the fast synaptic transmission of GABAergic and dopaminergic

neurons[55-57]. The α5 and β3 subunits, however, have neither the principal nor the complementary component for functional ACh binding sites but are considered auxiliary subunits that can replace the canonical non-binding subunits, such as β2[52,58]. The α5 subunits co-assemble with both the α4β2 and α3β4 configurations and have been shown to mediate nicotine aversion in mouse models[59]. α5 knockout mouse models show increased nicotine consumption compared to controls, suggesting a role for the α5 subunit in reward and aversion behavior in mice[60,61].

Risk variants associated with nAChRs

Genome-wide association GWA studies use statistical associations of probability to identify a causal variant within a population that contributes to a complex disease[62]. Specifically, these studies can identify common genetic variants: single nucleotide polymorphisms (SNPs) which can have two alternative base pairs at a specific locus[63]. The allelic frequencies of SNPs reflect its prevalence within a population of individuals. For example, a particular SNP variant with a minor allele frequency of 0.34 would correspond to 34% of a population of individuals. GWAS studies identify SNPs in linkage disequilibrium (LD), a measurement of whether the linkage of a gene is interrupted by meiosis, as a function of distance or as simplified by Slatkin[64] the nonrandom association of alleles at two or more loci. This is represented in terms of an r^2 correlation value. The higher the r^2 value, the more likely the inheritance of any calculating the LD of a SNP would allow a GWAS to associate the inheritance of a SNP with other phenotypes and compare between populations using the HapMap database. In 2009, a using data collected by the Collaborative Genetic Study of Nicotine Dependence

(COGEND) [65,66], Bierut et al[66] identified several SNPs associated with increased risk of addiction phenotypes.

For this study, one of the top SNP variants, selected due to the highest statistically significant associations (r^2= 0.15, minor allele frequency of 0.34), was rs16969968. This SNP is positioned within the CHRNA3-CHRNA5-CHRNA4 gene cluster that codes for the α3, α5, α4 subunits of nAChR, respectively, is located in the 15q25 region [66,67]. More importantly, this variant encodes an aspartic acid (D) to asparagine (N) amino acid change at amino acid 398 located within the α5 accessory subunit, making it non-synonymous. Other non-synonymous variants within this particular gene cluster have previously been associated with the negative effects from nicotine addiction such as higher levels of plasma nicotine and its derivative cotinine, to a higher chance of developing lung cancer[52,68]. These findings suggest that a genetic change within the CHRNA3-CHRNA5-CHRNA4 cluster contributes to addiction behaviors.

Studies using animal models provide some clues on how the rs16969968 SNP in the α5 nAChR subunit may contribute to addiction behaviors. α5 knockout mouse models exhibit increased nicotine consumption compared to controls, suggesting a role for the α5 subunit in modulating reward behavior[60,61]. The N398 α5 subunit, when selectively expressed in the VTA DA neurons of Chrna5$^{-/-}$ mice, produced a partial loss of function of the receptor and increased nicotine self-administration[69]. Mechanistic studies using similar systems have also concluded that the functional change in N398 is likely due to intracellular modulation of the receptor[70]. In the chick, α5 is associated within the α4β2 subtype and has been shown to have a higher conductance, desensitization rate, and calcium (Ca^{2+}) permeability[71]. Similar studies have reported that

the incorporation of rs16969968 SNP at the 398 subunit location reduces Ca^{2+} permeability and increases short-term desensitization to nicotine[52,72]. These findings suggest that the intracellular modulation of this receptor may mediate the effects of genetic risk variants giving us some clue as to their contributions to addiction behaviors. Specifically, these studies highlight an important role of the auxiliary α5 subunit in mediating synaptic activity upon nicotine stimulation.

However, several factors limit the conclusiveness of these studies. For example, oocyte injection experiments do not take into consideration extracellular factors that can affect nicotine addiction such as the composition of native nAChRs. Even though carefully controlled mouse models have been quite successful in understanding the general mediating factors of motivational and reward behaviors, attempts to study more complex human diseases may correlate poorly and results can become difficult to interpret given the evolutionary distance between mice and humans. This effect has been demonstrated in inflammation models[73], spinal cord injury[74], and neurodevelopmental disorders[75]. To circumvent the limitations of previous work, and to better highlight the functional consequences of the N398 genetic variant of CHRNA5, we will use human stem cells. To do this, we will use subject-derived iPSC lines to generate human midbrain-like DA and glutamatergic neuronal cultures resembling midbrain VTA neurons, a pathway whose performance is altered in addiction[76,77]. The findings from past studies and the results of our work will pave the way to understanding how genetic variants contribute to drug abusing behaviors at a synaptic level.

GIRK channels: targets of alcohol abuse

G protein-coupled inward rectifying potassium channels (GIRK) are responsible for maintaining the resting potential of neurons [78,79]. GIRK channels restore resting membrane potential following depolarization by increasing the outward current of potassium (K^+) [79]. Although first cloned from rat heart, GIRK channels can be found in brain and pancreatic tissues and are composed of several subunits; named GIRK1-4 (Kir 3.1-3.4 in mouse). The most common GIRK channels found in the brain are GIRK1, GIRK2 and GIRK3[80,81]. GIRK1 and GIRK3 are incapable of making functional channels and form heteromultimers[82]. GIRK2 channels however, form homotetramers or co-assemble with GIRK1 and GIRK3[83,84]. Functional GIRK channels consist of a core region with two transmembrane domains containing a P-loop between the N and C terminals [85]. All GIRK combinations are activated via the GPCR/ G beta-gamma complex (Gβγ) transduction pathway[86]. Specifically, activation of GIRK2 channels occurs though G-protein (G_i and G_o) βγ dimers (Gβγ) via their C terminal domains[84,87,88]. GPCRs that activate GIRK channels, include D2 dopaminergic[89] and μ-opioid[90] receptors, suggesting that the ligands which bind to these GPCRs may play an important role in mediating the hyperpolarity of neurons. Specifically, GIRK channels are activated by neurotransmitters such as dopamine, opioids and ethanol.[91]

GIRK2 (encoded by the KCNJ6 gene) channels, unlike the other functional potassium channels, open upon binding to ethanol. Blednov and colleagues observed this effect through a reduced response during analgesic hot plate experiments on weaver mice (GIRK2 knockout mice) [92]. To further determine the effects of ethanol, Kobayashi et al.[93] used Xenopus oocyte expression assays to show that ethanol activation of brain-specific

GIRK channels did not occur though G-protein activation, but at some other location on the channel. Recently, Aryal et al.[94] identified a discrete ethanol-binding pocket. Their experiments mutating this pocket residue (a leucine residue within the βD to βE regions of the GIRK channel), reduced alcohol mediated activation. Thus illustrating that ethanol activation is directly related to GIRK channels and highlights the role of ethanol in mediating neurological activity within the brain.

While this past work strongly suggests a role of ethanol activation of GIRK channels, a study by the Collaborative Study on the Genetics of Alcoholism (COGA) sought to determine the genetic contribution to alcoholism[2]. To identify genetic variants, this GWAS study focused on oscillations from electroencephalogram (EEG) recordings following oddball task paradigm experiments. The use of EEGs allows for the recording of spontaneous brain activity and is a method of measuring cholinergic brain activity[95]. Past work from Lukas et al.[96] used EEGs as means of measuring theta activity in alcoholics as theta frequencies are associated with prefrontal and posterior brain corresponding to memory performance[97]. Additionally, the EEG theta phenotype is considered an endophenotype; a measureable heritable trait related to alcoholism [2,98]. The GWAS study associated subjects with reduced EEG frequencies at 3-7 Hz to three SNPs located on chromosome 21 within KCNJ6. These SNPs are located synonymously within exon 4 of KCNJ6 (rs702598) and within the intronic region between exon 3 and 4 (rs2835872 and rs2385880). These SNPs are assigned as a haplotype, thus are a combination of alleles along the same chromosome inherited as a unit[99]. The presence of these SNPs as a haplotype may suggest an increased impact on its association with the risk of AUDs. Given the behavioral effects of ethanol in GIRK2 knockout mouse studies

and GWAS studies associating GIRK2 in the increased risk of alcohol addiction, it is evident that ethanol exposure mediates synaptic response. Thus it becomes important to determine the contributions of genetic variants on a biological mechanism that associates them to the risk of AUDs.

Induced Pluripotent Stem Cells in studying neurodegenerative diseases

To overcome the lack of a renewable source of human neurons to study the role of human nAChR genetic variants, we used subject-specific induced pluripotent stem cells (iPSCs). This technology was developed in 2006, when Takahashi and Yamanaka reprogrammed somatic cells to a pluripotent state by the over expression of transcription factors OCT4, cC-MYC, SOX2, and KLF4[100]. Once reprogrammed, iPSCs are able to produce cell types that are specific for any of the three germ layers in the same way as embryonic stem cells[100]. This methodology allows for the creation of subject specific iPSCs to model human neuropsychiatric disorders or genetic mutations at a cell biological and mechanistic level as diagrammed by Marchetto et al.[3] in Figure 3[101-105]. Additionally, the technology of iPSCs will allow us to identify novel therapeutic strategies to circumvent the mechanisms that cause addiction phenotypes while minimizing the use of animal models. Specifically, we will utilize various iPSC neuronal differentiation protocols.

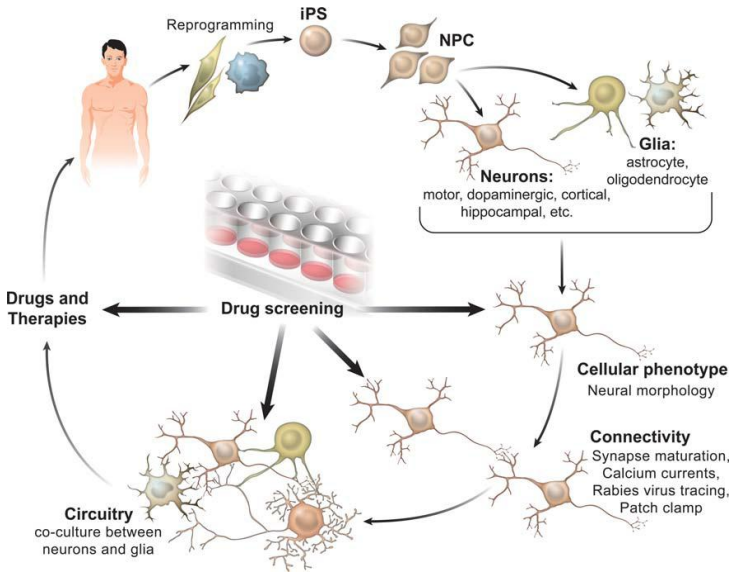

Figure 3 Marchetto et al.[3] illustration for the uses for iPSC technology

This diagram illustrates the potential use of iPSC neural differentiation protocols to streamline drug screenings to alleviate phenotypes of diseases related to circuitry, connectivity and neural phenotype.

In order to study neurological diseases, much work has been done focusing on developing various neuronal subtype specific differentiation protocols, including direct lentiviral induction [106], small molecules[107] and combinatorial viral- small molecule methods[108]. These differentiation protocols have been used to model neural development in an in vivo system, from autism spectrum disorders (ASDs), to Parkinson's disease as described in a recently summarized report following a Banbury meeting[109]. Furthermore, these stem cell model based system have been utilized to identify the synaptic properties that contribute to neurodegenerative disorders. Using fibroblast generated iPSCs from Rett syndrome patients, Marchetto and colleauges[110] observed synaptic alterations during differentiation, including reduced glutamatergic synapse numbers and X- inactivation. In another study, Brennand and colleagues showed aberrant migration in neurons derived

from iPSCs from patients with schizophrenia [109,111]. In generating iPSC models from GWAS studies, Nguyen et al[112] generated cell lines that carry the G3019S point mutation in the leucine repeat-related kinase 2 (LRRK2) gene associated with Parkinson's disease, and found increased expression of oxidative stress-associated genes and variation in hydrogen peroxide sensitivity. Additionally, recent work has attempted to identify the mechanisms underlying risk alleles. One such example was from work by Lieberman et al.[113], who identified altered expression of $GABA_A$ subunit genes from iPSC derived neurons carrying a synonymous SNP rs279858 within the GABRA2 subunit. Overall, the result of these studies highlights the impact and power of using iPSCs as a model system for neurodegenerative diseases. Our experiments will involve the characterization of neurons derived from iPSC lines from subjects carrying the major or risk-associated minor alleles of KCNJ6 and CHRNA5 genes.

Rationale

To elucidate a source of the predisposition for addiction behaviors of subjects who carry minor allele SNPs that are associated with nicotine or alcohol use disorders, we will utilize iPSC differentiation technology to probe the synaptic relationship between individual neurons. We hypothesize that the presence of these single nucleotide minor allele genetic variants contributes to modulating neurological activity. First, in the case of CHRNA5 minor allele variant, we hypothesize that the minor allele modulates the synaptic response of excitatory and dopaminergic neurons contributing to the addiction behaviors. Given that variation in α5 expression alters nAChR expression and function[114], the non-synonymous variants within α5 are likely to affect physiological

functions contributing to addiction behaviors[66]. Previous work with mice carrying the rs16969968 minor allele variant have shown increased intracranial self stimulation (ICSS) for nicotine [61]. Additionally, studies in Xenopus oocytes have shown increased desensitization of constructs that include the α5 subunit within the most common composition of nACHRs[115]. In the following chapters, we will show that inherent synaptic activity of neurons that carry the genetic variant is altered upon naïve nicotine stimulation. This work uses a novel approach of cell lines from those who carry the variant and test our hypothesis on a cell-by-cell basis.

Our second study involves identifying the minor allele SNPs in the inward rectifying channels GIRK2 and their contributions to addiction behaviors. We hypothesize that these SNPs alter the genetic profile by modulating splicing variations which may alter gene expression of GIRK2 channels thus modulating the overall inward reactivity of neurons. Recent work on the GIRK channels suggests that ethanol is a direct activator as GIRK2 knockout studies have shown reduced effects of ethanol[92,93]. Recent work has also identified a specific ethanol binding pocket outside of the GPCR activating domain[116]. This suggests a role of GIRK2 in mediating ethanol activity and thus we expect an alteration of synaptic activity in the response to ethanol. The results of this work provide important and supportive insights on how gene variants within familial populations may affect neuronal activity though the use of in vitro human iPSC derived neurons.

CHAPTER 1: CHRNA5 minor allele variant N398 contributes to increased synaptic frequency and desensitization

In an effort to determine the contributions of genetic variants to addiction disorders, we have established *in vitro* reward pathway models that differentiate iPSC differentiation into dopamine and excitatory neurons, typical targets of nicotine. Results obtained from the following work should be directly applicable to contribute to previous animal studies involved in understanding the genetic association with the increased risk of addiction.

IPSC Characterization: subject identification and reprogramming

Nicotine dependent subjects were selected from the Collaborative Genetic Study of Nicotine Dependence (COGEND) collection [65,66]. Dependent subjects were classified by Fagerström test of nicotine dependence (FTND) scores of 4 or more (out of a total of 10) [117]. These subjects carry the homozygous minor allele (AA) of rs16969968 as well as the presence of homozygous major alleles for other SNPs known to affect addiction behaviors and/or nAChR function: rs880395 (GG), rs8192475 (GG), rs12914008 (GG), and rs56218866 (TT) (Table 1). Non-nicotine-dependent control subjects who smoked came from the same collection, and were homozygous for the major allele of rs16969968 (GG) but matched at the other SNPs. One male and two females were selected for each group. Verification of risk-associated SNP rs16969968 was done in the lab of Dr. Alison Goate of Washington University, using DNA prepared from iPSC samples.

Table 1 Genotypic profile of subjects used in this study
List of subject cell lines profiles including, ID number (RUID), Gender, minor SNP status, allele of SNP (minor allele in red) and CHRNA5 amino acid group. All SNP genotypes (were confirmed by PCR in iPSC DNA.

Cell Line (RUID)	Gender	Status	rs880395	rs16969968	rs1799971	rs8192475	rs12914008	rs56218866	Group
03NA10370	Male	Affected	GG	AA	AA	GG	GG	TT	N398
03NA11467	Female	Affected	GG	AA	AA	GG	GG	TT	N398
04NA12831	Female	Affected	GG	AA	AA	GG	GG	TT	N398
03NA10137	Female	Control	GG	GG	AA	GG	GG	TT	D398
04NA12973	Female	Control	GG	GG	AA	GG	GG	TT	D398
03NA09641	Male	Control	GG	GG	AA	GG	GG	TT	D398

Somatic cells were reprogrammed to a pluripotent state by expression of critical transcription factors shown to maintain the pluripotency in both early embryos and embryonic stem cells[118]. In this project, CD4+ T-cells were used as a somatic cell population to be reprogrammed to iPSC. The $CD4^+$ T cells are prepared from cryopreserved lymphocytes obtained from RUCDR Infinite Biologics®. T- cells were transduced to iPSCs with Sendai viruses containing cDNA encoding transcription factors OCT4, SOX2, KLF4, and C-MYC (CytoTune™, Life Technologies) as described in the methods section. After transduction, we then characterized the iPSC lines for pluripotency.

IPSC Characterization: Indicators of pluripotency

To verify that the transformation process from iPSCs produced from somatic T-cells produced iPSCs, we characterized the lines using an array of indicators. We first defined the ability of iPSCs to differentiate into all three germ layers through embryoid

body immunocytochemistry (not shown) and by gene expression studies, including the PluriTest algorithm[119] (Table 2). According to Müller et al.[119], pluripotency can be identified via the PluriTest in two ways. The first is the pluripotency score; which uses hundreds of both pluripotent and differentiated samples from many research labs to identify a pattern of genes separating pluripotent from non-pluripotent samples. The ranking of samples are according to genes that separate the samples the most. The threshold for pluripotency is a score greater than 20. The second indicator of pluripotency is the novelty score, a measurement of the biological variations with respect to the gene expression of data set. For pluripotency, a novelty score less than 1.67 is required. As a control comparison for the results of PluriTest, a human embryonic stem cell (H1 hESC) sample was used as a control for pluripotency. To serve as controls for differentiated cells, we used cryopreserved lymphocytes (CPL) and enriched CD4+ T-cells. In order to compare scores for the source CPL, T-cell samples, and the resulting iPSC from the same source we used cell line 04NA15503 from an unrelated study. All iPSC prepared for this project pass these thresholds.

Table 2. PluriTest algorithm values
Comparisons of pluripotency scores (Pluripotency raw and Novelty) between iPSC, EPSC and parental lines. Sufficient pluripotency status is determined with a pluripotency score higher than 20 and a novelty score greater than 1.67 grouping the iPSCs with hESCs together from parental T-cell (TiPSC) and CPL lines.

Subject	Stage	Group	Pluripotency raw	Novelty
H1	ESC	hESC	20.863	1.53
04NA15503	CPL	CPL	-105.33	3.04
04NA15503	T-cell	T-cell	-93.18	2.862
04NA15503	iPSC	TiPSC	32.179	1.657
03NA10370 (P26)	iPSC	TiPSC	28.115	1.519
03NA10370 (P13)	iPSC	TiPSC	28.238	1.507
03NA09641	iPSC	TiPSC	38.518	1.491

We then confirmed pluripotency by two immunocytochemistry (ICC) markers OCT4 and TRA-1-60 that are traditionally found in carcinoma and embryonic stem cells. OCT4 is a SOX2 binding protein which acts to enhance the expression of fibroblast growth factor (FGF2) and Nanog [120-122] and TRA-1-60 is a pericellular matrix peptidoglycan protein[123]. All iPSC prepared for this project stained positively for these pluripotent markers as shown by representative imaging in Figure 4. These results demonstrate that subject-specific T-cell derived iPSCs for this project have been successfully reprogrammed to a pluripotent state regardless of presence of N398 variant.

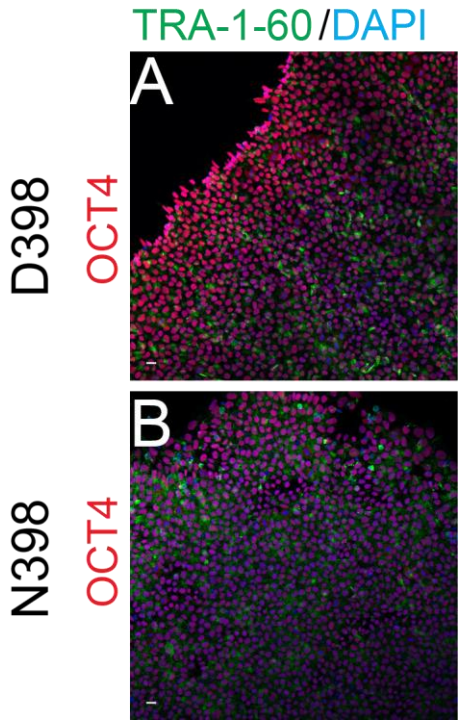

Figure 4 Immunocytochemistry for pluripotency markers
Positive ICC for OCT4 (Red) and TRA-1-60 (Green) of D398 A) and N398 B) iPSCs

Differentiation of iPSC to midbrain-like DA neurons: Dual SMAD inhibition

To study the functional consequences of the N398 genetic variant of CHRNA5, we used each of the six subject-derived iPSC lines to generate human midbrain-like DA neuronal cultures. We began with modeling midbrain VTA DA neurons as they are critical mediators of the mesolimbic system, a pathway whose performance is altered in addiction [76,77].

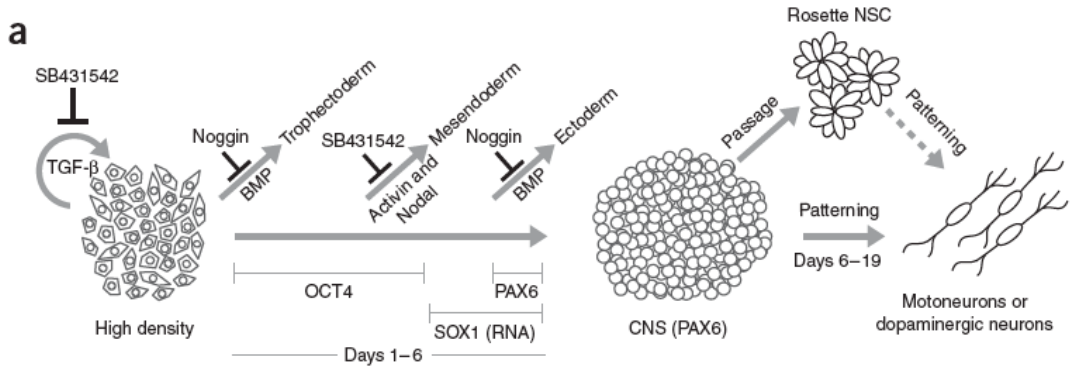

Figure 5 Schematic of dual SMAD inhibition protocol diagrammed by Chambers et al.[124]
The protocol by Chambers et al.[124] used small molecules (SB431542, Noggin) to inhibit SMAD proteins involved in the downstream signaling of TGFβ and BMP. This protocol in a time dependent manner, directed iPSC differentiation towards an endodermal fate and further into a final state of midbrain dopamine neurons.

Numerous studies have demonstrated the importance of Noggin, an inhibitor of the BMP signaling pathway, in neural induction and in the inhibition of neuronal differentiation [125,126]. To mimic midbrain DA neuron induction via BMP/TGFβ mediated signaling, we used a small molecule based modified dual SMAD inhibition protocol by Kriks et al. [107] who had developed modified version from Chambers et al.[124] (Figure 5). However we must note that the neurons from these protocols are intended to mimic DA induction and we realize that this culture system does not completely possess all of the synaptic inputs of a developing midbrain. Because of this, we can only accurately refer to neurons generated from dual SMAD inhibition protocol as "midbrain-like". The expressed mature neuronal markers in midbrain-like DA neurons was confirmed by positive staining of the rate-limiting enzyme in dopamine production tyrosine hydroxylase (TH), the early neuronal dendritic marker beta III tubulin (known by its antibody name as TUJ1)[127] and a more mature neuronal marker microtubule associated protein (MAP2) (Figure 6A and 6B). We quantified the population of mature neurons that co express TH. More than 75% of MAP2 and TUJ1 labeled cells co expressed TH,

indicative of mature dopamine neurons. We also probed for co-expression of TH and vesicular DA transporter (DAT). The cultures had punctate DAT and TH staining distributed throughout the culture (Figure 6D). There was no significant difference in the population MAP2 $^{+}$ TH^{+} cells of midbrain-like DA neurons between both genotypes (D398 75.0% ± 0.092, n=3; N398 78.4% ± 0.027, n=3). To confirm that TH^{+} cells were post mitotic, cultures were incubated with EdU for 24 hours to label cells in S phase. Only a small fraction of TH^{+} cells stained positive for EdU (Figure 7D 3.0 ± 0.007% for D398; 2.02 ± 0.008% for N398, n=3), indicating that nearly all cells were post mitotic. These results clearly show that the dual SMAD inhibition protocol produces post-mitotic midbrain-like neurons whose generation is not affected by the N398 genotype (Figure 6). However, the dual SMAD cultures also contained a small minority of serotonergic (5-HT positive) and inhibitory (GAD6 positive) neurons (Figure 7). ICC also identified cells that were both TH^{+} and $VGluT^{+}$ (Figure 7) seen in both rat and monkey [128] [129,130] and suggests that some DA neurons could potentially co-release glutamate which may modulate dopamine activity.

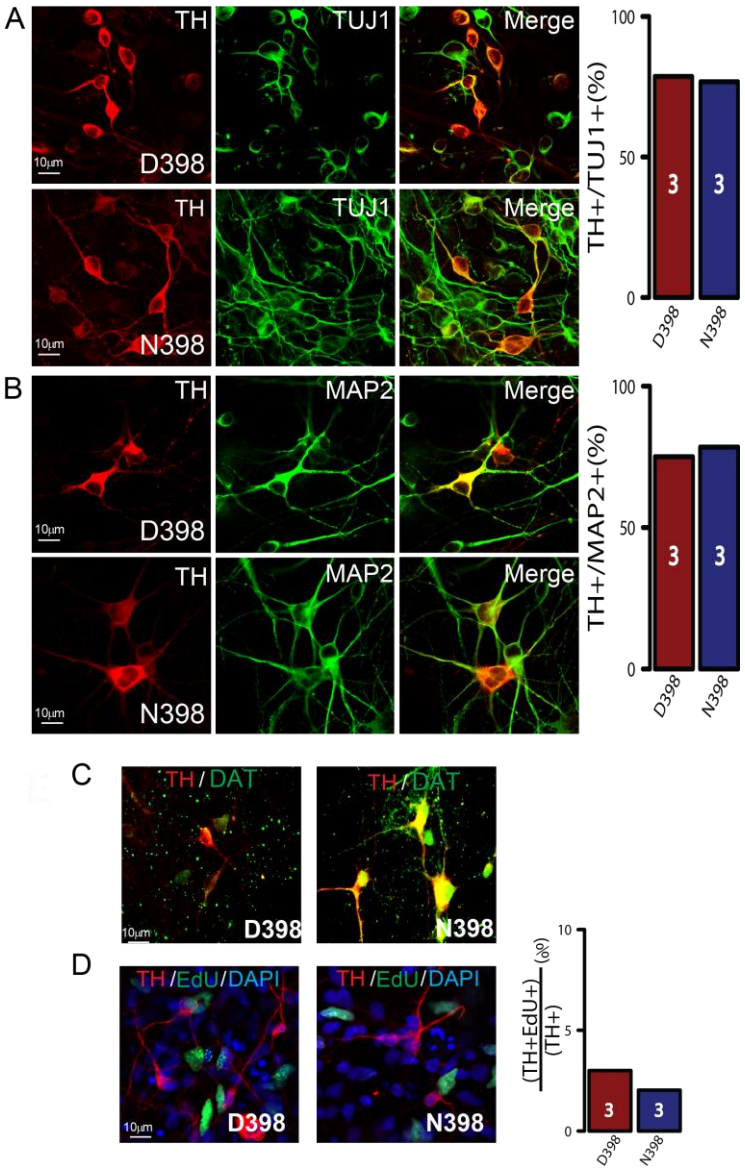

Figure 6 Pan neuronal immunocytochemistry of Dual SMAD inhibition neuronal cultures

Majority cells in iPSC-derived DA cultures expressed both TUJ1, MAP2^{+} and DAT (green) cells and TH (red) in both D398 A-C) and N398 groups. D) Few TH^{+} were labeled with a pulse of EdU (green), indicating that most cells were post mitotic

Functional assessment of midbrain-like DA neurons: The release of dopamine and expression of nAChR subunit mRNA

To determine whether the midbrain-like DA cultures were capable of releasing DA in response to nAChR activation, we used high performance liquid chromatography (HPLC) analysis. For this experiment, the DA culture medium was replaced with buffer containing 1 mM nicotine for 30 minutes. The HPLC analysis was done by Jessica Verpeut in the laboratory of Dr. Nicolas Bello in the department of Animal Sciences at Rutgers University. The medium was analyzed for DA content as described in the general methods. A distinct peak consistent with DA retention time indicates that the extracellular levels of dopamine due to nicotine activation via nAChRs in neuronal cultures and was not affected by either genotype (Figure 7). Similar retention time was seen with cultures exposed to 40mM of KCl (not shown). Taken together, the results are consistent with the presence of midbrain-like DA neurons.

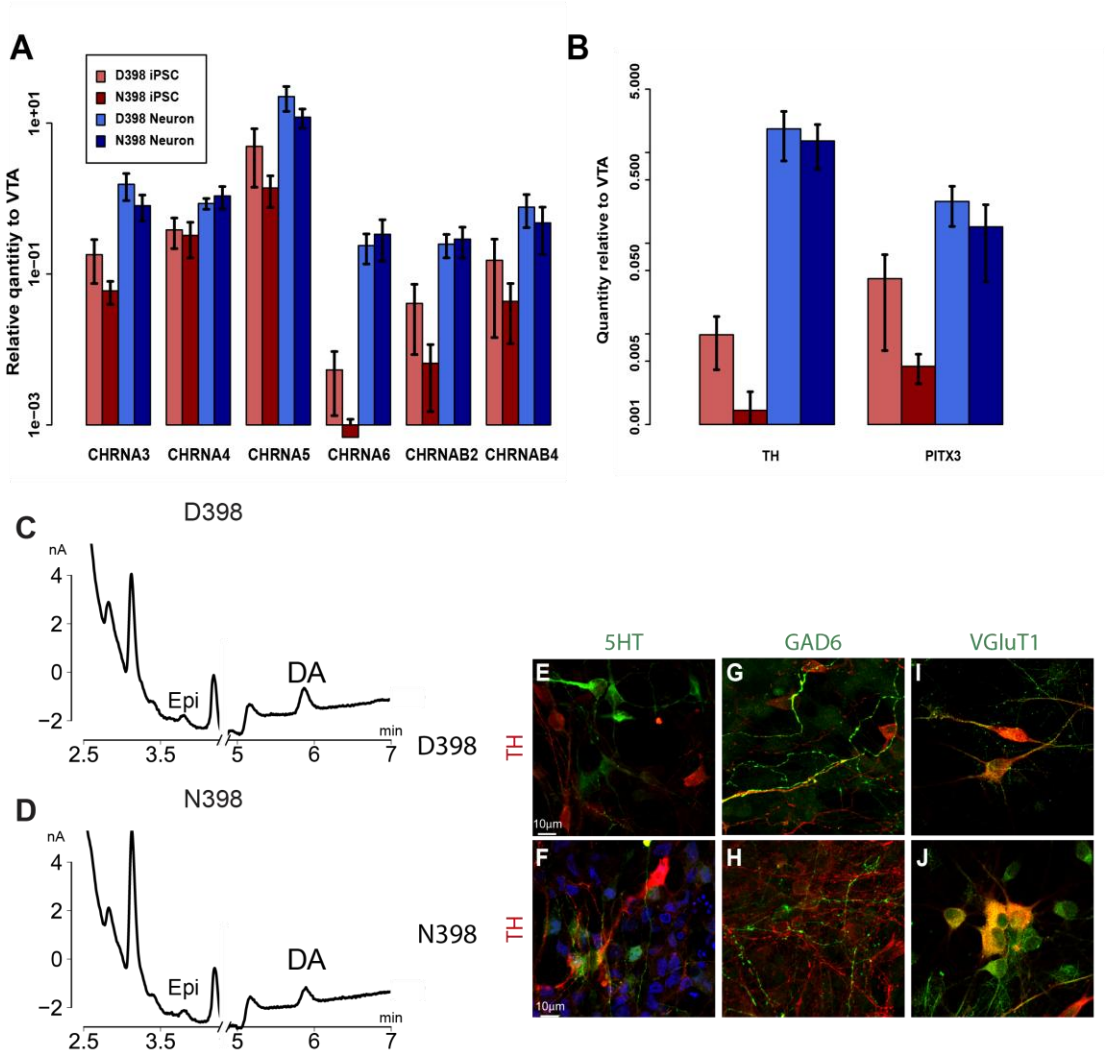

Figure 7 Genetic and functional analysis of DA neurons

A) qPCR analysis of nAChR subunit-encoding mRNAs α3, α4 ,α5 ,α6, β2, β4, of D398 (red) or N398 (blue), for either iPSC (lighter) or DA (darker) cultures. mRNA levels are normalized to GAPDH and human fetal VTA RNA. Cultures were also assayed by qPCR for mRNAs encoding (H) TH and the midbrain marker PITX3. For all qPCR assays, DA neurons were different from iPSC cultures (ANOVA, $p<0.05$) but there was no difference between N398 and D398. HPLC chromatogram demonstrates the presence of dopamine released by (C) D398 or (D) N398 cultures following KCl treatment. Midbrain-like DA cultures were stained with TH (red) and either 5HT (E, F), GAD6 (G, H), or VGluT1 (I, J) (green).

Having confirmed the DA neural lineage of the cultures through biochemical methods, we then used qPCR to determine if the neurons express not only mature

dopaminergic neuronal markers, but also the mRNAs encoding the nAChR subunits. As a control to ensure results are similar to levels of the developing brain, we used human fetal VTA mRNA generously provided by Drs. Yuka Imamura Kawasawa and Nenad Sestan from Yale University. Both the N398 and D398 40-day differentiated midbrain-like DA cultures expressed mRNA specific for nAChR subunits α3, α4, α5, α6, β2, and β4 at levels similar trends to that found in the VTA of 13-25d rats [131] (Figure 7). To further confirm the midbrain-like lineage of our culture, we observed mRNA expression for TH and the classic midbrain marker, PITX3 (Figure 7). All nAChR subunit and marker mRNAs increased significantly upon differentiation from iPSC to midbrain-like DA neuron cultures (ANOVA, $p<0.05$), indicating the active transcription of nAChR receptors. There was some variability between iPSC lines derived from different subjects, as depicted by the large error bars shown in Figure 7A, there was no significant difference in expression of subunit mRNAs between CHRNA5 variant groups. Therefore, the rs16969968 SNP in CHRNA5 does not affect the generation of the DA cellular phenotype through the dual SMAD inhibition protocol.

Functional assessment of midbrain-like DA neurons: Electrophysiological recordings reveal active and mature DA neurons

Next, we established the exhibition of an excitable membrane potential to confirm the functionality of iPSC derived midbrain-like DA neurons. Through whole cell patch clamp recordings done by Guohui Li from the lab of Dr. Zhiping Pang, both the D398 and N398 midbrain-like DA neurons produced robust and repetitive spontaneous action potentials (APs), and had similar membrane

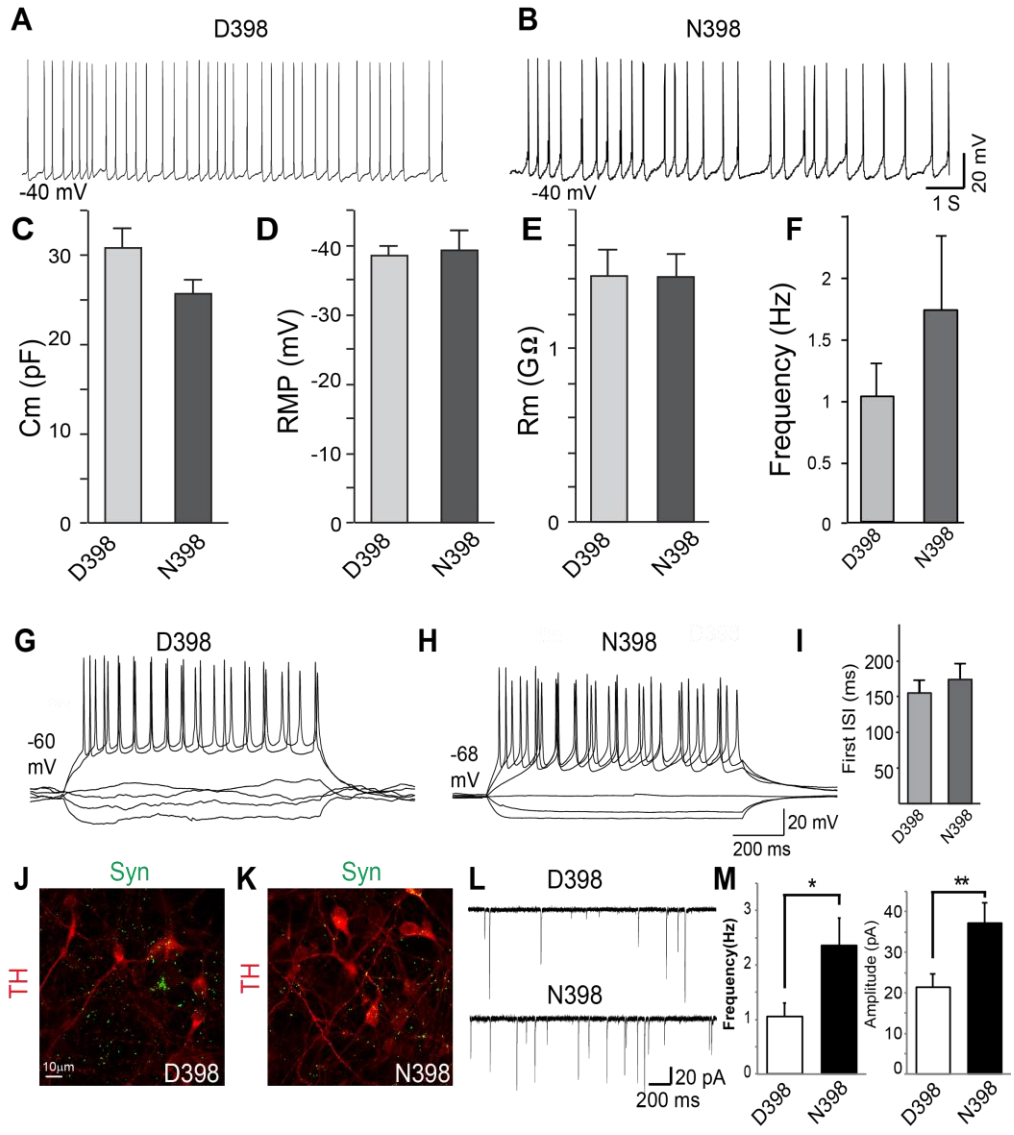

Figure 8 Electrophysiological analysis of midbrain-like DA cultures

A-B) Spontaneous action potentials of D398 and N398 DA neurons. C) Membrane capacitance, D) Membrane resistance, E) Resting membrane potential (RMP), and F) Spontaneous firing frequency of D398 and N398 DA neurons. G-H) Repetitive action potentials from depolarizing current injections in D398 and N398 DA neurons. I) Interstimulus intervals of induced action potentials of D398 and N398 DA neurons. J-K) ICC of TH (Red) and Synapsin (Green) for D398 and N398 DA neurons. L) Spontaneous postsynaptic currents of D398 and N398 DA neurons. M) Frequency of inward currents from D398 and N398 DA neurons.

properties, including membrane capacitance, resting membrane potentials, and input resistance, confirming the maturity and functionality of the neurons (Figure. 8). While the spontaneous APs in midbrain-like DA neurons of both genotypes have statistically

similar frequencies (p=0.258), the N398 neurons tend to fire more APs (Figure 9F). Next, we tested the intrinsic excitability of the midbrain-like DA neurons by inducing APs using different current injected amplitudes. Neurons of both genotypes exhibited similar frequency of induced APs, suggesting similar neuronal excitability (Figure 8G and H). This suggests that the N398 variant in CHRNA5 does not impair the propensity for neuronal excitability, nor does it produce any major changes in the passive membrane properties of D398 or N398 neurons (Figure 8C-E). However, the N398 variants have a slightly higher frequency of spontaneous APs (Figure 8F), which could be due to differences in synaptic network activity. Since the midbrain-like DA neuronal cultures also form synapses, as revealed by synapsin puncta (Figure 8J and K), we turned to measurements of postsynaptic activity.

To test whether the N398 variant alters synapse function, we measured spontaneous postsynaptic currents (sPSCs, Figure 8L). Both N398 and D398 neurons exhibited robust sPSCs, indicative of mature synapse formation and synaptic transmission. Interestingly, consistent with the slightly greater spontaneous AP firing frequency in N398 DA neurons, the N398 DA neurons also exhibited greater spontaneous post-synaptic activity (Figure 8L and M), indicated by the increased frequency and the amplitudes of the sPSCs in N398 neurons when compared to the D398 DA neurons. Therefore, neurons in the N398 cultures have a higher excitability due to more synaptic activity.

RNA sequencing highlights link to alterations in calcium response mechanisms

Our goal was to identify genes that may contribute to or result from the functional differences observed between D398 and N398 human neurons. To confirm the cellular identity of midbrain-like DA cultures gene expression profiling was done by RNA sequencing (RNAseq). We used replicate cultures from single donors from each variant group (Figure 9). This was done to reduce the noise from using multiple individual samples. However this approach raises the possibility that the gene expression analysis would be limited to that particular individual and not the risk variant itself. This was shown in RNAseq analysis within isogenic mutants versus control subjects, where there the variability between individuals was much greater than an isogenic pair of a mutant line[132]. The expression analysis was compared to hESC-derived NSCs at two stages of differentiation (leading to primarily glutamatergic neurons, day 0 and day 5) [133] Also included in the data analysis was RNAseq data from DA cultures published by the Studer lab [134]. Clustering shows that D398 and N398 cultures are more similar to midbrain-like DA neuron cultures than to glutamatergic (cortical) NSC (Figure. 9A)[107]. Additionally, we found similar expression levels of several mRNAs known to be associated with DA neurons in midbrain-like DA, D398, and N398 cultures (Figure 9B). These genes included, CORIN is a floor plate cells cell surface marker originally found as an activator of atrial natriuretic peptide (ANP) cardiac hormone[135], and it has been associated with OTX2 during dopamine neurogeneis[136]. FOXA1 is a positive regulator of NGN2, NURR1 and EN1[137]. LMX1A also targets NGN2 by repressing HES1[138]. Lastly, NR4A2, a ligand mediated receptor normally expressed in the developing midbrain, binds to TH where NURR1 knockout mice have an irregular movement [139],[140].

Additionally, the midbrain-like DA neurons expressed the paired-like homeodomain transcription factor 3 (PITX3) which is found within the substantia nigra and VTA neurons during embryonic day 10[141]. Overall, the mRNAs of these factors are all prominent within midbrain-like DA cultures providing more evidence that the genetic profile is similar to levels found in previously published midbrain-like DA cultures.

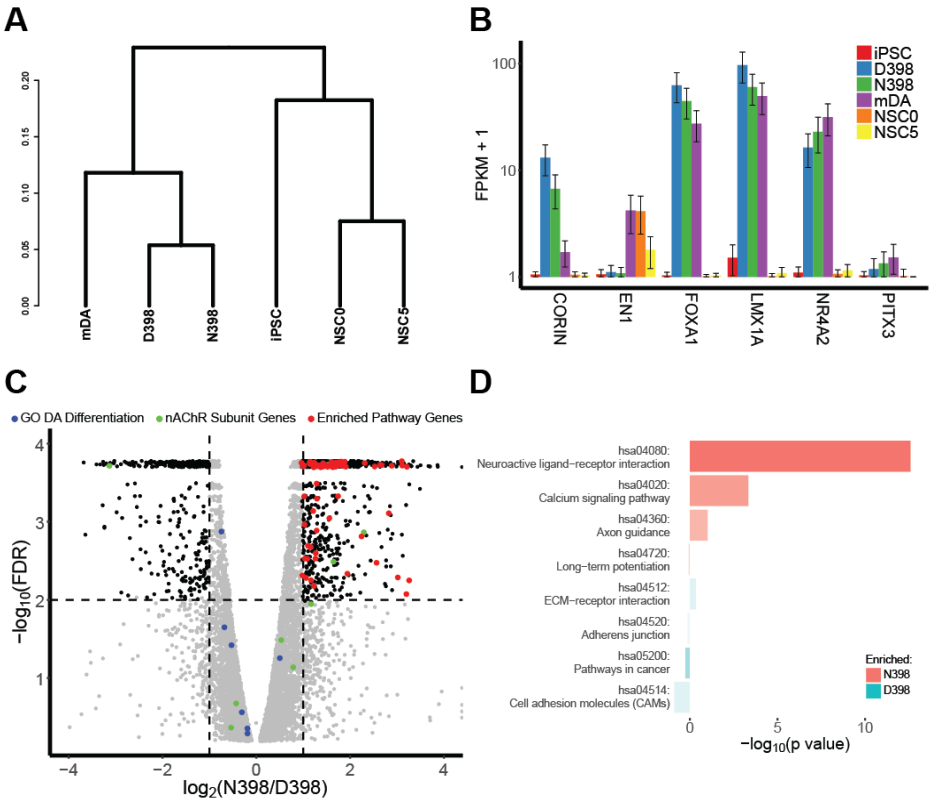

Figure 9 RNA sequencing analysis of midbrain-like DA cultures
A) Hierarchical clustering of D398 and N398 DA cultures, iPSC or iPSC-derived NSC (NSC0), or NSC differentiating into glutamatergic neurons (5 days of differentiation, NSC5). The dendrogram shows relative distances (based on the Jenson-Shannon divergence metric) for the top 500 genes varying by group. (B) Expression patterns for genes characteristic on midbrain DA neurons. The mean FPKM is plotted ± the 95% confidence interval, n=3/group. (C) RNAseq volcano plot. The horizontal axis shows the log2 fold-change, comparing N398 to D398. The vertical axis shows the false discovery rate (FDR) as the –log10 of the value. Points are plotted as individual genes not significantly different (grey dots) or significantly different (black dots) at 1% FDR (horizontal dashed line) and at least 2-fold different (vertical dashed lines). Colored dots indicate the nAChR receptor neuronal markers (green), GO dopamine differentiation genes (blue) and differentially regulated genes belonging to the significantly-enriched pathways relatively increased in N398 (red). (D) Pathway (KEGG) analysis identifies three functional groups as enriched in the list of genes increased in N398. Bar colors indicate enrichment in N398 (red) or D398 (blue). The bar length indicates the FDR, and the color intensity (alpha) indicates the number of genes enriched.

Furthermore, the majority of mRNAs detected in these cultures was expressed at similar levels in either D398 or N398 DA neurons, as depicted by the grey dots within the

vertical dashed lines indicating 2-fold differences and below the horizontal p-value cut-off dashed line in Figure 9C. The set of nAChR subunit mRNAs (Figure 9C green dots), as previously detected by qPCR (Figure 8A), was primarily within the 2-fold difference range (vertical dashed lines), except for CHRNA5, which was relatively increased in D398 (8.7-fold higher, 0.02% FDR). QPCR assay (Figure 8) indicated a similar difference although it was not statistically significant. Other groups of genes indicative of neuronal identity or maturity, including the gene ontology group members specific for dopaminergic differentiation (Figure 9C, blue dots) were unaffected by the variation. This again confirms that the genetic variants in this study do not affect the differentiation into neurons further suggesting a more downstream effect.

We then focused on differences between D398 and N398 cultures, where 1,194 genes were significantly different (≤1% FDR and at least 2-fold different, dashed lines; black dots in Fig. 9C). Taking the 349 genes that were relatively lower in N398, only two KEGG pathways were found to be enriched at relatively low confidence levels (blue bars in Fig. 9D), as determined by DAVID software[142,143]. However, the 845 genes relatively increased in N398 were significantly enriched in neuroactive ligand-receptor interaction, Ca^{2+} signaling pathway, and axon guidance KEGG pathways (red bars in Figure 9D) highlight neuron activity-specific biological processes. This predicts that N398 DA neuron cultures are likely to exhibit functional differences in response to ligand, potentially through changes in calcium influx. This also implies that the N398 variant may contribute to the excitatory response of neurons during nicotine exposure and that deregulated mRNAs may be due to intracellular signaling events far downstream of the nicotine receptor variants.

Neuronal activity upon stimulation by nicotine

Ca^{2+} -imaging analysis suggests increased network activity in N398 affected subjects

As an initial first step to survey the network-wide activity within cultured midbrain-like DA neurons, Ca^{2+} imaging was done in response to nicotine stimulation. Observed Ca^{2+} transients, though not providing direct evidence of synaptic activity, give meaningful information about intracellular Ca^{2+} levels in living cells, because Ca^{2+} is a key intracellular signaling ion, particularly for vesicular release at the synapse [144,145]. Neuronal Ca^{2+} transient responses to nicotine were recorded during perfusion of 3 μM nicotine in either D398 or N398 midbrain-like DA neurons, using replicate cultures from a single individual from each group to reduce the phenotypic variability between subjects. A nicotine concentration of 3 μM while not physiologically relevant to humans[146] has been shown to cause a significant increase in desensitization in Xenopus oocytes expressing the N398 variant[115]. In order to mimic past work, we began with a higher nicotine exposure. After trials with nicotine were completed in each field, only cells that showed an increase in Ca^{2+} signal after perfusion with 40 mM KCl solution were considered neurons and selected for analysis. This allowed us to distinguish neurons from glia in the co-culture system. For the time resolution of our assays (1 frame per second) we usually observed bursts of transients as a single, aggregated peak in a pattern similar to burst firing found in substantia nigra sections of rats[38] (an example from Smetters et al.[5] is shown in Figure 10).

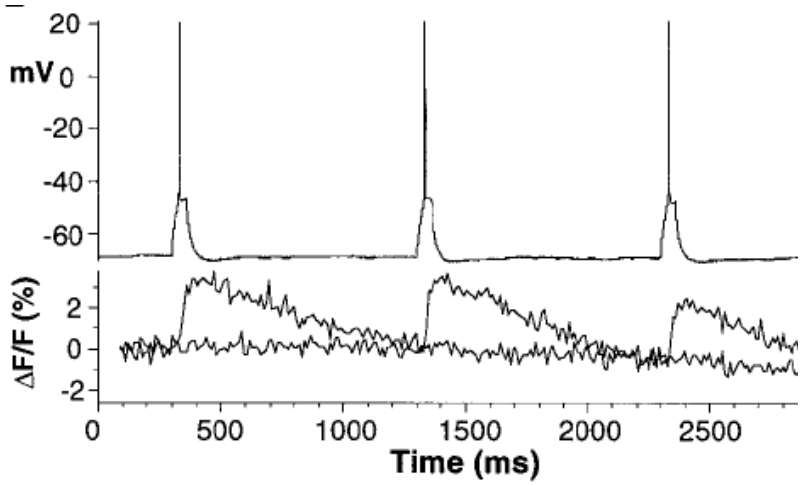

Figure 10 Calcium imaging correlation to action potential depicted from the work of Smetters et al.[5]
This sample of perforated patch clamping during calcium imaging displays similar amplitude and responses between action potential measurements and calcium fluorescence.

Only fluctuations in fluorescence intensity in the neurons after the addition of nicotine were classified as events. This was done to ensure that results from each neuron analyzed were due to nAChR activation. Each neuron within the field of view was further classified as one of the following: Oscillators, whose fluctuations in fluorescence intensity preceded nicotine application and continued after nicotine application (Figure 11A, B); Nicotine responders, which exhibited increased fluorescence intensity only after application of nicotine (Figure 11C, D); and nicotine non-responders (not shown), which failed to exhibit fluctuations in fluorescence intensity following the application of nicotine. Results from neuronal cultures with the N398 genotype displayed an increased number of nicotine responder neurons when compared to the D398 neurons (Figure 11E). This suggests that neurons carrying the N398 variant show increased network activity compared to D398 neurons.

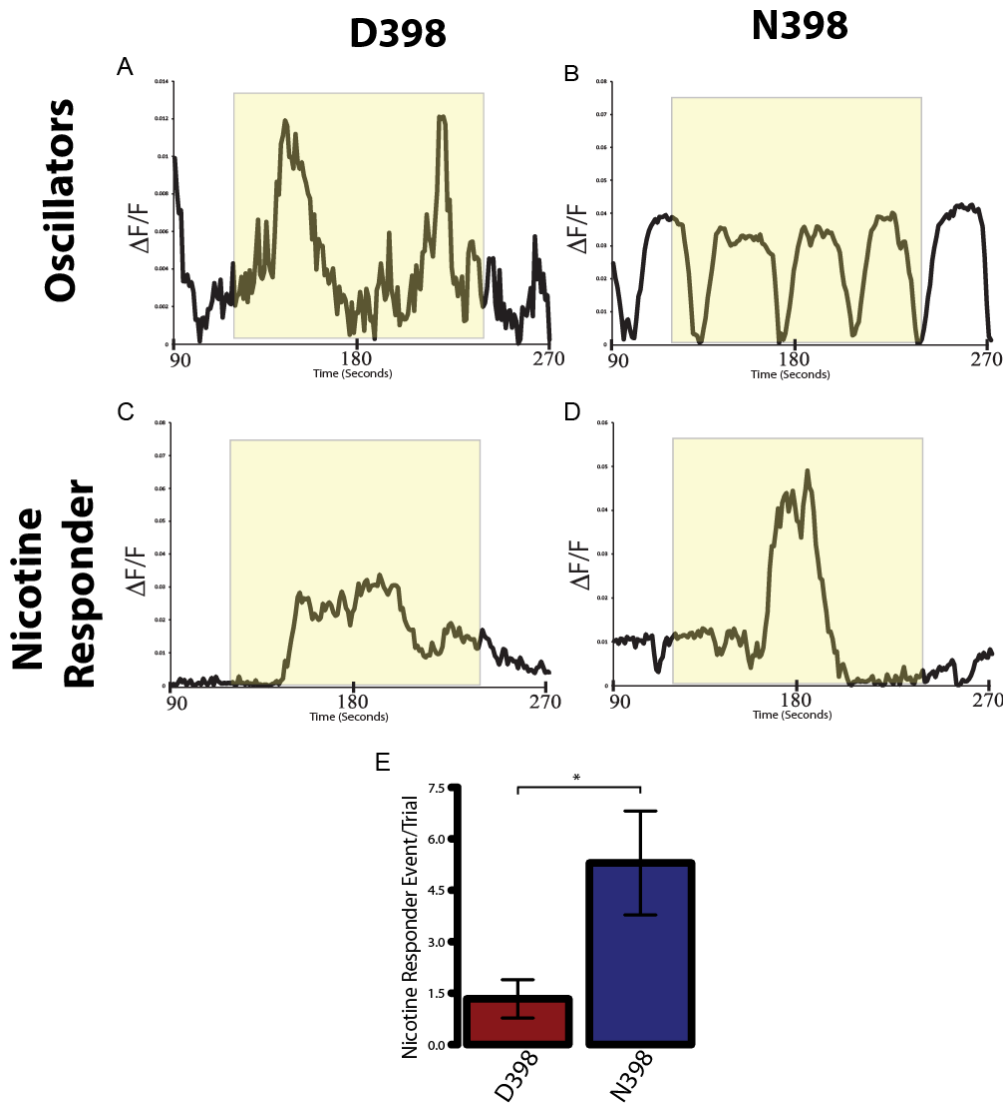

Figure 11 Representative traces of Ca^{2+} events
Ca^{2+} imaging detects patterns of cells identified as oscillators or nicotine responders. The time phase shown as the yellow box is when the flowing buffer was supplemented with 3 μM nicotine, which was then washed out and followed with 40 mM KCl (not shown). (A, C) Representative trace of an Oscillator event and a nicotine response event in D398 DA neurons. (B, D) Representative trace of an Oscillator event and a nicotine response event in N398 DA neurons E) Summary of nicotine response events per trial between D398 and N398 subject groups.

These results are consistent with the predictions from gene expression analysis and increased basal EPSC frequencies (Figure 8). Overall, the results of the calcium imaging

focused on the global neural network activity following exposure to high levels of nicotine. During the calcium imaging analysis, we observed increased network activity in neurons with the N398 variant. We then reasoned that to further elucidate the cell-to-cell synaptic properties of the N398 variant, nicotine exposure experiments needed to be done using whole cell patch clamping.

Increased excitatory response to nicotine exposure

The results from qPCR and RNAseq analysis suggest that the contributions of the rs16969968 minor allele variant may lie with an altered synaptic response to nicotine. To

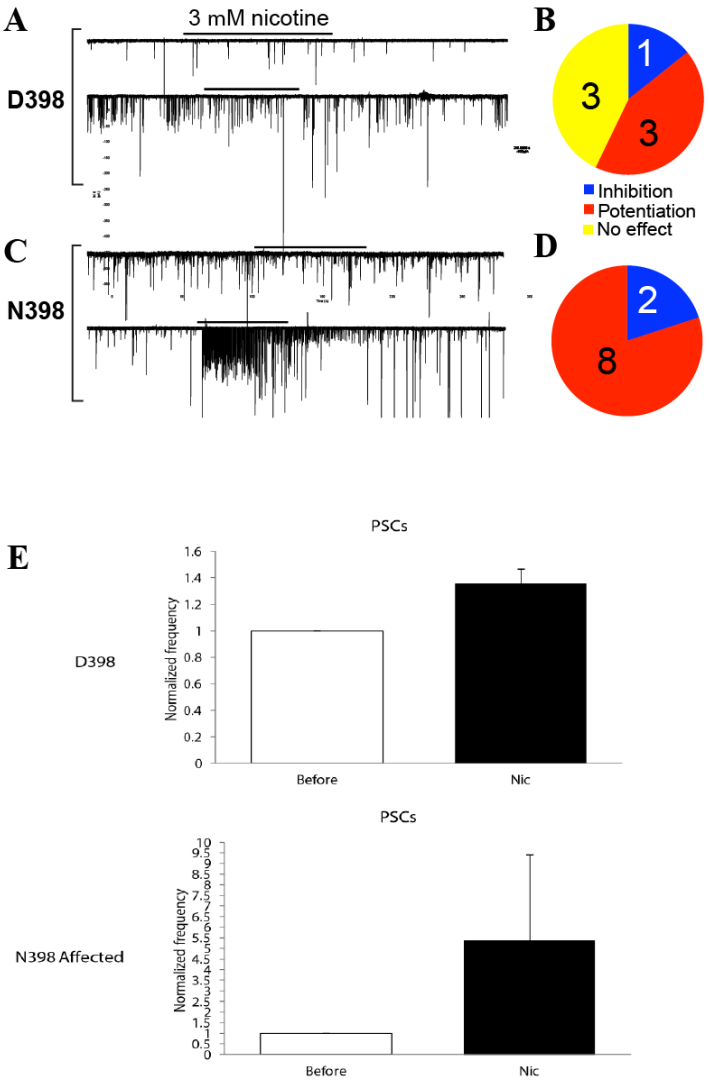

Figure 12 Excitatory response following high dose of nicotine
A) Representative traces of PSCs observed after 3 μM nicotine exposure to D398 DA neurons. B) Pie graph showing the number of cells showing different responses to nicotine application in D398neurons. "Potentiation, inhibition and no effect" reflect the frequencies of PSCs during the applications of nicotine, when compared to before the application of nicotine, were higher, lower or no change, respectively. C) Representative traces D) Pie graph showing the number of cells with different responses to nicotine application in N398 neurons. E) Quantification of EPSCs observed after 3 μM nicotine exposure to N398 DA neurons.

test this hypothesis, postsynaptic electrophysiological analysis on both the D398 and N398 DA neurons was conducted in response to 3 μM nicotine. Results illustrate that D398 DA neurons respond variably to nicotine exposure, as some are potentiated and others are inhibited in response to nicotine (Figure 12A and B). The N398 DA neurons, however, are potentiated more frequently following 3 μM nicotine exposure (Figure 12C and D). We also observe the frequency of EPSCs following nicotine exposure is higher compared to basal levels in the N398. Our work thus far has suggested that the nAChR α5 subunit variant contributes to a phenotypic difference between these two populations of neurons in the form of increased synaptic response to nicotine. Additionally, our basal electrophysiology, calcium imaging, and genetic studies have suggested that subjects with this variation may react differently to nicotine exposure. However, such a concentration would not be suitable for understanding how physiologically relevant levels of nicotine[146] affect the N398 risk variant. Thus we designed our next set of experiments to determine if there is any altered synaptic activity after a dosage curve with physiologically relevant levels of nicotine.

Glutamatergic N398 neurons exhibit increased activity following nicotine exposure

Results from the dual-SMAD-derived midbrain-like DA cultures suggest that human DA neurons may co-release glutamate (Figure 7) and that the release of glutamate was likely differentially affected by the N398 or D398 nAChR variants due to increased basal EPSCs in the N398 (Figure 8). Furthermore, gene expression patterns predict a difference in neurotransmitter response pathways, particularly for glutamate signaling (Figure 9). We considered whether the difference in response between N398 and D398

variant nAChRs could be observed in cultures of purely excitatory neurons. Additionally, forebrain excitatory glutamatergic neurons are modulated by nAChRs[30]. To study the impact of nicotine on synaptic transmission N398 and D398 iPSC were differentiated into excitatory neurons using induced neuronal (iN) protocols[147]. The iN protocol uses a lentiviral transduction method to increase the uniformity of excitatory cultures through puromycin drug selection (Figure 13). Our previous results displayed increased EPSC frequency, thus we hypothesize that the N398 variant would have a greater functional impact on excitatory neurons.

The induced excitatory neurons produced from this protocol expressed mature neuronal markers based from positive ICC of vesicular glutamate transporter (VGluT1), Synapsin1 and MAP2 (Figure 14). The expression of vesicular glutamate transporter is indicative of the ability to release glutamate, a major transmitter in excitatory neurons located within the synapses of excitatory neurons and has been found within the VTA[148]. Additionally, the presence of the synaptic vesicle permeable protein synapsin[149] illustrates the ability of the excitatory neurons generated by the iN protocol to shuttle neurotransmitters such as glutamate.

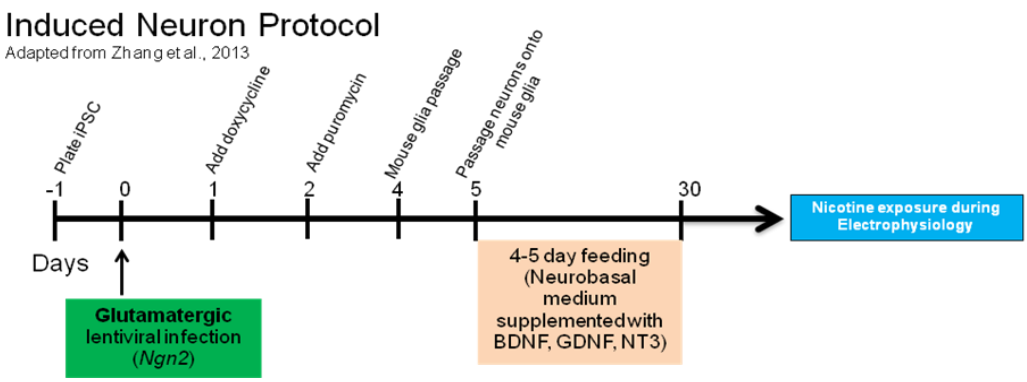

Figure 13 Schematic of adapted induced neuronal protocol from Zhang et al.[6]
The induced neuronal protocol begins with an infection of lentiviruses containing a doxycyline inducible Neurogenin2 (NGN2). Following puromycin selection, iN neurons are passaged onto mouse glia and supplemented with neural maturation factors BDNF, GDNF, and NT3. After a 30 day maturation period, excitatory neurons are subjected to nicotine dosage experiments until 30 days post infection.

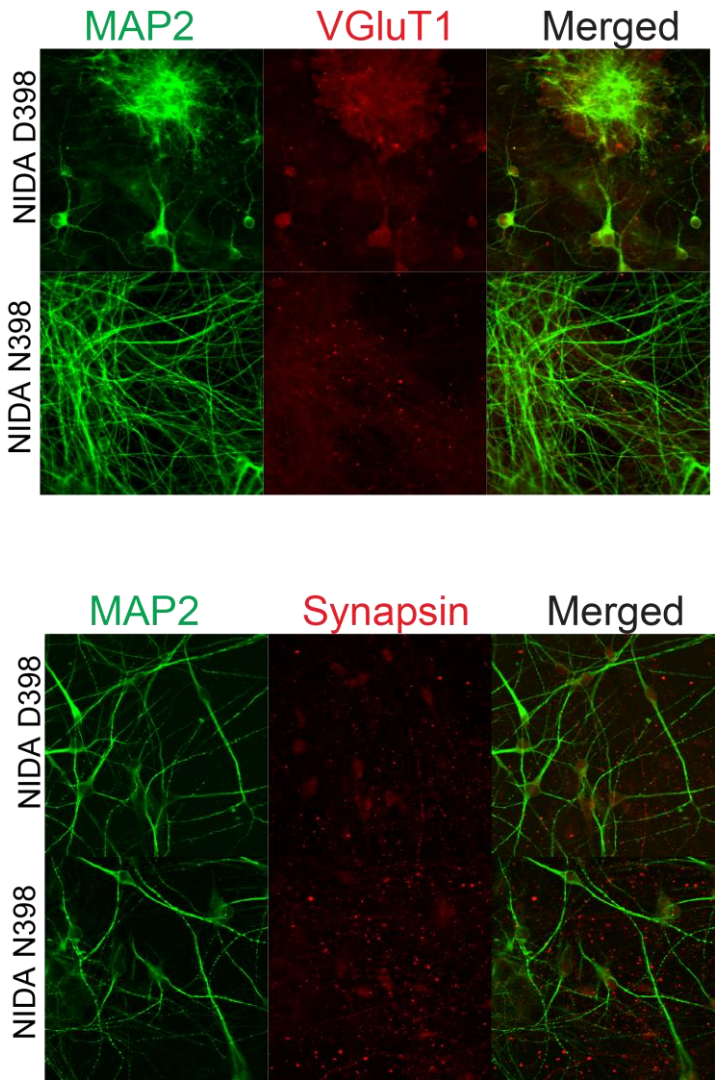

Figure 14 ICC of Glutamatergic iN cultures
Positive staining for mature glutamatergic neurons: MAP2 (green), vesicular glutamate transporter 1 (VGluT1, top, red), and Synapsin (bottom, red).

The effects of nicotine on spontaneous excitatory PSCs (sEPSCs) in both D398 and N398 human excitatory neurons were examined by whole cell patch clamping performed by Apoorva Halikere in Dr. Zhiping Pang's laboratory (described in the methods section). Excitatory post-synaptic potential (EPSC) responses were recorded

during a single increasing exposure dose of nicotine ranging from 0.1 μM to 6 μM every three minutes. Within 30 s of 0.1 μM nicotine exposure, frequencies of sEPSCs were significantly increased in the N398 subjects compared to the D398 controls (Figure 16C). Interestingly, following the dramatic increase of the sEPSCs in N398 neurons at low doses, the facilitatory effects appeared to decrease over time in the continued presence of nicotine, likely due to the desensitization of the receptor, which mimics the desensitization reported with ectopic expression studies in Xenopus oocytes[150]. Similarly, the amplitude of response trended higher during the initial 30 s but then fell below D398 shortly thereafter (Figure 15D). The difference in response at 0.1 μM nicotine was not limited to a single outlier cell or to cells prepared from a single subject (Figure 15E and F, with an example trace in A). The distribution of responses was variable but showed clearly that multiple cells from multiple subjects exhibited increased EPSC frequencies and amplitudes following the application of nicotine (Figure 15). These effects of nicotine even more convincing due to the fact that the frequencies of sEPSCs in that both N398 and D398 neurons were stable before the application of nicotine (Figure 15B-D). This suggests that the increased frequency and amplitude were in response to the application of nicotine.

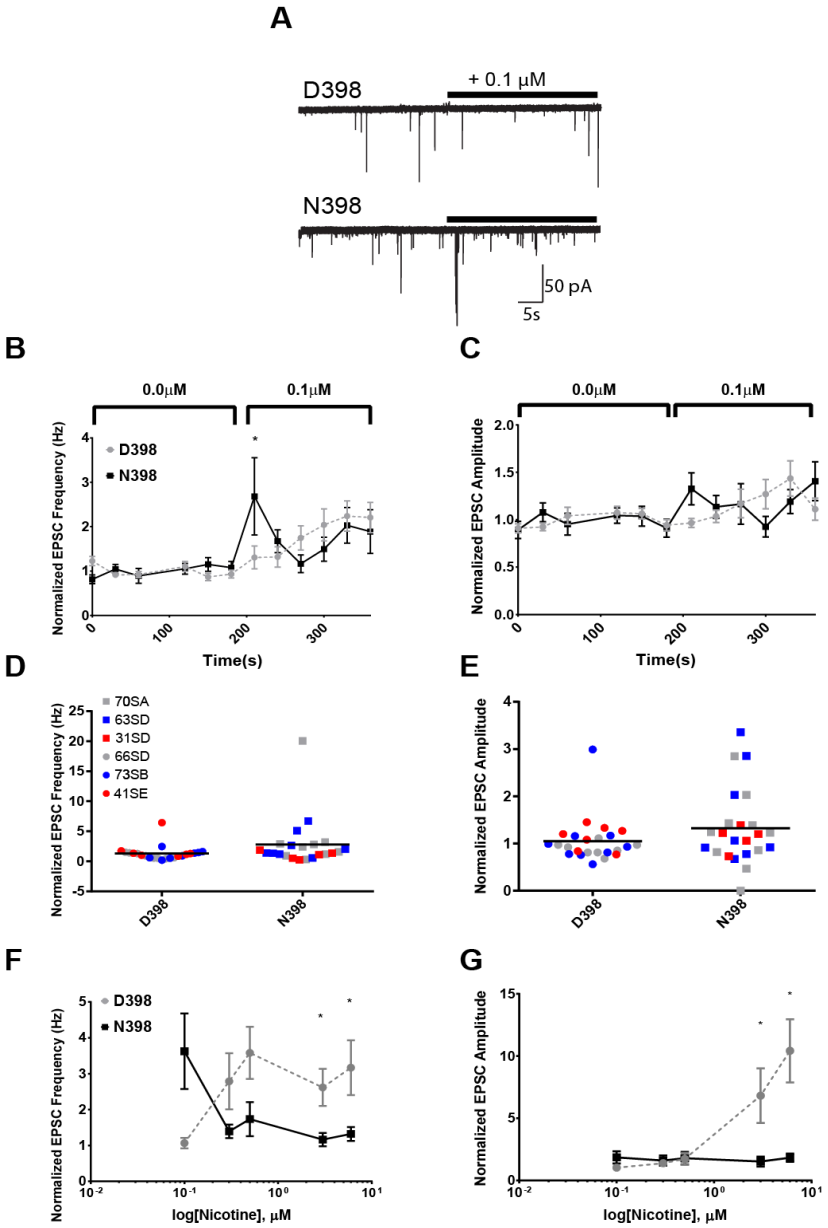

Figure 15 Nicotine dose response curves

Example traces from a patched neuron to show changes in response upon introduction of 0.1 μM nicotine (indicated by bar). Patched neurons increased frequency (C) and amplitude (D) during initial exposure to 0.1 μM nicotine. By 60 s after nicotine addition, frequency trended lower in N398 cells, although not significantly. Plotting the initial response to 0.1 μM nicotine for individual cells, it is clear that the changes in frequency (E) or amplitude (F) in N398 was not due to a single cell or subject. D398 samples are plotted as circles and N398 as squares. Color denotes cells from individual subjects (Table 1). However, subsequent additions of increasing doses of nicotine had reduced initial frequency (F) and amplitude (G) in N398 compared with D398 cells. N398 was different in frequency response from D398 as assessed by a Tukey post-hoc test of a general linear mixed-effects model with repeated measures ($p=0.00046$, $n=115$ cells per genotype; 5 cells per culture; 5-7 cultures per individual cell line).

Creating isogenic iPSCs for the CHRNA5 SNP

The result of this work addresses the role of rs16969968 SNPs in individual synaptic activity within an in vitro nicotine simulated neuronal network. Based on the results of electrophysiology, gene expression and calcium imaging, we have made the case for a possible role of N398 variants in the mediation of neuronal nicotine responses through increased frequency and desensitization. For our experiments, we used control lines from subjects that were unrelated to N398 subjects, each with their own unique genome. The use of these types of controls raises the possibility of diluting subtle phenotypes that can become overshadowed by differences between individuals, thus we run the risk of misinterpreting phenotypical differences between individuals as if they were due to the risk variant. This will require a better way to validate phenotypes seen from iPSC-derived neurons. To address this issue, we will need to create isogenic pairs of iPSC lines.

For the creation of isogenic lines, we utilize genome editing technology based on clustered interspaced palindromic repeats (CRISPR) developed by Doudna et al.[151]. To make isogenic iPSC lines, we will replace the CHRNA5 exon5 rs16969968 minor allele with a major allele sequence.

CHRNA5 editing: Donor plasmid cloning

For successful production of isogenic cell line, genome editing technology relies on several components. First is the Cas9 protein, which creates double stranded breaks, specifically at regions that contain clustered short interspaced repeats (CRISPR). To ensure that the Cas9 protein successfully targets CRISPR sites, the Cas9 protein must

complex with a small trans-activating RNA sequence RNA (tracrRNA) which activates RNA-guided DNA cleavage[152]. The tracrRNA sequences bind to the target sequence and a proto spacer motif or PAM site, located immediately upstream of the target site. A double stranded break (DSB) is created once the Cas9/tracrRNA complex binds to target sequences. Cellular mechanisms to repair a DSB include non-homologous end joining (NHEJ) or homologous recombination. In order to modify the target sequence, one can rely on potential replication errors during NHEJ which would disrupt intended target. Additionally, one could replace the target sequence by homologous recombination of a donor plasmid. Since NHEJ may create a mutation within the CHRNA5 coding sequence that may affect synaptic activity, we chose to replace the entire CHRNA5 exon 5 with the major allele using homologous recombination of a donor plasmid (diagrammed in figure 16).

The donor plasmid contains many features to ensure selection of repaired iPSC lines. The first feature of our plasmid is a fusion puromycin/EGFP backbone. This selection will allow for visualization and positive drug selection of transfected cells. LoxP sites flank the puromycin/EGFP, which provides the option to remove the sequence using the Cre recombinase if the puromycin/EGFP sequence is found to altered cell dynamics or undergone non-homologous recombination. As a negative selector for non-homologous recombination of the entire donor plasmid, we included a herpes virus thymidine kinase (TKHSV) gene. During successful homologous recombination, the TKHSV is lost as it is outside the right homologous flanking region. Thus the inclusion of TKHSV gene within the genome (non-homologous recombination) will increase the sensitivity to DNA polymerase inhibitor, gancyclovir, causing cell death[153,154]. The donor

plasmid consists of the CHRNA5 exon 5 containing the major allele flanked by homology regions to ensure recombination at the correct locus (Figure 16).

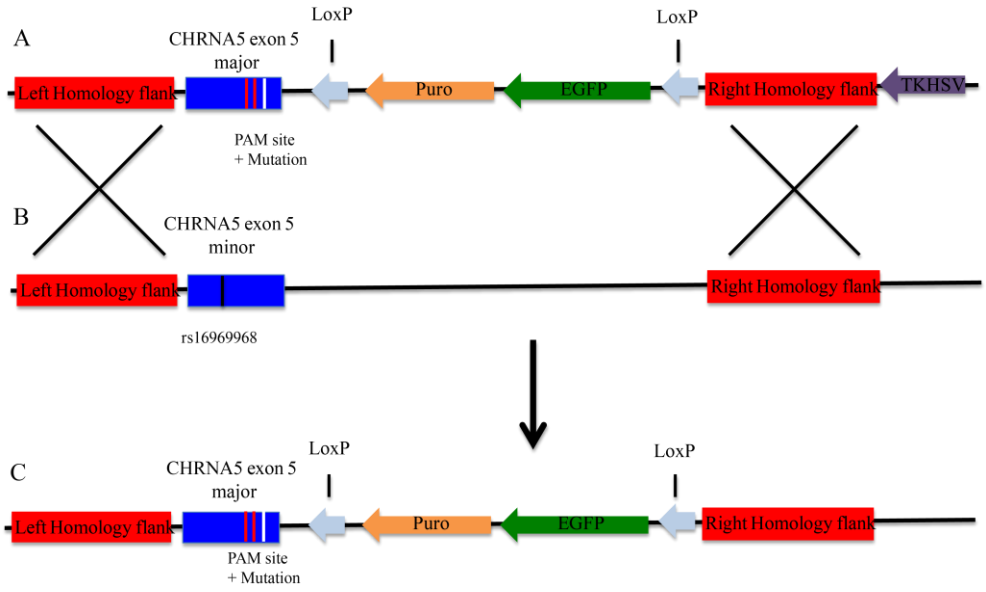

Figure 16 Homologous insertion profile of CHRNA5 exon 5 CRISPR repair donor plasmid

A) Plasmid map of CHRNA5 donor plasmid. Illustrated from left to right is the CHRNA5 exon5 left homologous flank, the major allele of the CHRNA5 exon 5 sequence, which contains a synonymous cytosine base changes at the PAM site. Following the CHRNA5 exon5 sequence, the PGK promoter driven Puromycin/EGFP fusion sequence is flanked by loxP sites. The homology region then finishes with the CHRNA5 exon5 right homology flanks. To the outside of the homology region is the TKHSV gene. B) Genomic region of minor allele CHRNA5. C) Expected sequence following homologous recombination of CHRNA5 donor plasmid.

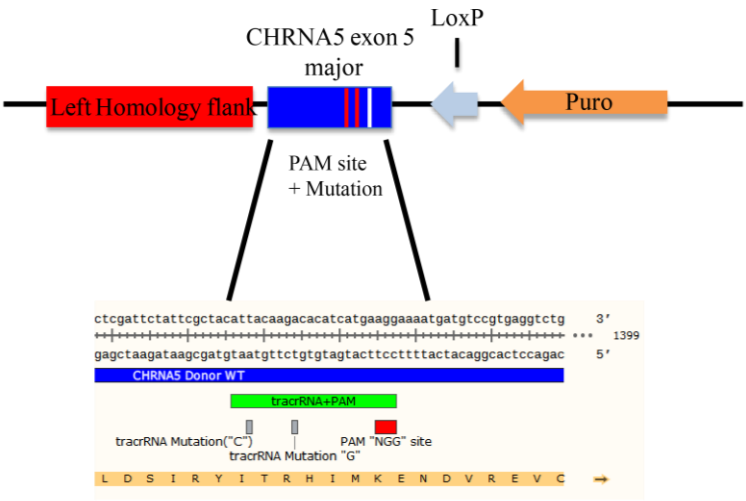

Figure 17 TracrRNA binding site mutation
To prevent targeting from the Cas9 protein, the binding sequence of the tracrRNA sequence was synonymously mutated in the donor plasmid. These mutations were within 15 nucleotides upstream of the PAM sequence

However, when modifying a genome using a donor plasmid, simply recombining the same sequence (with the exception to the intended correction) raises the possibility of plasmid targeting or retargeting of repaired sequence following recombination by the Cas9 protein. To circumvent this, we designed the repaired sequence with synonymous mutation within the tracrRNA binding site as illustrated in Figure 17 under "PAM + mutation". The presence of CHRNA5 homology sequences, mutated PAM sites within the final donor construct should allow for efficient and direct isolation of minor allele corrected isogenic iPSC lines.

To construct the donor plasmid, we used the Gibson assembly protocol developed by Barnes[155] and licensed by New England Biolabs. This exonuclease based cloning

protocol assembles multiple DNA fragments by generating and ligating complementary adjacent overhangs. In our case, we required the assembly of the CHRNA5 exon 5 and its homology regions within a puromycin GFP fusion plasmid. This first required the generation of PCR fragments of the major allele of CHRNA5 exon 5 and its homology regions. To produce the homology fragments, we designed PCR primers within sequences that flanks either side of the CHRNA5 exon 5 using genomic DNA from a minor allele iPSC line. For the major allele CHRNA5 exon 5 sequence, we used a synthetic oligo. Following amplification, complementary extension overhangs were generated from an additional PCR reaction for each fragment. The assembly of the donor plasmid occurred in several Gibson reactions. Each reaction required a gel-purified, restriction enzyme-linearized form of the fusion plasmid along with the repair flanks containing the extension overhangs. CHRNA5 minor allele containing iPSC lines were electroportated with the fusion repair plasmid, following sequence verification.

CHRNA5 editing: edited iPSC selection

Following electroporation of editing components (donor clone, tracrRNA, and Cas9 protein), iPSC cultures were allowed to recover and grow to 80% confluency. Cultures were then replated into a 96 well plate (15,000 cells per each well) to easily harvest single colonies following puromycin selection. Puromycin selection then began in a stepwise fashion; by increasing from 50 μg/ml, 150 μg/ml every three days to a final concentration of 300 μg/mL. This stepwise treatment is designed to allow for expression of puromycin resistance gene product to be produced. Following puromycin selection, surviving iPSCs clones were expanded, cryopreserved and harvested for DNA extraction.

CHRNA5 editing: Culture screening

Once expanded, the candidate potentially edited iPSC samples were harvested for genomic DNA to screen for rs16969968 minor allele correction. To identify homologous recombination of the donor cultures, we used the formation of PCR products from primer pairs designed within and outside the recombination site (Figure 18). The first primer pair is located within the puromycin gene. We expected a PCR product as the iPSC clones survived puromycin treatment. However, only three out of the four cultures had a PCR product (Figure 19A). This may have been due to poor priming since the puromycin gene has a high GC content. The next PCR reaction was to determine the presence of homologous recombination. These PCR primers were located upstream of the loxP site between the right homology flank and into the adjacent genomic DNA. Thus genomic DNA (gDNA) isolated from the minor allele iPSC line would fail to amplify, since the PCR product can only be made if the donor sequence is homologously inserted into the genome. We used this concept as our negative control for homologous insertion of the donor plasmid. We also designed a synthetic oligo containing the sequence overlapping the loxP site to the right homologous region. This construct would act as a positive control, since this sequence produced by the PCR product is unique only if there is homologous insertion of the donor plasmid. All of the candidate isogenic iPSC lines produced a homology PCR product (Figure 18A). Lastly, to determine if there was non-homologous recombination insertion of the entire donor sequence into the genome, we designed a primer pair within the TKHSV gene. Interestingly, all of the candidate edited iPSC lines produced a TKHSV PCR product. This suggests that while we have

homologous insertion of our donor sequence, there is the possibility of other insertions of the entire donor plasmid somewhere within the genome.

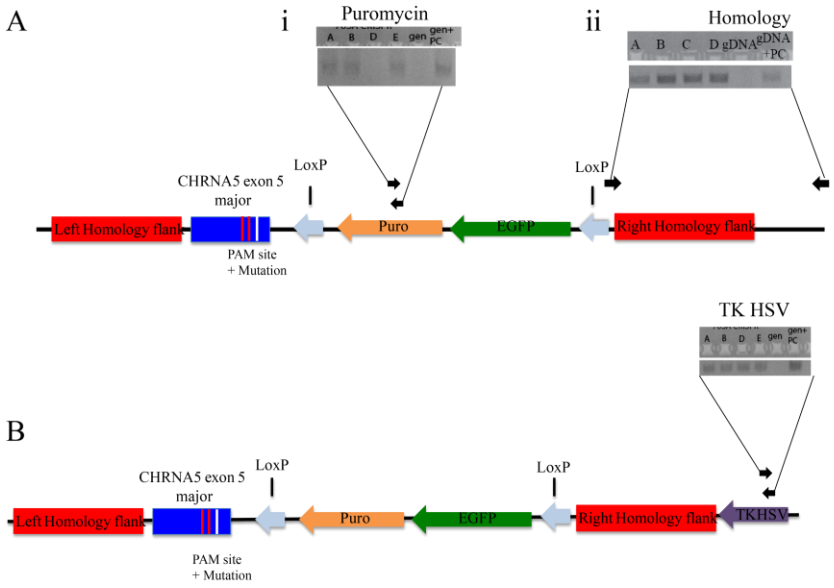

Figure 18 Detection of homologous CRISPR repair through PCR in candidate isogenic iPSC lines
A) PCR confirmation of homologous recombination of donor plasmid due to Ai) PCR product within the puromycin gene was detected in three out of the four candidate isogenic iPSC lines (lettered lanes) and synthetic positive control oligo. Aii) PCR product of homologous insertion, in all four candidate isogenic iPSC lines (lettered lanes) and synthetic positive control oligo. B) PCR confirmation of non-homologous insertion of donor plasmid due to PCR product within the TKHSV gene was detected in all four candidate isogenic iPSC lines.

So far, we have shown possible replacement of the minor allele of the CHRNA5 exon 5 sequence which would provide an isogenic control iPSC line. To confirm this finding we will need to conduct sequencing of the CHRNA5 exon 5 at the location of the rs16969968 SNP from the candidate iPSC lines. Upon sequencing confirmation, the isogenic iPSC lines will allow for a more appropriate comparison of phenotypes while confidently excluding the individual genetic background. We expect to validate the findings of this chapter by isolating the increased desensitization and EPSC frequency

within the minor allele carrying subject lines. We also expect to reverse this phenotype in the edited lines.

Discussion of Chapter 1

The major goal of this work is to identify the synaptic activity of neurons during initial nicotine exposure in subjects who carry the rs16969968 minor allele SNP. While past studies in mouse and Xenopus oocytes reveal potential effects on reward circuitry, we hypothesized that subtle affects of the α5 subunit genetic variants on nAChR would be detectable at the cellular level.

We first began by selecting donors carrying homozygous rs16966968 major or minor allele, encoding the D398 or N398 variant of the nAChR α5 subunit, respectively. IPSC were prepared from de-identified, cryopreserved lymphocyte repository specimens collected as part of a large genetics study (COGEND) previously used for genome-wide association studies[65,66].

To begin to test CHRNA5 variant function, we first generated midbrain-like DA neuronal cultures in order to mimic the VTA, an important member of the reward/addiction circuit[76,77]. Neuronal cultures were made through a dual-SMAD inhibition method generating cultures of relatively high purity midbrain-like DA neurons with co-expression of fundamental neuronal markers such as TuJ1 and MAP2 (Figure 6A and B). TH^+ cells were also labeled with DAT antibody (Figure 6D), indicating that the midbrain-like DA neurons could potentially possess the capability of releasing dopamine. This was followed up through HPLC analysis which confirmed DA release

into the medium following depolarization. Lastly, we demonstrated that midbrain-like differentiation protocol produced TH^+ cells were post-mitotic as a small percentage labeled with EdU (Figure 6E), as would be expected for mature neurons. From these results, we conclude that dual SMAD inhibition protocol produces midbrain-like DA neurons.

Although our results are consistent with the presence of midbrain-like DA neurons, the cultures also contained a small minority of serotonergic (5-HT positive) and inhibitory (GAD6 positive) neurons (Figure 7). We have also identified cells that were both TH^+ and $VGluT1^+$ (Figure 7), consistent with the notion that some DA neurons also co-release glutamate[129,130]. Thus these results suggest that while the N398 variant does not alter the process of differentiation, it remains possible that a heterogeneous mixture of neurons with any type of cell-cell synapse could be formed and may modulate synaptic function in response to nicotine.

Functionally, the presence of the N398 variant does not interfere with the generation of mature DA neurons, as determined by the expression of neuronal markers (Figure 7). Similarly, the basic membrane properties, and the capacity for generating action potentials, were not different between the two CHRNA5 variants (Figure 8). However, it appears that N398 neurons are receiving more synaptic inputs, as revealed by an increased PSC amplitude and frequency in N398 compared with D398 (Figure 8M). This is consistent with a possible increase in excitability of N398 neurons, or reduced input from inhibitory neurons, suggested by the relative higher frequency of spontaneous action potentials. This correlates with results from Morel et al.[156] and others[61,70] who suggest that while the $\alpha 5$ subunit does not contribute to nicotine binding with nAChRs,

the loss or alteration of α5 contributes to a shift in nicotine response, specifically in VTA DA neurons[69]. These results further suggest that an altered N398 DA neuronal response to nicotine can subsequently change the extracellular concentration of dopamine into areas of the brain responsible for addiction behaviors such as the PFC and SN.

To investigate intracellular regulatory processes of global gene expression we utilized RNAseq analysis. This type of analysis determines the gene expression from the number of transcript reads and can be used to screen for genes that are differentially expressed between variants which can be further validated[157]. The RNAseq results demonstrate identifiable differences between cultures based on CHRNA5 genotype and they predict that N398 cells will have altered response to stimuli. The most informative and significant functional enrichment from our analysis was for KEGG pathways specific for neuroactive ligand receptor interaction, calcium signaling, and axon guidance (red bars in Figure 9D). The gene expression patterns are consistent with the presence of midbrain-like DA-like neurons in our cultures and that the N398 and D398 cultures are most similar to the previously-published midbrain-like DA cultures[107]. Coincidentally, some of the differentially regulated genes were components of the glutamatergic pathway, and because we detected a minority of excitatory glutamatergic neurons in the midbrain-like DA cultures (not shown), it is also possible that some TH^+ cells co-release glutamate[128] thus the genetic differences may be due to $TH^+/VGluT^+$ neurons. Whether the altered expression of these genes is an effect of the N398 variant or whether it is only a correlation due to differences in neuronal function, the RNAseq results demonstrate

identifiable differences between cultures based on CHRNA5 genotype and they predict that N398 cells will have altered response to stimuli.

Our experiments suggest that N398 neurons are predisposed for an increased neuronal network activity upon initial nicotine exposure. Calcium imaging was used to indicate synaptic activity in response to nicotine stimulation. Cells were classified by the pattern of response to nicotine (Figure 11A-D). Results demonstrate a significant increase in nicotine responders in N398 (Figure 11E). It is possible that this increase is due to nAChR activity in the DA neurons or the response may be due to pre-synaptic input from other cells in culture. However, the results of Ca^{2+} imaging confirm the prediction from RNAseq that N398 cells exhibit a more robust network activity response to nicotine. This enhanced activity was confirmed by assessing postsynaptic currents in response to nicotine (Figure 12). This could be due, for example, to an altered activity of the individual receptor or to increased synapse formation. It is also possible that the increased excitability in midbrain-like DA cultures may be due to nAChR mediated activity in the DA neurons or to pre-synaptic input from other cells in culture—possibly an excitatory input.

Postsynaptic electrophysiological analysis on both the D398 and N398 DA neurons was conducted in response to 3 μM nicotine. Results illustrate that D398 DA neurons respond differently in response to nicotine exposure, as some are potentiated and others are inhibited (Figure 12A). The N398 midbrain-like DA neurons, however, are potentiated more frequently following 3 μM nicotine exposure (Figure 13B). Not only are the N398 neurons potentiated more frequently, but also the frequency of EPSCs

following nicotine exposure is higher compared to basal levels when compared with the D398 DA neurons. In conjunction with spontaneous EPSCs we show that the excitatory output of N398 DA neurons following nicotine exposure. Thus it appears that nicotine enhances the synaptic strength of the circuit more so in subjects with N398 genetic variant.

To test the possible effect on nicotine on excitatory neurons, we differentiated iPSC into glutamatergic neurons and exposed them to an increasing dosage of nicotine. Results from our nicotine dosage experiments had an increased frequency of EPSC in N398 iN cells at the lowest dose tested (0.1 μM). EPSCs at higher doses were consistent with desensitization of the receptor, which was observed in α2β4-containing nAChRs of a Xenopus oocyte injection model[150].This difference in response occurs at nicotine concentrations typical of heavy smokers (0.025-0.5μM)[146]. The results of this work indicate that the N398 variant of CHRNA5 is associated with greater excitability, which suggests that dopamine neurons are affected postsynaptically. These results suggest that individuals who carry the N398 variant may be subject to the dynamics of increased synaptic frequency followed by rapid desensitization of DA neurons at physiological and high doses of nicotine (Figure 12). This dynamic may enhance the pleasurable response to nicotine increasing the amount of extracellular DA in areas responsible for motor movement thus increasing possibility for reward seeking behavior. Consequently, these repeated elevated nicotine responses during nicotine exposure may further increase and potentiation leading to a feed forward cycle of addiction behavior. This series of events

may potentially contribute to the increased risk of nicotine addiction of those carrying the N398 variants [158].

However, we must take into consideration the possibility that the inherent genetic variability between individuals may overwhelm any subtle disease-associated phenotypes[159-162]. Indeed, our previous RNAseq analyses demonstrate broad variability among subject iPSCs, even among members of the same family [132]. The most convincing solution to this problem is the creation of isogenic pairs of cells differing only in a single locus, usually by genetic engineering techniques[163,164]. We have begun to implement techniques of isogenic repair using CRISPR genome editing technology. More specifically, we have isolated potential edited lines, but need to further verify repair by sequencing at the location of the rs16969968 variant.

The results derived from different human subjects tested a number of subject-specific iPSC and neuronal subtypes that are consistent and reasonably capture sufficient variability while identifying for reproducible phenotypes based on the non-synonymous SNP. Therefore in combining the increased neuronal activity identified by both Ca^{2+} imaging and PSC responses to nicotine, and supported by the increased basal frequency of PSC and the predicted pathway changes revealed by RNAseq, we conclude that the N398 variant produces neurons with increased responsiveness to nicotine. These results would agree with work from CHRNA5 knockout mouse models where reduced α5 subunit caused substantial behavioral effects such as increase nicotine intake[60,61].

CHAPTER 2 Elucidating the role of genetic variants associated with Alcohol Use Disorders

Alcohol Use Disorders (AUDs) affect millions of Americans, where large components of these behaviors are heritable. The ranges of heritability of these behaviors can be from 51-59%[165]. In 2012, a family genome wide association study (GWAS) sought to identify genetic variants associated with the increased risk of alcohol addiction[2]. The genetic variants from that study are associated with decreased frontal theta oscillations and are found within the KCNJ6 gene and encode a G-protein coupled receptor stimulated inward rectifying potassium channel (GIRK2). This channel modulates the hyperpolarization of neurons by forcing the membrane voltage towards the resting potential, decreasing neuronal activity[166]. For this study, we have developed a culture-based model to identify the physiological and genetic mechanisms among patients with AUD behaviors and their GWAS risk-associated SNPs. We have derived neurons and neuronal stem cells from AUD patient-specific induced pluripotent stem cells (iPSCs).

IPSC Characterization: pluripotency

To begin this study, we identified subjects with alcohol dependence from collections of Dr. Bernice Porjesz of SUNY Downstate Medical Center, Brooklyn, NY. These subjects each carry the three most significantly-associated haplotype SNPs identified by Kang et al.[2] (rs2835880, rs702859, and rs2835872; Table 3). Cell lines from alcohol dependent subjects with the KCNJ6 SNPs were identified as “KCNJ6 Affected”. Non-alcohol-dependent control subjects came from the same collection, and were

homozygous for the major alleles and corresponding cell lines were referred to as "KCNJ6Control".

Table 3 iPSC lines derived from cryopreserved lymphocytes provided from the COGA repository by RUCDR

List of subject cell lines profiles including, ID number (RUID), Gender, minor SNP status, allele of SNP (minor allele in red) and karyotype result. All SNP genotypes.

Cell Line (RUID)	Gender	Status	rs702859	rs702860	rs283872	Karyotype result
AA6376	Male	Affected	GG	GG	AA	Normal
AA11246	Male	Affected	GG	GG	AA	Normal
AA7351	Female	Affected	GG	GG	AA	Normal
AA10233	Female	Affected	GG	GG	AA	Normal
AA6472	Male	Control	AA	AA	GG	Normal
AA6407	Male	Control	AA	AA	GG	Normal
AA10474	Female	Control	AA	AA	GG	Normal
AA10171	Female	Control	AA	AA	GG	Normal

Cryopreserved lymphocytes from selected subjects were obtained from RUCDR Infinite Biologics®. T-cells were reprogrammed by RUCDR to iPSCs using Sendai viruses containing cDNA encoding four transcription factors shown to maintain pluripotency (OCT4, SOX2, KLF4, and C-MYC; CytoTune™, Life Technologies) as described in the methods section. After transduction, we verified the presence of risk-associated SNPs in iPSC lines by sequencing gel purified PCR products (not shown),

During the process of reprogramming, iPSCs are at risk for induced copy number variations and chromosomal aberrations[167,168]. To ensure that reprogrammed iPSCs maintained the same chromosomal profile as their corresponding somatic cell lines, we probed the samples for karyotyping analysis, which was done by Drs. Mary Konsolaki and Li Deng of RUCDR. IPSC lines were found to have the full set of normal

chromosomes and did not contain extra chromosomal bands, thus were judged to be karyotypically normal (Table 3, representative analysis in Figure 19).

Pluripotency of subject iPSC lines was first confirmed by mRNA gene expression analysis using microarray results and the PluriTest algorithm[119], which was performed by RUCDR. PluriTest analysis yields a pluripotency and a novelty score set as defined by Müller et al.[119]. The pluripotency score distinguishes a pattern of genes separating pluripotent from non-pluripotent using many samples from multiple laboratories. The samples are then ranked according to the genes that separate them the most; the threshold score for determining pluripotency is greater than 20. The second indicator of pluripotency is the novelty score. This is defined by measuring the biological variations with respect to the gene expression where the threshold for pluripotent cultures should be less than 1.67. All eight iPSC lines passed the pluripotency thresholds (Table 4). The failure of PluriTest novelty thresholds is due to a PluriTest algorithm to instrument update. However, the process of passaging iPSCs over time selects for the most pluripotent cells[169] and reduces copy number variations[167]. Furthermore, all eight lines positively expressed pluripotent markers through immunocytochemistry (ICC) following the PluriTest. Additionally, subsequent experiments were able to successfully differentiate the iPSC lines into neural stem cells (NSCs) and neurons.

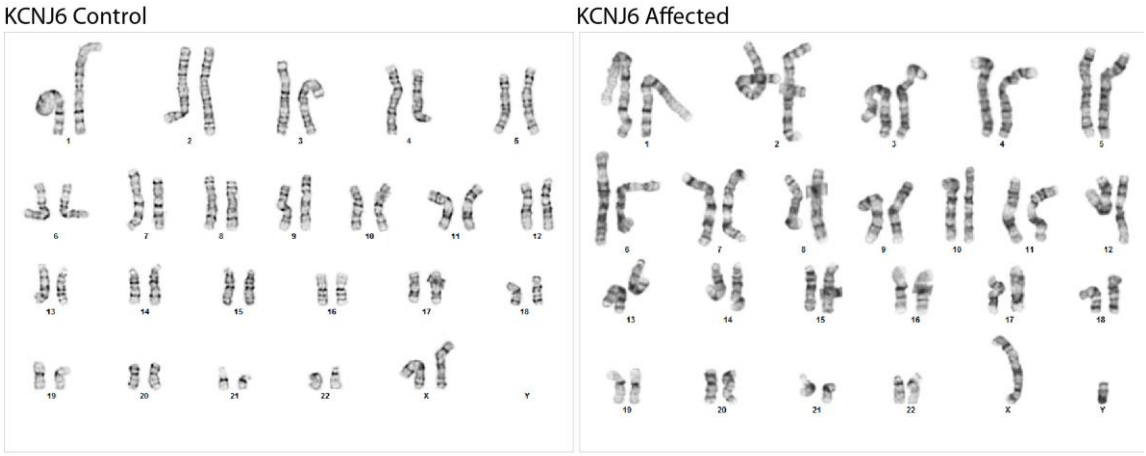

Figure 19 Representative karyotyping from subject-derived iPSC lines
Karyotyping analysis shows similar chromosomal make up of iPSC lines regardless of variant

Table 4 PluriTest analysis of pluripotent gene expression of iPSC lines
Pluripotency scores (Pluripotency raw and Novelty) for KCNJ6 iPSC lines. Sufficient pluripotency status is determined with a pluripotency score higher than 20 and a novelty score greater than 1.67.

KCNJ6	Cell Line (RUID)	Pluripotency	Novelty
Control	AA10171	25.857	1.816
	AA10474	21.854	1.913
	AA6472	26.171	1.858
	AA6407	29.25	1.95
Affected	AA6376	21.109	1.961
	AA7351	25.82	1.72
	AA10233	29.201	1.864
	AA11246	32.63	1.97

Pluripotency was further confirmed by positive ICC of markers traditionally found in carcinoma and embryonic stem cells: OCT4 and TRA-1-60 (Figure 20). OCT4 is a SOX2 binding protein that acts to enhance the expression of fibroblast growth factor (FGF2) and TRA-1-60 is a pericellular matrix peptidoglycan protein [120,121,123]. Overall, these results demonstrate that subject-specific T-cell derived iPSCs have been successfully reprogrammed to a pluripotent state regardless of presence of KCNJ6 variant.

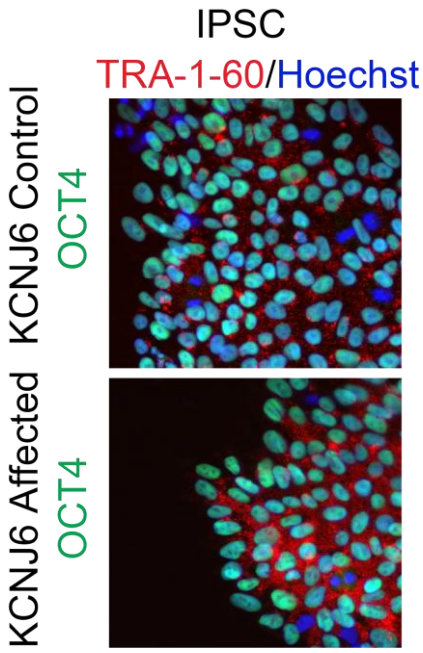

Figure 20 Representative ICC for pluripotency markers Oct4 and TRA-1- 60
Positive ICC for OCT4 and TRA-1-60 in Control and Affected iPSC (A, B)

Differentiated neural stem cells express neural markers[170]

We wanted to identify a neuronal mechanism that is associated with subjects carrying the AUD related SNPs. We reasoned that the most significant effect of ethanol would be regulating gene expression, since previous work has suggested that alcohol

affects neural stem cells (NSCs) by altering DNA transcriptional regulatory mechanisms[171,172] inhibiting growth, and reducing migration. Thus, we began our study by differentiating iPSCs into (NSCs).

NSCs are homogenous, self renewing multipotent cells that have the ability to differentiate into a neural ectodermal fate producing neurons, astrocytes and oligodendrocytes[173]. By identifying the effects of ethanol in neural progenitor cells, we can determine what intrinsic features of KCNJ6 risk variants contribute to AUD behaviors. More specifically, NSC are similar to the precursor cells within the fetal brain that may be exposed to high ethanol concentration when the majority of adult neurons are made during the third trimester[174]. To differentiate iPSC into NSC, we utilized an NSC differentiation medium from Gibco (described in the methods).

The transition from iPSC to NSC results in loss of OCT4 and TRA-1-60 pluripotency factors (not shown), but other factors such as Sox2 and Pax6 are expressed. Full NSC differentiation was confirmed by positive expression of NSC markers such as: Nestin, an intermediate filament protein which is a major cytoskeletal protein in the mammalian CNS[175], neural RNA binding protein, Musashi[176], PAX6, which is expressed in early development of the CNS modulating NSC self renewal and cell cycle progression[177], and SOX2, required for NSC maintenance[178] (Figure 21). The result of this analysis confirms that regardless of genotype, the NSC differentiation protocol developed by Gibco produces NSCs that stain correctly for neural progenitor markers.

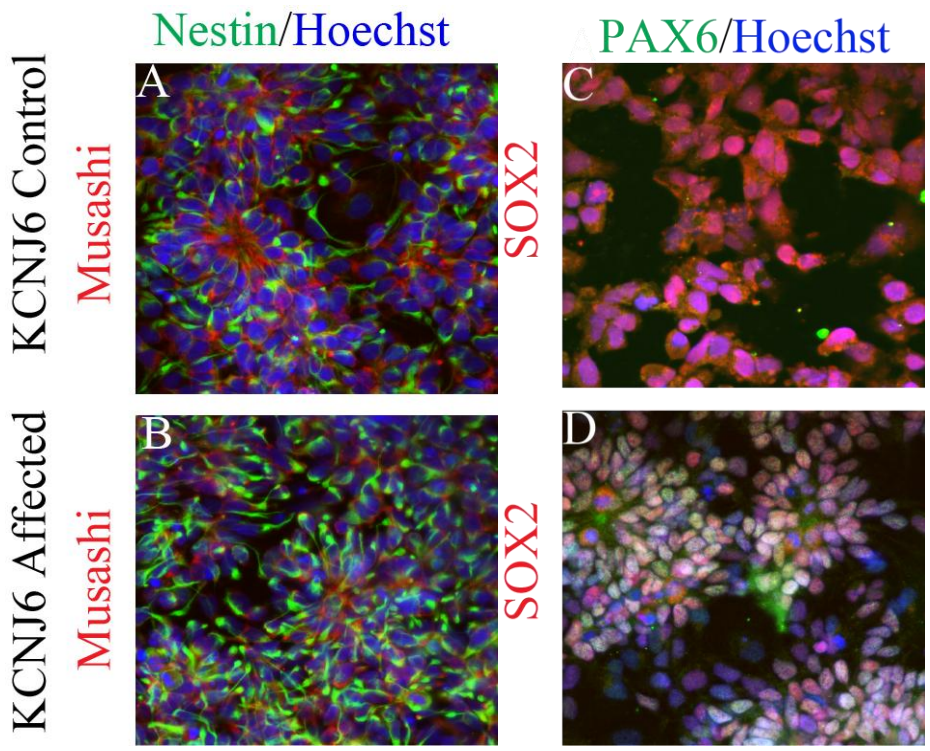

Figure 21 Representative positive ICC staining of neural lineage markers in KCNJ6 lines differentiated NSCs
Positive ICC of Nestin (green) Musashi (red), SOX2 (red), PAX6 (green) and Hoechst (blue) in Control (A, C) and Affected (B, D) NSCs

Ethanol exposure does not affect the growth characteristics of NSCs

Previous work has noted the negative effects of alcohol on neurogenesis and cell cycle genes, specifically during NSC proliferation as reviewed by Oni et al[179]. This paper reviewed as series of studies including work by Hicks et al.[171] who showed that ethanol disrupts growth factor-mediated cell cycle progression. The work by Vangipuram et al.[180] identified a significant reduction in gene expression of at least five major signaling pathways involved in neural differentiation. Additionally, Liu et al.[181] showed altered methylation following ethanol treatment in NSCs. These studies suggest that ethanol exposure mediates the intrinsic growth characteristics of NSCs. We hypothesized that the

ethanol treatments would not cause massive cell death, but may alter growth dynamics of the NSCs. This would include genes involved in growth and neurogenesis. To address this hypothesis, we began by assessing growth and expansion of NSCs during ethanol exposure. Over the course of 72 hours, we determined the effects of cell viability and number in NSCs that were exposed to ethanol (-/+ 75 mM in sealed flasks) collecting samples every 12 hours. This experimental set up is an effective way to maintain near-constant ethanol levels in culture as shown by personal correspondence from Dr. Lily Deng. A concentration of 75 mM that is high, but within range of blood alcohol levels (BAC) of alcohol dependent subjects[182]. We began to study NSC growth with this high dose, and future work will also assess NSC growth dynamics at BAC levels of non-alcoholics which are around the 10 μM- 15 μM range[171,180,181,183].

Comparing all eight cell lines, there was no significant variation in cell diameter or cell viability between genotypes, with or without exposure to 75 mM ethanol at any time during the 72 hour exposure. There was also no change in doubling time between genotype and treatment (Figure 22). These results are in contrast with published work, where cell growth in NSC is reduced after ethanol exposure [184]. Other studies have suggested that the effects of ethanol exposure on NSCs may occur following more chronic ethanol exposure, possibly affecting the neural differentiation scheme[185].

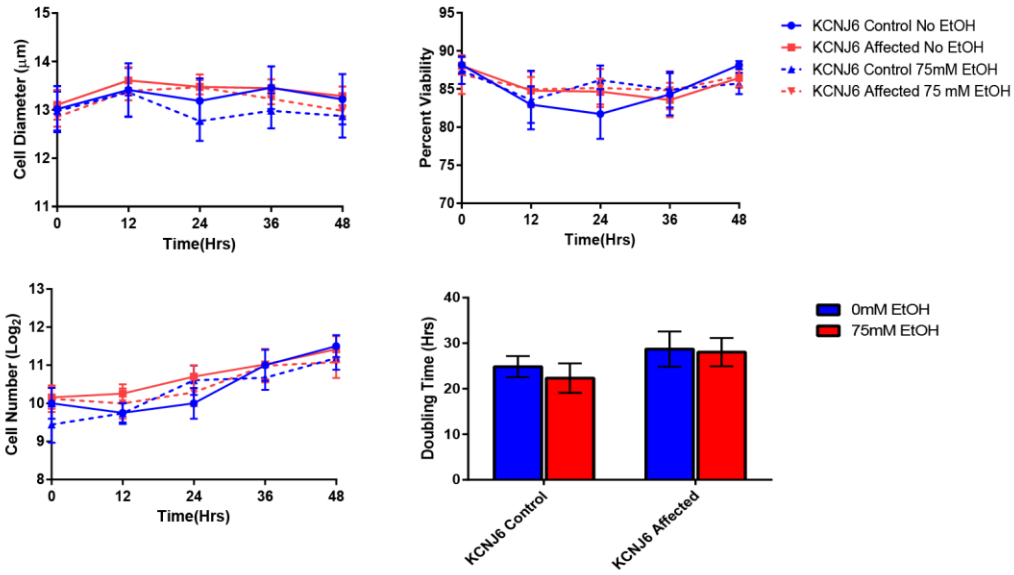

Figure 22 Effect of 75mM on growth dynamics of Neural Stem Cells
(A-C) Cell diameter, number, and viability following 72 hours of 75 mM ethanol exposure to NSCs. D) Quantification of Doubling time +/- ethanol exposure. There was no change in any measurement between samples

KCNJ6 variants differentially express neural development genes

We hypothesized that the contributions of the AUD risk variant SNPs may alter the ethanol mediated synaptic response capacity of neurons. This may be due to changes in the gene expression of GIRK2 channels in neuronal precursors following ethanol exposure. Our first step in addressing this question was identifying changes in gene expression between KCNJ6 variants using RNAseq analysis (method described previously). Using ethanol exposure methods described previously, iPSC derived NSCs were exposed to 75 mM ethanol for 24 hours in order to determine the effect of ethanol exposure following a full NSC cell cycle and cell pellets were collected for RNAseq analysis.

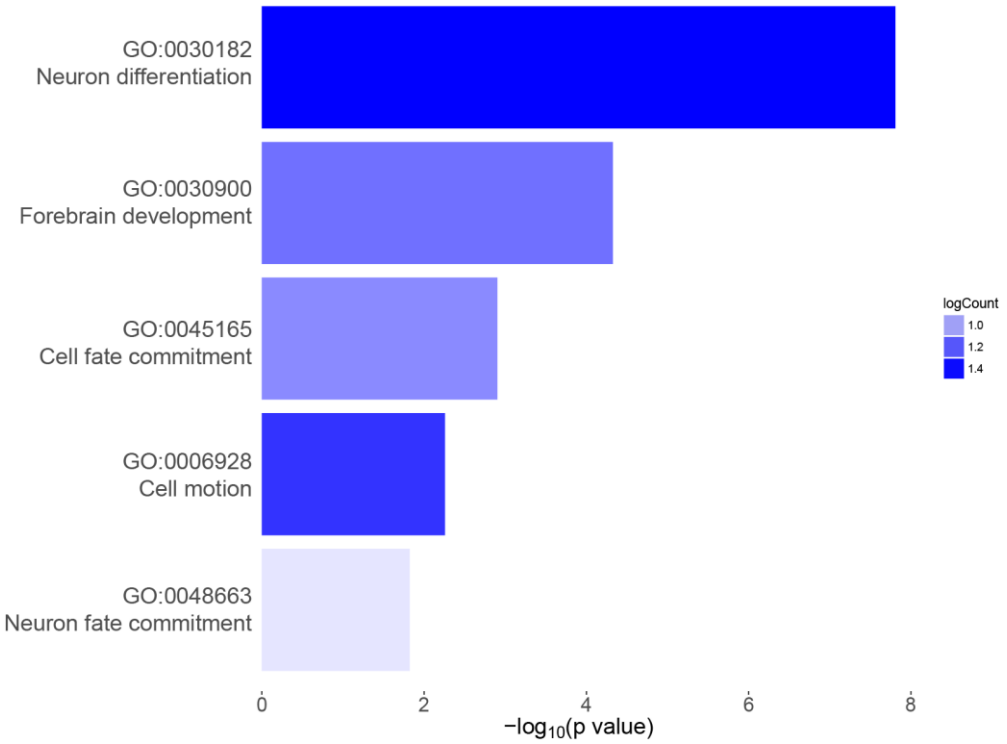

Figure 23 RNAseq functional enrichment analysis
Differentially expressed in NSCs of KCNJ6 affected and control subjects after 24 hours exposure to 75mM of ethanol. These differences were seen- by genotype in neuronal differentiation, and forebrain development. The bar lengths are the -log10 of the false discovery rate. The color intensity is the log10 of the number of genes in that GO group, as indicated by the key (logCount)

The results of the RNAseq analysis revealed genes that were involved in neuronal differentiation and cell fate commitment. These genes were more enriched in subjects with the KCNJ6 variant (Figure 23). Top genes included forkhead box F2 (FOXF2), a gene recently identified to play a role in blood brain barrier and palate development[186,187], and receptor tyrosine kinase (ROR2), which is involved in Wnt pathway activation[188] (Table 5). Thus these results suggest that acute ethanol exposure affects genes involved in development, as ethanol exposure plays a role in altering the expression of genes involved in the cell cycle as seen in previous work[171]. To expand on this, we performed

qPCR expression analysis on genes previously found to be altered during ethanol exposure[171,172]. These genes include G1 regulators (CCND1, MCM5 and E2F7) and G2 regulators and DNA binding transcription factors (PTTG1, BUB1, SOX2, MECP2 and CUX2). We followed a similar dosage and time scale as the growth curve (Figure 22) but used a single control NSC line to determine if there were any inherent effects of ethanol without the KCNJ6 variants (Figures 24-26). The results of this assay found that 24 hours of ethanol exposure induced a slight increase in expression of G1 and G2 related genes (Figure 24A-B, Figure 25A-B) while the opposite was true in M phase related genes (Figure 26A and C). Our finding, while preliminary, suggests that there is a slight cycling effect on gene expression over the course of 72 hours with the largest expression difference with or without ethanol at 24 hours. However, the effects of ethanol did not translate in altering the cell growth or viability during this period. Which suggests that the observed gene expression effects may not mediate NSC proliferation dynamics but may alter the ability of NSCs to exit the cell cycle affecting differentiation [180,189]. We will need to expand this experiment to all NSC lines to confirm if there are any significant effects of ethanol on cell cycle genes. Additionally, we will need to determine whether the effects of ethanol on NSCs lies in modulating their differentiation scheme by differentiating ethanol treated NSCs and quantifying the number of mature neurons produced.

Table 5 List of top ten genes differentially expressed between KCNJ6 variant and control subject NSCs

Top genes from RNAseq that were differentially expressed between the KCNJ6 minor allele variant and control major allele variant were isolated based on edgeR ANOVA modeling. Differential expression between genotypes was noted by the log2 fold change of gene expression compared to control lines. The false discovery rate (FDR) notes the rate of type I (rejection of the null hypothesis), for each gene.

Gene	log_2 Fold change	False Discovery rate (FDR)
FOXF2	2.825	4.194E-07
LOC253039	2.255	5.477E-06
ROR2	0.999	2.779E-04
SLC45A3	-0.899	3.900E-04
MSX1	2.228	4.471E-04
ALX4	2.388	7.852E-04
DSP	1.483	8.955E-04
WSCD2	3.322	1.288E-03
CDH6	1.124	1.927E-03

.

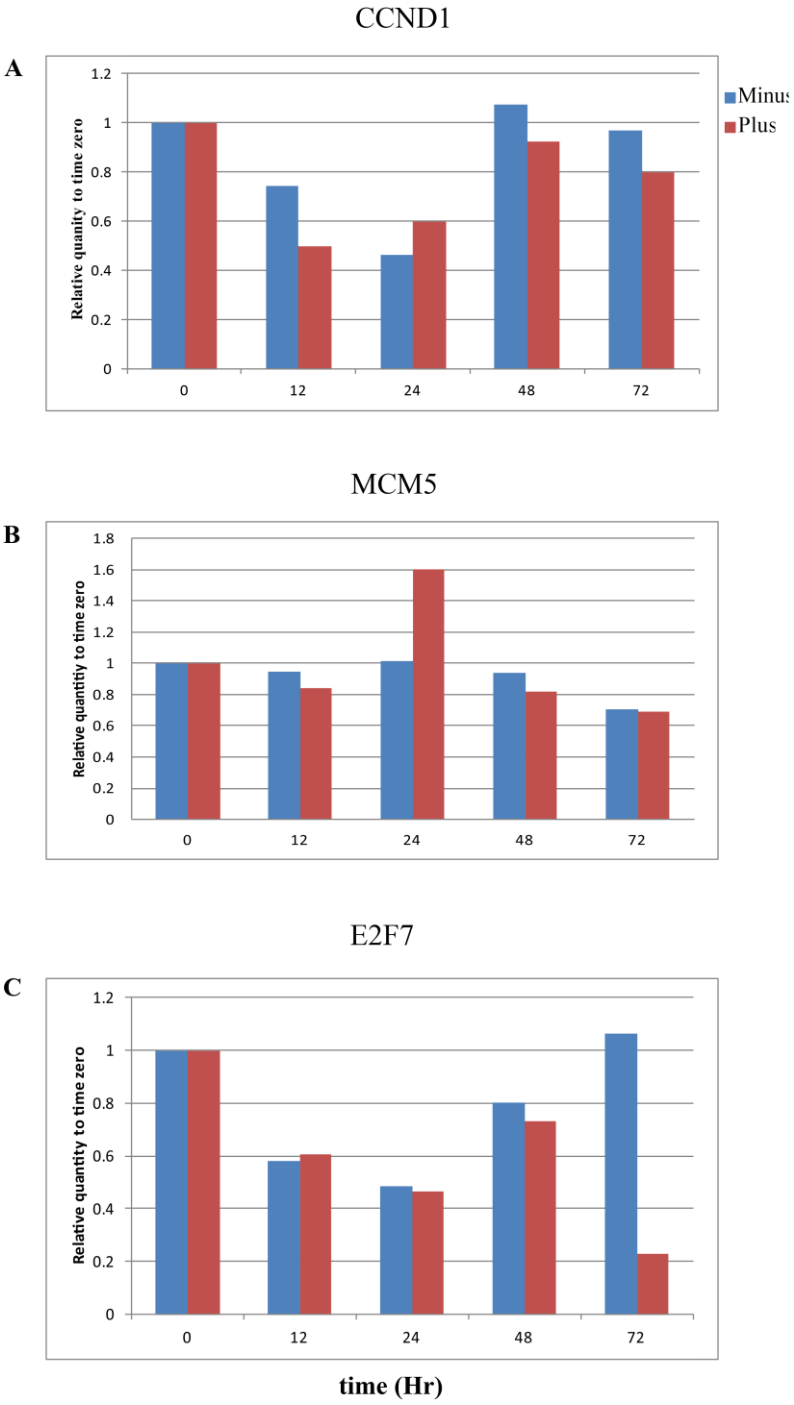

Figure 24 Quantitative PCR from following 75mM ethanol treatment of G1 cell cycle genes: CCND1, MCM5 and E2F7
Control cell line "KCNJ6 72" NSCs were exposed to 75mM ethanol and probed for expression of various cell cycle genes A) CCND1 B) MCM5 C) E2F7.

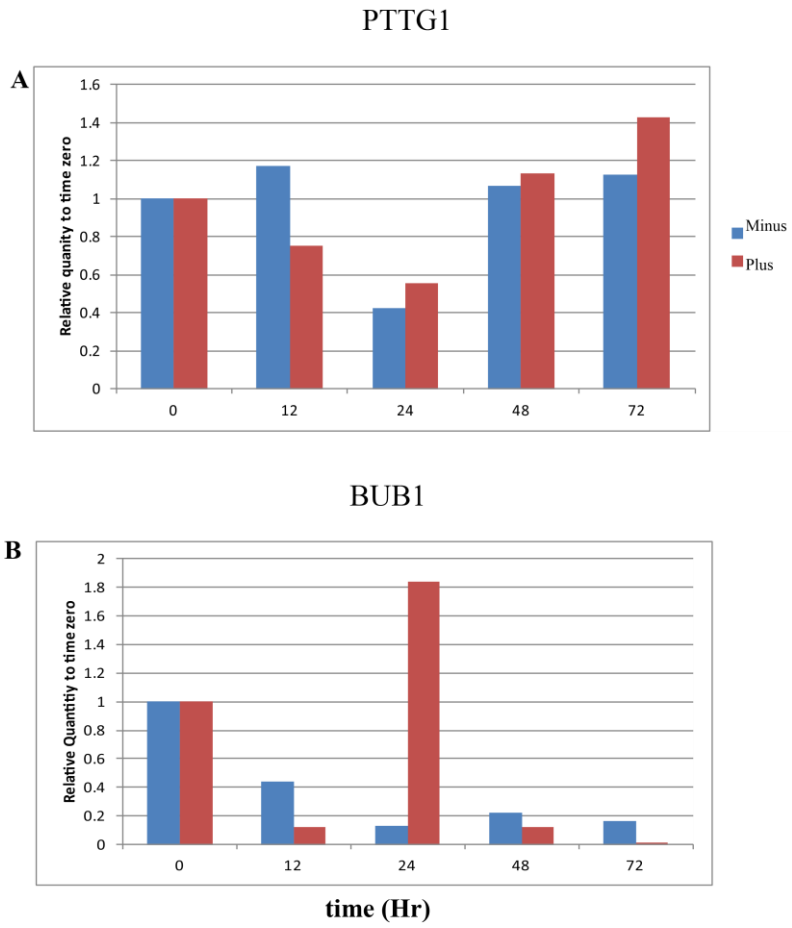

Figure 25 Quantitative PCR of genes involved in G2 phase from following 75mM ethanol treatment
Control cell line "KCNJ6 72" NSCs were exposed to 75mM ethanol and probed for expression of various cell cycle genes A) PTTG1 B) BUB1

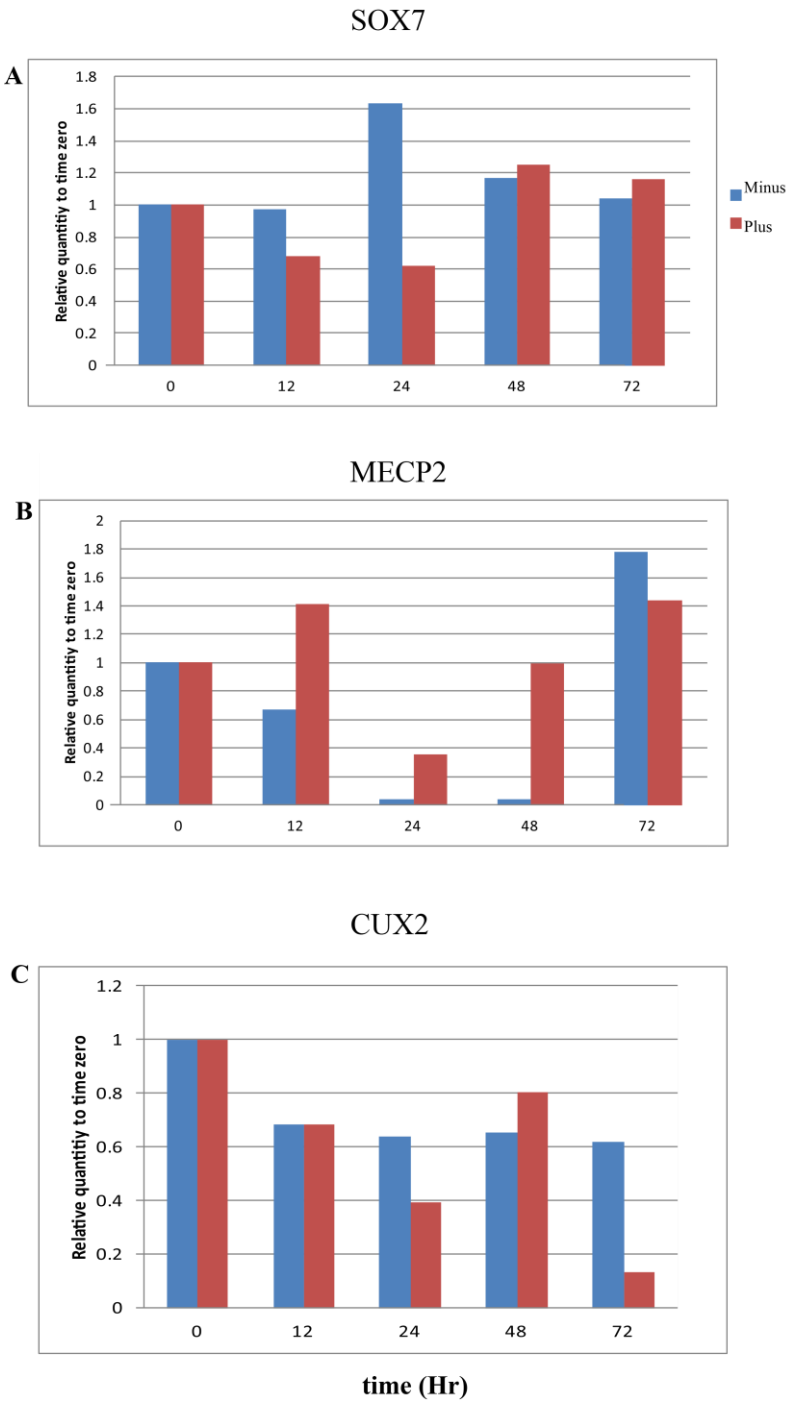

Figure 26 Quantitative PCR of genes involved in M phase following 75mM ethanol treatment
Control cell line "KCNJ6 72" NSCs were exposed to 75mM ethanol and probed for expression of various DNA binding transcription factors: A) SOX7 B) MECP2 C) CUX2

Neuronal activity in the presence of ethanol

In addition to modulating the gene expression profile of NSCs, ethanol directly targets GIRK2 channels though a distinct binding pocket[94]. Ethanol modulates the excitation of DA neurons. This is done through the decreased firing of GABAergic neurons via the μ- opioid receptor a activity [190]. Past work from Zhang et al.[191] demonstrated a minor allelic SNP (rs1799971) within the OPRM1 gene reduces mRNA expression and lowers μ-opioid protein yield. Similarly, Duan et al.[192] showed decreased mRNA stability and protein expression in DA receptors with synonymous SNPs. These studies suggest that the synonymous KCNJ6 variants may contribute to reduced gene expression of GIRK2 channel. We hypothesized that the risk variants alter the gene expression of GIRK2 channels and modulate the synaptic activity. To address this, we started by determining synaptic response of excitatory neurons, but first needed to optimize culture conditions. KCNJ6 variant iPSC were differentiated into excitatory neurons using an induced neuronal (iN) protocol[147]. The iN protocol uses a lentiviral transduction method to increase the uniformity of excitatory cultures through forced expression of transcription factor, Neurogenin 2 (NGN2). Neurogenin 2 is a transcription factor involved in neurogenesis, and whose forced expression in stem cells produces excitatory neurons[193]. Generally, the NGN2 iN differentiation protocol uses a common basal medium (Neurobasal, Gibco). However, work by Bardy et al[194]. argues that Neurobasal medium is not physiologically suitable for production of neuronal cultures and interferes with neuronal differentiation. Thus, they developed a novel neural basal medium, which is more physiologically similar to cerebrospinal fluid, a commonly used medium during electrophysiological analysis, which they named “BrainPhys.” We

decided to use this protocol and expected this medium would enhance the reliability and quality of synaptic experiments using excitatory neurons.

Following a modified differentiation scheme (found in methods), excitatory neurons were produced and cultured for 45 days. We then determined the neuronal phenotype from both variants using ICC markers for excitatory neurons: vesicular glutamate transporter (VGluT1), synapsin (hSyn), and microtubule associated protein (MAP2) (Figure 27). The expression of VGluT1 and hSyn together is indicative of the ability of the neurons to formulate synaptic vesicles and release a major excitatory transmitter (glutamate)[149]. The KCNJ6 variant neuronal cultures had similar VGluT and hSyn expression patterns. From these results, we illustrate the ability to generate excitatory neurons by the protocol from Bardy et al.[194] regardless of genotype. From here, we will explore the neural circuitry effects of the KCNJ6 variants.

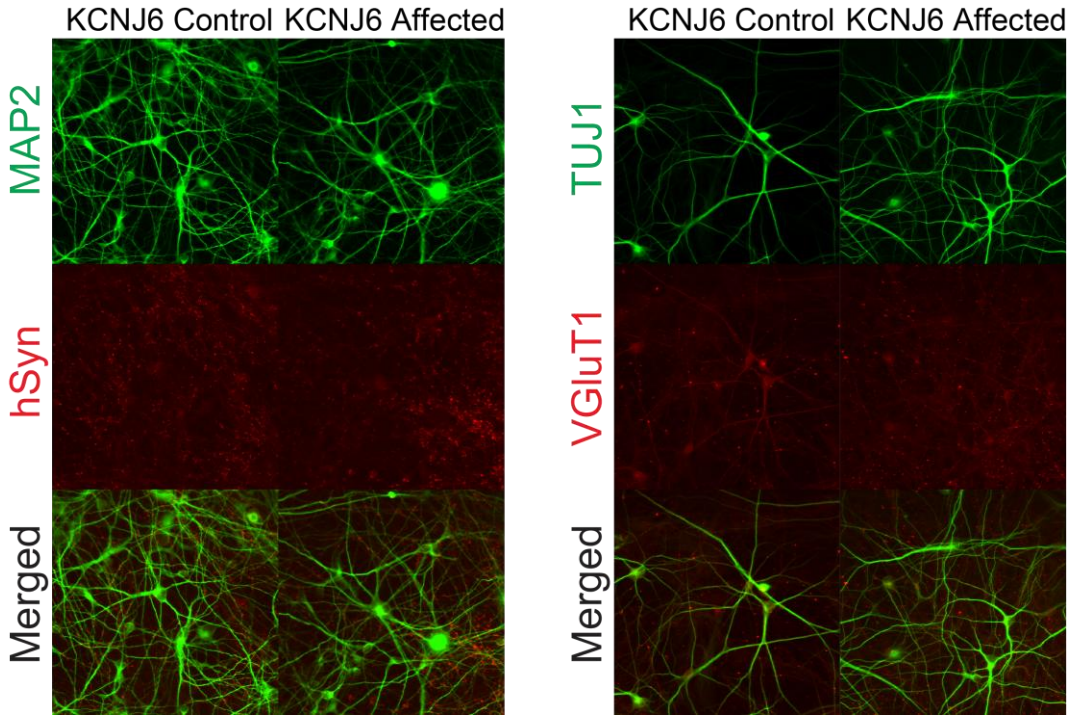

Figure 27 Neuronal differentiation through Ngn2 induction produces spontaneously active excitatory neurons using BrainPhys basal medium
A, B) ICC of iN cultures (day 40) shows expression of VGluT1, hSyn and MAP2, indicative of maturing excitatory neurons. Excitatory neurons were induced using the NGN2 protocol.

Calcium imaging

To determine whether changing the basal culture medium would significantly enhance activity of the iN neuronal cultures, we used calcium imaging (Ca^{2+}). Because Ca^{2+} is a key intracellular signaling ion, particularly for vesicular release at the synapse [144,145] we can observed Ca^{2+} transients, though not providing direct evidence of synaptic activity, this assay provides meaningful information about intracellular Ca^{2+} levels in living cells. We shipped day >40 neuronal cultures in both neurobasal and BrainPhys to the laboratory of Dr. Paul A. Slesinger at Mount Sinai. Neuronal cultures were incubated

with the calcium-chelating agent Fluo-4AM, as described in methods, and assessed for spontaneous synaptic activity. Results from preliminary experiments showed an increased amount of spontaneous Ca^{2+} influx in BrainPhys cultures (Figure 28). While this work is ongoing, our initial results using two types of medium find the BrainPhys medium to be more suitable for our continued experiments. As our main goal is to determine basal synaptic activity between KCNJ6 variants in the presence of alcohol, we are currently continuing Ca^{2+} imaging to observe the circuitry effects of ethanol exposure. We are conducting single cell electrophysiology experiments in coordination with the laboratory of Dr. Zhiping Pang.

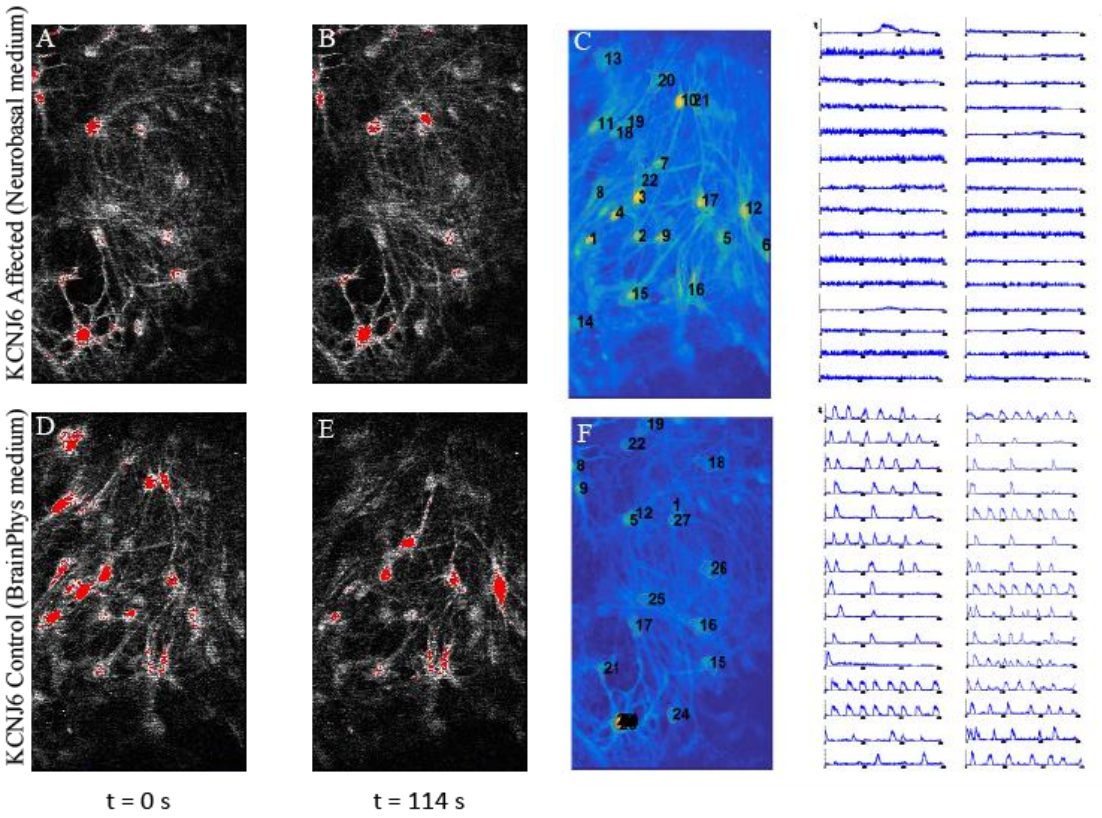

Figure 28 Representative images of Ca^{2+} activity show increase in Ca^{2+} spikes in cultures grown in Neurobasal (A-C) BrainPhys medium (D-F)
D) Time lapse of Ca^{2+} activity from panel shows stable Ca^{2+} signals in neurons cultured with Neurobasal medium (C), as compared to more dynamic Ca^{2+} signals in neurons cultured with BrainPhys (F).

Alternative splicing variants

The work by Isomoto et al. [195] identified KCNJ6 splicing variants within GIRK2 channel by screening mouse brain cDNA libraries. These particular splicing variants altered the length of the of GIRK2 channel at the C-terminal domain which plays a role in binding to Gβγ GCR[196]. While there are predicted alternatively spliced GIRK2 mRNAs in the human genome, there have not been published reports verifying their presence in human cells. To identify whether alternatively spliced isoforms of KCNJ6 gene are

present in NSC lines we needed to identify candidate variants. We began by isolating predicted KCNJ6 isoforms using assembled transcript maps from assembled by cufflinks[197] of ethanol treated NSC RNAseq data. Candidate novel isoforms were termed T433 and T434. We also used a GIRK2 cDNA variant, designated AK313997, that was identified by the New Energy and Industrial Technology Development Organization (NEDO), who created a cDNA library from a functional analysis of protein and research application project (Figure 29). Additionally, we used the NM_002240 Reference Sequence (RefSeq) from the National Center for Biotechnology Information (NCBI) database as the base sequence for KCNJ6.

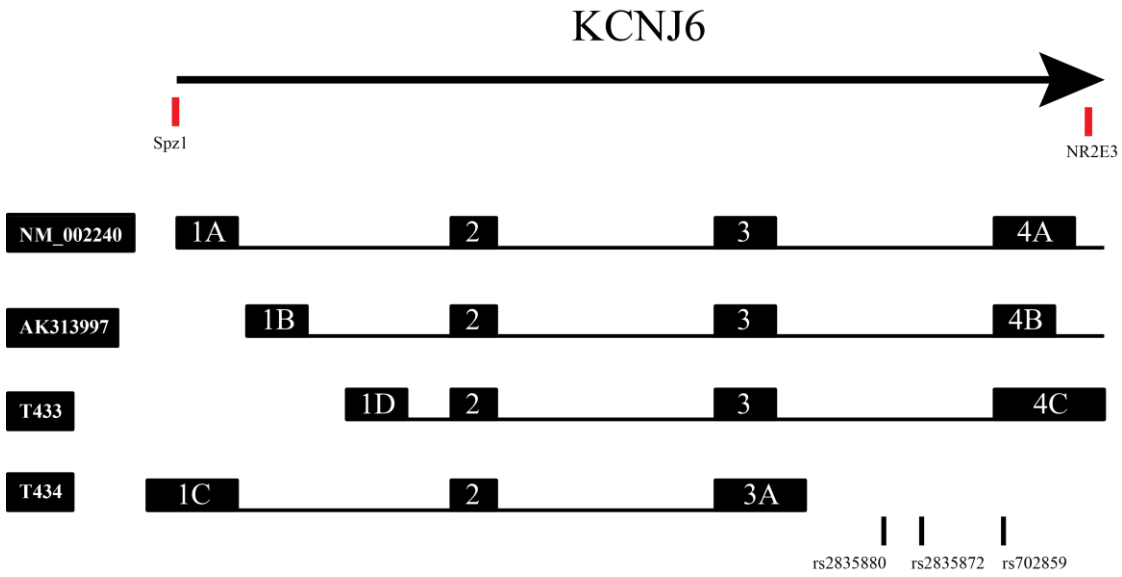

Figure 29 Transcript map of KCNJ6 gene
KCNJ6 transcript map listing possible splicing variants from ethanol treated NSC RNAseq analysis, and predicted cDNAs. Sequence is not to scale due to space limitations. NM_002240 is the NCBI Reference Sequence (RefSeq) NCBI database with "NM" as the accession molecule identification for mRNA. AK313997 is a predicted cDNA variant from (NEDO). T443 and T434 are predicted splicing variants isolated by RNAseq analysis from ethanol treated NSC lines. The locations of the KCNJ6 synonymous SNPs identified by Kang et al.[2] is noted at the end of this diagram. Highlighted in red are predicted SpzI and NR2E3 transcription factor-binding sites.

We designed primers to determine the presence of these splicing variants from PCR products of >40 day neuronal cultures (Figure 30). The PCR reaction products overlapped the RNAseq predicted splicing variants (T433 and T434), AK313997 and GAPDH as an input control. To differentiate between variants, PCR primers were designed to produce products within an exon sequence or between two different exons crossing exon-exon junctions. As a control, we designed a primer pair that would create a product that is common for all variants (Exon3). The presence of PCR products would be indicative of the presence of corresponding variant. Results in Figure 30 revealed bands from all lines, with the exception of line "71", which may have been due to low RNA yield especially since the GAPDH control also failed to amplify. Overall, there were strong PCR bands between exon 3 and 4 and exon 4A and 4C. This suggests that the neuronal cultures express the RefSeq mRNA, AK313997, and predicted isoforms T433 and T334. Interestingly, the PCR product spanning exon 1B to 3 revealed bands with varying intensity. However, the intensity of the splicing isoform PCR products was variable and was not specific to any particular subject or variant. At the same time, these results suggest that all three predicted isoforms are present in neuronal cultures regardless of KCNJ6 variant. Because this type of endpoint PCR is not quantifiable, we then reasoned that the splicing isoforms within each subject line needed to be quantified by qPCR.

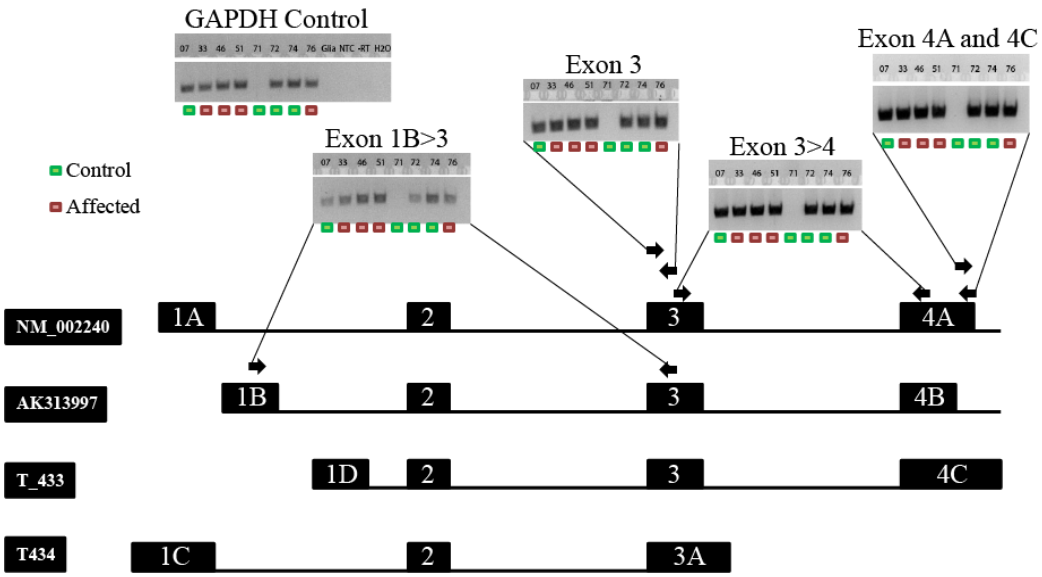

Figure 30 PCR analysis to determine presence of predicted and verified KCNJ6 splicing variants

KCNJ6 (NM_002240) and predicted variant splicing forms are illustrated above. Sizes are not to scale. PCR primers were designed to assess the presence of each splicing variant within all subject samples. The last number of the RUID was used for space constrains. The colored boxes denote which cell line contains the KCNJ6 variants (Green, control, Red, Affected). Primers were within common KCNJ6 exons (Exon 3 and Exon3>4) and across predicted exon-exon junctions (Exon 1B>3, Exon4A and 4C). GAPDH was used as a control for mRNA expression. KCNJ6 Affected line "71" did not amplify in any PCR reaction.

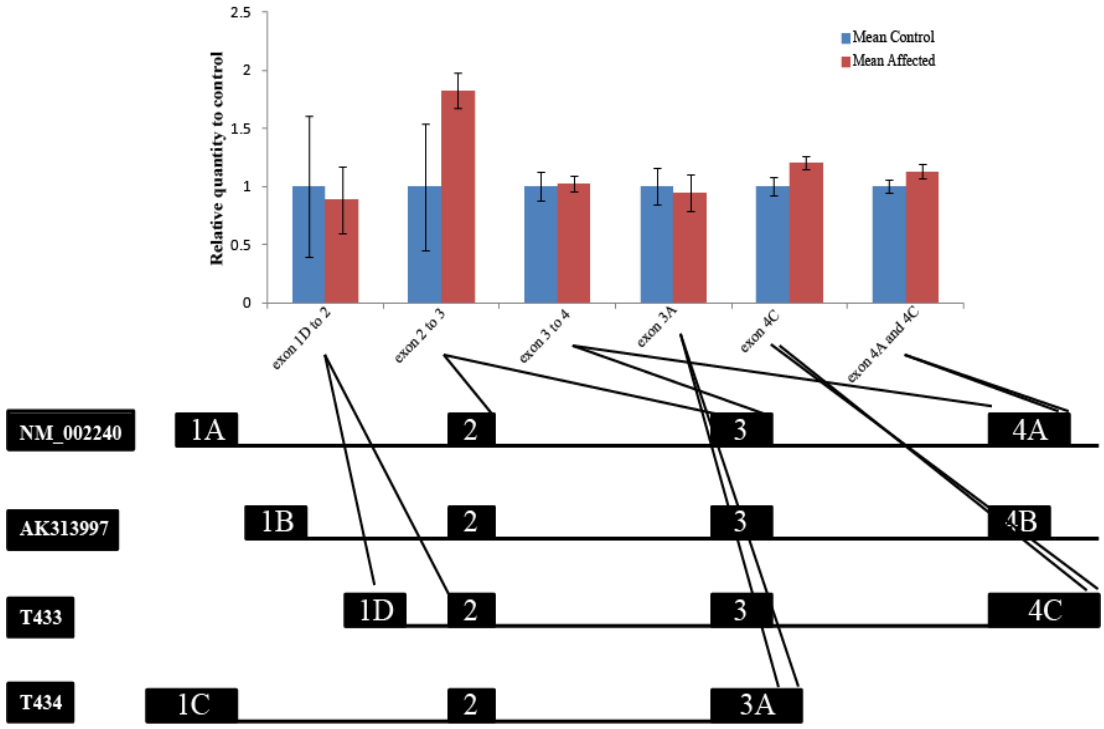

Figure 31 qPCR analysis to determine quantity of KCNJ6 splicing variants
KCNJ6 (RefSeq: NM_002240) and predicted variant splicing forms are illustrated above. Sizes are not to scale. qPCR primers were designed to cross exon-exon junction for quantification of each splicing variant.

To quantify the predicted splicing variants, we designed qPCR primers spanning over the exon-exon junctions (Figure 31). We used the mean cycle threshold (CT) values of the exon 2 to exon 3 splice site as a baseline as it was common between all variants. The results suggest a slight non significant variation in the expression of splicing isoforms between KCNJ6 affected and control populations, specifically in isoform T433 exon 4C that contains a predicted binding site for NR2E3 (Figure 30), a human nuclear receptor involved in retinal differentiation[198]. Additionally, exon 4 contains the 3' untranslated region (UTR), which could be a possible target for microRNAs and have been shown to mediate $GABA_A$ channel expression by deadenylation [199,200]. Following analysis from TargetScan software[201] we identified microRNAs such as let7-5p and miR-

96 whose expression is significantly increased in the serum of subjects with AUD[202]. Furthermore, in exon 1, there is an Spz1 transcription factor binding sites predicted by Portales-Casamar and colleagues[203] located within the "1C" variant upstream of exon 1 transcription start site. Spz1 is a part of the basic-helix-loop-helix (bHLH)-leucine zipper (Zip) family of proteins that are involved in spermatogenesis and is a candidate oncogene[204,205]. Overall, the qPCR results suggest that subjects carrying KCNJ6 variants contain splicing isoforms which targets of transcription factors that can alter GIRK2 expression or activity, which could lead to downstream variations in synaptic activity during ethanol exposure, thus changing the concentration of GIRK2 channels that are expressed on the cell membrane[192]. Currently, neuronal cultures are being assessed for alterations in synaptic dynamics and splicing isoforms of induced neuronal cultures following ethanol exposure.

Summary and future directions of Chapter 2

The goal of this work was to identify genetic and phenotypic profiles that highlight the contributions of risk associated SNPs. These risk variants were identified by reduced EEG theta waves and are located within intronic and one exon regions of the GIRK2 potassium inward rectifying channel gene KCNJ6. This channel is responsible for decreasing neuronal activity [166] and may play a role in mediating addiction behaviors.

We began by using an *in vitro* stem cell model, differentiating subject specific iPSCs into NSCs and excitatory neurons. We have demonstrated that subject iPSCs were appropriately reprogrammed and have normal karyotypes (Figure 19 and 20). Additionally, the NSCs derived from iPSC consistently expressed the neural stem cell

markers Nestin, Musashi, SOX2 and PAX6. This suggests that the NSC differentiation protocol produces robust NSCs whose differentiation was not affected by the presence of KCNJ6 SNPs.

Although past work has identified migratory and growth changes in NSC following ethanol exposure[171] [170], our experiments demonstrated no change in cell proliferation or viability during within a 72-hour time exposure to 75 mM ethanol, regardless of the presence of the KCNJ6 variant (Figure 22). These results suggest that acute ethanol exposure may not alter population dynamics (cell growth, viability) of NSCs[170,171]. Some have suggested that the effect of ethanol on NSC growth dynamics is due to the resilience of NSCs to acute ethanol exposure, but also note that ongoing proliferation of NSC may still be affected[184]. Rat models showed reduced NSC proliferation after chronic ethanol exposure, these findings conflict with our findings, and implies that this model may be more appropriate for chronic ethanol exposure.[185,206]. Furthermore, our experimental setup of whole cell live/dead counts may not have the resolution to determine subtle changes in the amount of dividing NSCs during chronic exposure. Perhaps a more sensitive experiment such as Bromodeoxyuridine (BrdU) labeling would be able to address this. This type of analysis would allow us to visualize the total number of cells proliferating overtime by labeling actively dividing NSCs. Overall, our NSC model, warrants further study into the long-term proliferative effects (>5 days) of ethanol exposure. In the meantime, we continued to explore the effects of acute ethanol exposure on the gene expression of NSCs.

To assess the gene expression effects of acute ethanol exposure, we conducted RNAseq analysis following a 24-hour ethanol treatment of NSCs. The results of our

analysis presented genes associated with development that were enriched in subjects within KCNJ6 risk-associated variants (Figure 23). These genes included FOXF2 and ROR involved in Wnt pathway activation (Table 5). These results suggest that genes involved in development may be expressed differentially following acute ethanol exposure in subjects who carry the KCNJ6 SNP. Additionally, qPCR experiments following ethanol treatment highlight slight differences in differentiation and cell cycle genes such as MECP2, PTTG1 and SOX7 (Figure 24). This may affect ability of the NSCs to differentiate and/or migrate as demonstrated by Zhou et al[170]. However, our qPCR analysis was done using a single control NSC line. We plan to expand this analysis to the remaining subject lines, which will give a more comprehensive phenotype of gene expression during ethanol exposure.

Since the KCNJ6 SNPs are located in non-coding regions and are synonymous, we do not expect the SNP to alter the overall activity of GIRK2 channels, but may modulate mRNA expression or stability through splice isoforms[207]. This could affect the population of GIRK2 channels on the synaptic surface and the potential synaptic response to alcohol[208]. To explore the possibility of multiple splicing variants, we have designed primers against predicted splicing isoforms from cDNA products listed in online genomic databases as well as from our own RNAseq data. Our preliminary PCR suggests that the neuronal lines variably express, by qPCR and PCR, predicted KCNJ6 splicing variants (Figure 30and 31), which may correlate with functional differences. However, these initial results were not consistent between genotypes.

To follow up with these findings, we designed qPCR primers to determine the relative quantity of predicted splicing variants in mature neurons. QPCR results indicated

differential expression of RNAseq predicted splicing variants specifically, splicing variant "T434". These results imply that there are multiple KCNJ6 splicing variants in neurons and their precursors. More specifically, these splicing isoforms have a slight non-significant differential expression between KCNJ6 variants; this may indicate a differential GIRK2 channel response to ethanol. To address this concept, we are planning experiments to identify the gene expression and synaptic activity following ethanol exposure.

We have also identified possible microRNAs (let7-5p and miR-96-5p) binding sites within the KCNJ6 3'UTR. The work of Ignacio et al.[202] have associated the increased expression of these microRNAs with those that have AUD behaviors. The presence of these predicted microRNAs binding sites at the 3'UTR of KCNJ6 along with their increased expression in those carrying AUDs, implies that these microRNAs affect the stability of KCNJ6 which may lead to downstream expression levels of the GIRK2 channel. This association warrants further verification of the expression of microRNAs let-7-5p and miR-96-5p in addition to their predicted KCNJ6 3'UTR binding site in NSCs and mature neurons.

Furthermore, our results raise the possibility that subjects carrying the KCNJ6 SNPs could have varying quantities of splicing variants. For example, in mouse there are at least five variants of Girk2 channel (Girk2-1, Girk2A-1, Girk2A-2, and Girk2B. Girk2C, Girk2D) [208]. However, these isoforms have no effect on the channel properties[80]. A closer look at the locations of alternatively predicted splice isoforms suggest that there are potential transcription factor binding sites, which may affect protein expression or trafficking. For example, the predicted isoform T434 contains a longer version of exon 1

and was expressed slightly more in the KCNJ6 affected subjects and may be a potential targeting site for bHLH-zip protein Spz1. Additionally, work from Ma et al.[209] showed splice isoforms mediating the expression of GIRK2 channels. Here, the authors used a fibroblast cell line or COS cells to identify ER export and post Golgi trafficking motifs from splicing variants of Girk2 (Kir3.1) in the N and C terminals in both hetero and homotetrameric channel formations. This implies that in order to identify the contributions of risk variants in synaptic behavior, the possible effects of these splicing variants may be identified in mature neurons following ethanol exposure.

We also plan to repeat RNAseq in mature neurons following ethanol exposure; this will allow us to determine if the differential gene expression effects seen from our ethanol treated KCNJ6 affected NSCs affect downstream gene expression. We should also be able to better measure differences in isoforms, and may discover novel isoforms not found in NSC. This would correlate with KCNJ6 variants that may mediate some of the effect of ethanol treatment, beginning at the neural progenitor stage. Splicing elements within the C-terminal region of GIRK2 channels can translate into altered pharmacological activity of GIRK2 channels[210] , which may lead to alterations in neuronal activity in the presence of ethanol. We also intend to follow up our gene expression studies in NSC with longer ethanol exposures using all KCNJ6 variant NSC lines in order to mimic chronic ethanol exposure and resolve whether these variants may affect synaptic activity.

Finally, we have seen from our PCR data that those carrying the minor allele KCNJ6 had a trend of increased mRNA expression of predicted alternative splicing isoforms. However, our qPCR experiments to quantify splice isoforms did not yield

significant changes between KCNJ6 variants, perhaps these differences may be enhanced in neuronal cultures following ethanol exposure. We can improve these experiments by adding more biological replicates from each subject cell line. This work argues for more effort to illuminate the role of GIRK2 channel risk SNPs within addiction phenotypes. Identifying the molecular mechanisms behind these behaviors would pave the way for a new source of possible drug targets or screening based off subjects who carry these risk variants.

DISCUSSION

With more emphasis on precision and personalized medicine, the identification of individual genetic risk factors of addiction diseases opens up new strategies for prevention and treatment. Studies have suggested that genetic variants may contribute to the risk of relapse and/or risk of addiction phenotypes[11,12]. To understand the genetic contributions to addiction behaviors, we have utilized a stem cell based approach. The use of iPSCs will allow us to identify novel therapeutic strategies to circumvent the mechanisms that cause addiction phenotypes while minimizing the use of animal models.

As our long-term goal is to identify novel therapeutic strategies for overcoming addiction mechanisms and circumventing the use of animal models, we utilized the technology of subject specific iPSCs that carry a genetic variant. This technology is powerful in that one can have an expandable cell population, which can be used to study the contributions of risk SNPs in multiple cells type or neuronal subtypes. In order to study the impact of risk variants using stem cells, much work has been focusing on developing various neuronal subtype specific differentiation protocols. One such example was from work by Lieberman et al.[113], who identified reduced expression of $GABA_A$ subunit genes from iPSC derived neurons carrying a synonymous SNP rs279858 within the GABRA2 subunit. Additionally, work by Duan et al.[192] determined that a combination of synonymous variants could contribute to the overall mRNA stability and receptor synthesis in the D2 dopamine receptor. These results imply that synonymous mutations could lead to quantifiable biological phenotypes. Moreover, stem cell-derived neuronal cultures are likely to be most similar to neurons present in early stages of human development, and not those in adults responding to repeated nicotine stimulation such as

in addiction. Thus, it is possible that a systems approach to studying risk variants in addiction phenotypes is possible within a stem cell based model.

Previous experiments using heterologous expression of CHRNA5 suggest that the N398 variant alters Ca^{2+} permeability and mediates nicotine consumption[60,61,69,150,211]. α5 knockout mouse models have resulted in increased nicotine consumption compared to controls, suggesting a role for the α5 subunit in reward and aversion behavior in mice [60,61]. While these carefully controlled mouse models have been quite successful in understanding the general mediating factors of motivational and reward behaviors, attempts to study more complex human diseases in mouse models may poorly correlate whose results can become difficult to interpret given the evolutionary distance between mice and humans, the inbred characteristics of the mouse model [73]. Additionally, knockout studies fail to take into account adaptations due to compensation for lost subunits and may carry alternate splicing variants[208 52]. To overcome the lack of living human neurons to study the role of human genetic variants, iPSC differentiation technology, now allows the use of human neurons derived from phenotypically variant subjects to model human neuropsychiatric disorders at a cell biological and mechanistic level

In addition to mouse studies work on genetic risk variants has been done using synthetic mRNA Xenopus oocytes CHRNA5 mRNA injections [71,212]. These studies have reported that along with other receptor components, the incorporation of N398 SNP variant reduces Ca^{2+} permeability and increases short-term desensitization to nicotine [52,72]. Overall, these studies highlight an important role of the auxiliary α5 subunit in mediating synaptic activity upon nicotine stimulation. However, oocyte injection

experiments do not take into consideration other intracellular factors that can affect nicotine addiction and may not correspond to native nAChRs.

Since our goal was to represent isolated genotypes in order to test the difference between the major and minor alleles within the CHRNA5 and KCNJ6 gene, we used control lines from subjects that were unrelated to N398 subjects. Indeed, our previous RNAseq analyses demonstrate broad variability among subject iPSCs and KCNJ6 splice isoform screen, even among members of the same family. This raises the possibility of diluting subtle phenotypes that can be overshadowed by differences between individual genetic backgrounds.

We believe that by testing a reasonable number of subject-specific iPSC lines we capture sufficient variability while searching for reproducible phenotypes. It has been suggested that cell lines from multiple patients and controls as well as multiple subclones from each patient should be analyzed to statistically provide a convincing cellular or functional phenotype. However, this approach can lead to a high workload can be time consuming and may not always practical for smaller research groups. This is a major obstacle to the identification of disease-associated phenotypes[159-161]. The most convincing solution to this problem is the creation of isogenic pairs of cells differing only in a single locus, by genetic engineering techniques[163,164]. Isogenic samples compared to unrelated controls can vastly reduce RNAseq variability demonstrated by Lin et al.[132]. To alleviate the issue, we are creating of isogenic cell lines from rs16969968 affected subjects. The creation of isogenic cells lines will eliminate the potential for genome variability between subjects allowing for analysis of subtle phenotypic differences between variants.

We must also take into consideration the co morbidity of nicotine and alcohol use disorders[13,213]. Behaviorally, the co-morbidity of these nicotine and alcohol use disorders was demonstrated by the work of Rose and colleagues, where peak human blood alcohol concentrations (BAC 0.03g/dl) potentiated the pleasurable effects of nicotine[214]. Evidence of the co-morbidity of alcohol and nicotine use disorders can also be found within the polymorphisms in the α4 subunit[215]. This polymorphism changes alanine to threonine at position 529 increasing the startle response amplitude, suggesting an enhanced activity of nAChRs following alcohol exposure. Our work provides a unique opportunity to determine the molecular phenotypes of these two comorbid disorders and how risk associated SNPs may contribute to them. Our stem cell based approach is a valuable way to assess contributions of these risk variants on the synaptic activity following the addition of nicotine, alcohol or both. For example, we can ask if the increased synaptic response seen in the CHRNA5 variant is exacerbated in the presence of levels of alcohol and nicotine present in heavy smokers and drinkers. Future experiments, could involve mimicking nicotine or alcohol pharmacological environments such as heavy smoking and fetal alcohol exposure. Synaptic activity would be assessed by either whole cell patch clamping or circuitry-based analysis (calcium imaging) following ethanol exposure. We could assess the downstream effects of gene expression or protein population after long term exposure to nicotine or ethanol.

Overall this work supports previous studies addressing the roles of addiction risk variants within the synaptic response to drugs of abuse thus affecting human neuronal functions[61,115]. We have observed this through alterations in synaptic response to nicotine, and gene expression changes with the acute exposure to alcohol and nicotine.

This work serves as a proof of principle and a systems approach to bridge the gaps from population genetics to molecular biology in understanding the cell-to-cell mechanics of those carrying a risk associated alleles. The techniques of this work can also be used as drug screens within subjects carrying genetic variants. Similarly, groups such as Germany's SysMedAlcoholism consortium[216] have begun to address the challenges in finding new ways to combat alcohol addiction by using a combined omics- informational approach (genetic transcriptome, neurodynamics and neuroimaging) to create predictive models which are subsequently validated by clinical sampling and animal models including iPSC. Continuing these studies is likely to lead to a better understanding of the impact of gene variants on human behavior and may identify intervention and treatment strategies that are more effective to combat addiction.

METHODS

iPSC generation from CPLs

Preparation of iPSC from human primary lymphocytes using Sendai viral vectors (CytoTune™, Life Technologies) has been described Moore et al [217]. Human induced pluripotent stem cells were maintained at 37°C, 5% CO_2, 4% O_2 on Matrigel™ (BD Biosciences)-coated wells in mTeSR medium (Stem Cell Technologies). Once every week or when wells were 70-80% confluent, cultures were cleaned of spontaneous differentiation material by hand-dissection. Colonies were dissociated into clumps using 1 U/mL Dispase (BD Biosciences, Franklin Lakes, and NJ) and plated on Matrigel (BD Biosciences, Franklin Lakes, NJ) coated plates in 1:12 dilution. Plating ratio was dependent on the well density prior to passaging. The medium was changed every day. All biomaterials were de-identified repository specimens and therefore are exempt from human subjects' regulations.

Neural induction via Dual SMAD inhibition

Midbrain dopaminergic (midbrain -like DA-like) neurons were generated using a dual SMAD inhibition protocol[107]. IPSCs were dissociated using Accutase (Stem Cell Technologies) and plated at a density of 6.0×10^6 cells per well in a 60 cm Matrigel (BD) coated dish 20 days after differentiation, neuronal cultures were dissociated using Accutase and passaged at a 1:1 plating ratio. 30 days after differentiation, midbrain-like DA-like neurons (1.5×10^5) were co-cultured with mouse glia (7.5×10^4 cells). Electrophysiological and Ca^{2+} imaging analyses were performed following at least 40 days of differentiation.

Glial cell isolation.

Forebrains were dissected from postnatal day 3-5 wild-type mice and were manually dissociated into ~0.5 mm2 pieces in a total of 2 ml of HBSS. A total of 500 μl of 2.5% trypsin were added and dissociated tissue was incubated at 37°C for 20 min. Solution was mixed every 5 min. Using a pipette, the remaining tissue was further dissociated and passed through a 70 μM nylon mesh filter (BD Biosciences) into DMEM with 10% Fetal Bovine Serum and L-glutamine. Glia cells were passaged three times before culturing with human neuronal cells. These procedures were approved by the Rutgers University Institutional Animal Care and Use Committee (#I11-073-10).

Neural induction via Induced Neuronal differentiation

To generate excitatory neurons, we will employ the exogenous expression of specific excitatory linage transcription factors that are introduced into iPSCs via a modified lentiviral-induced neuronal differentiation protocol described by Zhang et al. [147]. Transcription factors (NGN2) were generously provided by the Pang lab. On day -1 iPSCs were treated with Accutase (Stem Cell Technologies) and plated as 6 well plates (5×10^5 cells/well) with Y-27632 dihydrochloride (Tocris; also known as "Y-compound") on matrigel coated dishes. On day - l lentiviral infection cocktail consisting of Doxycycline TetO neuronal transcription factor to rtTA mix with a 1:1.5, ratio was added to cells to mTeSR medium with Y-compound. On day 1, the culture medium was replaced with neurobasal medium supplemented with B27/L-Glutamine (Invitrogen) with Doxycycline (10 ng/mL, MP Biomedicals) and Y-compound (10 ng/mL). On day 2 and

3, a 48 hour Puromycin (10 ng/mL, Fisher Scientific) selection of neurons begins with medium changes of Neurobasal medium with Doxycycline & Puromycin every 24 hours. On day 4, the culture medium was replaced with Neurobasal with Doxycycline medium. On day 5, infected cells (1.5×10^5) were dissociated with Accutase and co-cultured with mouse glia (7.5×10^4) to further promote synaptogenesis, with 50% of neurobasal containing 10 ng/ml of Doxycycline, BDNF, GDNF and NT3 in each well exchanged every 3 days. For the Bardy et al. protocol, iPSCs were infected as previously stated until day 4 where ½ of the medium was exchanged with iNC medium from the Bardy protocol. Using BrainPhys (Stem Cell Technologies) as a basal medium. The medium was exchanged ½ iNC every three days for three weeks. On day 21, infected cells (1.5×10^5) were dissociated with Accutase and co-cultured with mouse glia (7.5×10^4) to further promote synaptogenesis, with BrainPhys based iNM from the Bardy protocol supplemented with N2 and B27.

Neural Stem cell induction

To preferentially induce human NSC formation from hiPSCs, 25% confluent cells were passaged by disaggregation into clumps of cells (approximately 50-100 cells per clump) with 1 U/mL Dispase and plated at a ratio of 1:1 on matrigel coated dishes in mTeSR. HiPSCs were induced using Life Technologies PSC neural induction protocol (Gibco, 2013).

Real-time RT-PCR (qPCR)

Total cellular RNA preparations will use TRIzol reagent (Invitrogen). For qPCR, 500 ng of RNA was reverse transcribed using High Capacity cDNA reverse transcription

kit with RNAse inhibitor (Life Technologies). Human-specific TaqMan™ probes were purchased from Life Technologies and PCR conditions followed the manufacturer's recommendations. No amplification was detected in RNA prepared from only mouse glia (not shown). GAPDH was used as endogenous control. A sample of 17-week post-conception human fetal VTA RNA (a generous gift from Drs. Yuka Imamura Kawasawa and Nenad Sestan, Yale University) was used to normalize expression levels to obtain relative quantity (RQ) values. Data were analyzed by the ΔΔCt method for determining relative quantities (Ct=cycle threshold). qRT-PCR assays were performed on either the AB7500 Fast System or Viia7 system. Statistical analysis was performed using R software; ANOVA was used to compare control and affected group means.

PCR

Total cellular DNA preparations used Zymo Genomic DNA prep kit (Zymo). PCR amplification used the Q5 High Fidelity master mix (New England Biolabs), GAPDH was used as endogenous control. PCR products were run on a 0.8% agarose gel in 1X TBE buffer run with a 1K DNA ladder (Promega).

RNA sequencing (RNAseq)

RNA samples were used to prepare cDNA libraries with the TruSeq Kit (Illumina) and run on an Illumina HiSeq 2500 instrument by RUCDR Infinite Biologics® (Piscataway, NJ). The resulting data were aligned with human genome using a genome transcription map of hg19 from UCSC (from the Illumina iGenomes repository) using TopHat. Comparisons between groups used Cuffdiff and results were analyzed in R/BioConductor using the cummeRbund package [197,218]. Raw sequencing data can be

found in the NIH SRA archives under accession number SRP040275 and processed gene expression levels are in NIH GEO under accession number GSE56398. H1 hESC-derived NSC data for Days 0 and 5 are part of GEO series GSE56785. Datasets for midbrain-like DA neuron cultures were downloaded from SRA using the following accession numbers: SRR1030497, SRR1030496, SRR1030493, and SRR1030492 [134].

Dopamine release via High Performance Liquid Chromatography (HPLC)

Nicotine induced dopamine release was measured via HPLC, performed by Jessica Verpeut in the lab of Dr. Nicholas Bello at Rutgers University. After aspiration of medium, the cells were blanked using a HEPES external solution (140 mM NaCl, 5 mM KCl, 2 mM CaCl2, 2 mM MgCl2, 10 mM HEPES, 10 mM Glucose, Osm 36, pH 7.4) for 45 min. Medium was collected and flash frozen and replaced with either 20 mM of KCl, or 1 mM of nicotine for 30 min. Culture medium samples were analyzed by reverse phase high performance liquid chromatography (HPLC; Dionex Ultimate 3000) with electrochemical detection (Coulochem III). An acetonitrile-based phosphate buffer mobile phase (Thermofisher, Sunnyvale, CA) was used for all experiments. The internal standard, 3, 4-Dihydroxybenzylamine (DHBA), was added to all samples prior to extraction. To each sample, 385 μl of 0.1 N perchloric acid solutions was added, and then centrifuged at 12,000 rpm for 5 min. The supernatant was filtered using a 0.2 μm nylon disposable syringe filter prior to injection. This extraction procedure resulted in measurements of norepinephrine (NE), epinephrine (Epi), and dopamine (DA) by HPLC. Peak quantification was performed with Chromeleon 7.1 software (Thermofisher, Sunnyvale, CA).

Electrophysiology

Current clamp whole-cell recordings were used to record action potentials. This was performed by Guohui Li in the lab of Dr. Zhiping Pang at Robert Wood Medical School. The pipette solution for current-clamp experiments consisted of (in mM): 123 K-gluconate, 10 KCl, 1 MgCl2, 10 HEPES, 1 EGTA, 0.1 CaCl2, 1 K_2ATP, 0.2 Na_4GTP and 4 glucose. The pH of the solution was adjusted to 7.2 with KOH. A membrane potential of −65 to −70 mV was maintained during current-clamp recordings, and currents were injected into the cell in a step-wise manner to stimulate action potentials. For whole-cell voltage-dependent current recordings, the same internal solution as described above was used. For evaluation of synaptic function, the internal solution consisted of (in mM): 135 CsCl, 10 HEPES, 1 EGTA, 4 Mg-ATP, 0.4 Na_4GTP, and 10 QX-314, pH 7.4. The bath solution consisted of (in mM): 140 NaCl, 5 KCl, 2 CaCl2, 2 MgCl2, 10 HEPES, and glucose, pH 7.4. Stimulus artifacts in the recording, when stimuli were provided during evoked synaptic responses, were removed in the graphical representation of the data. Electrophysiological data are presented as mean ± SEM. All statistical comparisons were made using Student's t-test or with general linear mixed model packages in R/BioConductor.

Immunofluorescence and Confocal imaging

NSC, midbrain-like DA and excitatory neurons were fixed for 15 min in 4% paraformaldehyde (Electron Microscopy Sciences) in PBS at room temperature. Cells were incubated in blocking buffer (1X PBS, 1% goat serum, 4% BSA) for 1 hr. Cells were permeabilized in 0.2% Triton X-100 in PBS for 10 minutes and incubated overnight

with primary antibodies. The following primary antibodies were used: rabbit anti-Musashi (Abcam, 1:200), mouse anti-NESTIN (Millipore, 1:200), mouse anti OCT4 (Millipore, 1:2000), mouse anti- TRA-1-60 (Millipore, 1:1000), mouse anti-TH (Millipore, 1:1000), mouse anti-VGluT1 (Synaptic Systems, 1:500), mouse anti-TuJ1 (Covance, 1:1000), rabbit anti-SOX2 (1:100) rabbit anti-Synapsin (Abcam, 1:500), mouse anti-MAP2 (Millipore, 1:500), rabbit anti-DAT (Millipore, 1:250), rabbit anti-GAD6 (1:1000). After additional PBS washes, cells were incubated with fluorescently labeled secondary antibodies from Molecular probes (Alexa 488, Alexa 594, or Alexa 647) used at 1:500 dilution. The Click-iT EdU Alexa Fluor® 488 Imaging Kit was used to assess the mitotic state of TH^+ neurons. Confocal and spinning disk epifluorescence confocal imaging analysis was performed using a Zeiss LSM700 or Olympus Axiovert 100M confocal microscope (Carl Zeiss, Olympus). NSC imaging was performed using InCell6000 confocal microscope (GE) Cells were counted using Zeiss confocal microscope software (Zeiss). Ten images from one coverslip from two independent experiments were used for counting.

Ca^{2+} Imaging

Cultures were incubated with 1 μM Fluo4 AM (F-14201; Invitrogen) in the SMAD inhibition differentiation medium at 37°C for 20 min. Excess Fluo4 AM was removed from the neuronal cultures by washing twice in prewarmed HEPES-based extracellular solution (in mM): 140 NaCl, 5 KCl, 2 CaCl2, 2 MgCl2, 10 Glucose, 10 HEPES, pH 7.4, mOsm 290-300). Cultures were incubated in Neurobasal medium (Life Technologies) supplemented with 1 mM glutamate and 1X B27 supplement (Life

Technologies) at 37°C for 20 min to allow complete de-esterification of the Fluo4 AM loading dye. All calcium-imaging experiments were performed under the guidance of Dr. Kelvin Kwan of Rutgers University. Coverslips containing neurons from cultures were transferred to the bath chamber and placed in extracellular solution. Solutions flowed into the chamber on the Quick Exchange Platform (Warner Instruments, Holliston, MA) using a Valvelink 8 pressurized flow system configured with a programmable ValveBank Controller (Automate Scientific, Inc., San Francisco, CA). Neurons were perfused with extracellular solution, extracellular solution containing 3 μM nicotine or a 40 mM KCl solution. Extracellular solution was perfused into the bath chamber for 120 s, followed by extracellular solution containing 3μM nicotine for 120s and ending with extracellular medium for 120 s. For each field of view, this perfusion protocol was done a total of three times. To elicit a neuronal response, after the third perfusion step, cells were perfused with a 40 mM KCl solution (in mM: 100 NaCl, 40 KCl, 2 CaCl2, 2 MgCl2, 10 Glucose, 10 HEPES, pH 7.4, mOsm 290-300) for 120 s to depolarize cells and identify neurons.

Analysis of Ca^{2+} Signals

Changes in fluorescence intensity from different fields of view of a single coverslip of midbrain-like DA neurons were captured. The cell bodies, visualized in phase contrast, were defined as the region of interest in Image J (NIH). Changes in Fluo4 fluorescence intensity were determined via integrated density during the experimental period, extracted, and exporting into an Excel spreadsheet. Ca^{2+} fluctuations were calculated as ($\Delta f/f0$), where f is defined as the fluorescence intensity measured by sum of

pixels within the soma region of interest or “integrated density” when the cell is at rest (0 s) and Δf is the change in fluorescence intensity.

Nicotine exposure

Cultures were whole cell patch clamped as described previously. Nicotine was perfused in extracellular medium in increasing amounts 0.1 μM to 6 μM in 3 minute intervals. EPSC frequencies were counted using the pClampfit software (Molecular dynamics). Frequencies were normalized to the first 30 seconds of wash buffer and dosage frequencies were averaged over 30 second intervals within first minute. Amplitudes within each 10 second interval were also averaged in the same time frame.

Ethanol exposure

NSC cultures were fed with equilibrated neural induction medium (Gibco) in non-vented flasks with and without 75mM ethanol. Culture samples were dissociated every 12 hours with Accutase (Stem Cell Technologies) and assessed for cell viability (live/dead and total cell number) using the ViCell analyzer (Beckman Coulter). Cell viability was calculated using the slope over the course of the experiment.

REFERENCES

1 Zoli, M., Pistillo, F. & Gotti, C. Diversity of native nicotinic receptor subtypes in mammalian brain. *Neuropharmacology* **96**, 302-311, doi:10.1016/j.neuropharm.2014.11.003 (2015).

2 Kang, S. J. *et al.* Family-based genome-wide association study of frontal theta oscillations identifies potassium channel gene KCNJ6. *Genes Brain Behav* **11**, 712-719, doi:10.1111/j.1601-183X.2012.00803.x (2012).

3 Marchetto, M. C., Winner, B. & Gage, F. H. Pluripotent stem cells in neurodegenerative and neurodevelopmental diseases. *Hum Mol Genet* **19**, R71-76, doi:10.1093/hmg/ddq159 (2010).

4 Juarez, B. & Han, M. H. Diversity of Dopaminergic Neural Circuits in Response to Drug Exposure. *Neuropsychopharmacology*, doi:10.1038/npp.2016.32 (2016).

5 Smetters, D., Majewska, A. & Yuste, R. Detecting action potentials in neuronal populations with calcium imaging. *Methods* **18**, 215-221, doi:10.1006/meth.1999.0774 (1999).

6 Zhang, M., Scholer, H. R. & Greber, B. Rapid and efficient generation of neurons from human pluripotent stem cells in a multititre plate format. *J Vis Exp*, e4335, doi:10.3791/4335 (2013).

7 American Psychiatric Association. & American Psychiatric Association. DSM-5 Task Force. *Diagnostic and statistical manual of mental disorders : DSM-5*. 5th edn, (American Psychiatric Association, 2013).

8 Bramer, G. R. International statistical classification of diseases and related health problems. Tenth revision. *World Health Stat Q* **41**, 32-36 (1988).

9 United States. Public Health Service. Office of the Surgeon General. *How tobacco smoke causes disease : the biology and behavioral basis for smoking-attributable disease : a report of the Surgeon General*. (U.S. Dept. of Health and Human Services, Public Health Service
For sale by the Supt. of Docs., U.S. G.P.O., 2010).

10 United States. Public Health Service. Office of the Surgeon General. & National Center for Chronic Disease Prevention and Health Promotion (U.S.). Office on Smoking and Health. *Preventing tobacco use among youth and young adults : a report of the Surgeon General*. (U.S. Dept. of Health and Human Services, Public Health Service, Centers for Disease Control and Prevention, National Center for Chronic Disease Prevention and Health Promotion
For sale by the Supt. of Docs., U.S. G.P.O., 2012).

11 Chen, L. S. *et al.* Interplay of genetic risk factors (CHRNA5-CHRNA3-CHRNB4) and cessation treatments in smoking cessation success. *Am J Psychiatry* **169**, 735-742, doi:10.1176/appi.ajp.2012.11101545 (2012).

12 Lerman, C. *et al.* Role of functional genetic variation in the dopamine D2 receptor (DRD2) in response to bupropion and nicotine replacement therapy for tobacco dependence: results of two randomized clinical trials. *Neuropsychopharmacology* **31**, 231-242, doi:10.1038/sj.npp.1300861 (2006).

13 Hasin, D. S., Stinson, F. S., Ogburn, E. & Grant, B. F. Prevalence, correlates, disability, and comorbidity of DSM-IV alcohol abuse and dependence in the United States: results from the National Epidemiologic Survey on Alcohol and Related Conditions. *Arch Gen Psychiatry* **64**, 830-842, doi:10.1001/archpsyc.64.7.830 (2007).

14 Institute for Health Metrics and Evaluation. <http://www.healthmetricsandevaluation.org/gbd/visualizations/gbd-cause-patterns> (2013).

15 Stahre, M., Roeber, J., Kanny, D., Brewer, R. D. & Zhang, X. Contribution of excessive alcohol consumption to deaths and years of potential life lost in the United States. *Prev Chronic Dis* **11**, E109, doi:10.5888/pcd11.130293 (2014).

16 Hannigan, J. H. & Berman, R. F. Amelioration of fetal alcohol-related neurodevelopmental disorders in rats: exploring pharmacological and environmental treatments. *Neurotoxicol Teratol* **22**, 103-111 (2000).

17 Bouchery, E. E., Harwood, H. J., Sacks, J. J., Simon, C. J. & Brewer, R. D. Economic costs of excessive alcohol consumption in the U.S., 2006. *Am J Prev Med* **41**, 516-524, doi:10.1016/j.amepre.2011.06.045 (2011).

18 National Institute on Drug Abuse. *Principles of drug addiction treatment : a research-based guide*. Third edtion. edn, (National Institute on Drug Abuse, National Institutes of Health, U.S. Department of Health and Human Services, 2012).

19 Coe, J. W. *et al.* Varenicline: an alpha4beta2 nicotinic receptor partial agonist for smoking cessation. *J Med Chem* **48**, 3474-3477, doi:10.1021/jm050069n (2005).

20 Erwin, B. L. & Slaton, R. M. Varenicline in the treatment of alcohol use disorders. *Ann Pharmacother* **48**, 1445-1455, doi:10.1177/1060028014545806 (2014).

21 Alberg, A. J., Shopland, D. R. & Cummings, K. M. The 2014 Surgeon General's report: commemorating the 50th Anniversary of the 1964 Report of the Advisory Committee to the US Surgeon General and updating the evidence on the health consequences of cigarette smoking. *Am J Epidemiol* **179**, 403-412, doi:10.1093/aje/kwt335 (2014).

22 Chen, L. S. *et al.* CHRNA5 risk variant predicts delayed smoking cessation and earlier lung cancer diagnosis--a meta-analysis. *J Natl Cancer Inst* **107**, doi:10.1093/jnci/djv100 (2015).

23 Pidoplichko, V. I., DeBiasi, M., Williams, J. T. & Dani, J. A. Nicotine activates and desensitizes midbrain dopamine neurons. *Nature* **390**, 401-404, doi:10.1038/37120 (1997).

24 Mansvelder, H. D., Keath, J. R. & McGehee, D. S. Synaptic mechanisms underlie nicotine-induced excitability of brain reward areas. *Neuron* **33**, 905-919 (2002).

25 Fields, H. L., Hjelmstad, G. O., Margolis, E. B. & Nicola, S. M. Ventral tegmental area neurons in learned appetitive behavior and positive reinforcement. *Annu Rev Neurosci* **30**, 289-316, doi:10.1146/annurev.neuro.30.051606.094341 (2007).

26 Swanson, L. W. The projections of the ventral tegmental area and adjacent regions: a combined fluorescent retrograde tracer and immunofluorescence study in the rat. *Brain Res Bull* **9**, 321-353 (1982).

27 Margolis, E. B., Toy, B., Himmels, P., Morales, M. & Fields, H. L. Identification of rat ventral tegmental area GABAergic neurons. *PLoS One* **7**, e42365, doi:10.1371/journal.pone.0042365 (2012).

28 Hnasko, T. S., Hjelmstad, G. O., Fields, H. L. & Edwards, R. H. Ventral tegmental area glutamate neurons: electrophysiological properties and projections. *J Neurosci* **32**, 15076-15085, doi:10.1523/JNEUROSCI.3128-12.2012 (2012).

29 Nair-Roberts, R. G. *et al.* Stereological estimates of dopaminergic, GABAergic and glutamatergic neurons in the ventral tegmental area, substantia nigra and retrorubral field in the rat. *Neuroscience* **152**, 1024-1031, doi:10.1016/j.neuroscience.2008.01.046 (2008).

30 Mansvelder, H. D. & McGehee, D. S. Cellular and synaptic mechanisms of nicotine addiction. *J Neurobiol* **53**, 606-617, doi:10.1002/neu.10148 (2002).
31 Hikosaka, O., Sesack, S. R., Lecourtier, L. & Shepard, P. D. Habenula: crossroad between the basal ganglia and the limbic system. *The Journal of neuroscience : the official journal of the Society for Neuroscience* **28**, 11825-11829, doi:10.1523/JNEUROSCI.3463-08.2008 (2008).
32 Barrot, M. *et al.* Braking dopamine systems: a new GABA master structure for mesolimbic and nigrostriatal functions. *The Journal of neuroscience : the official journal of the Society for Neuroscience* **32**, 14094-14101, doi:10.1523/JNEUROSCI.3370-12.2012 (2012).
33 Velasquez, K. M., Molfese, D. L. & Salas, R. The role of the habenula in drug addiction. *Frontiers in human neuroscience* **8**, 174, doi:10.3389/fnhum.2014.00174 (2014).
34 Mansvelder, H. D. & McGehee, D. S. Long-term potentiation of excitatory inputs to brain reward areas by nicotine. *Neuron* **27**, 349-357 (2000).
35 Jhou, T. C., Fields, H. L., Baxter, M. G., Saper, C. B. & Holland, P. C. The rostromedial tegmental nucleus (RMTg), a GABAergic afferent to midbrain dopamine neurons, encodes aversive stimuli and inhibits motor responses. *Neuron* **61**, 786-800, doi:10.1016/j.neuron.2009.02.001 (2009).
36 Watabe-Uchida, M., Zhu, L., Ogawa, S. K., Vamanrao, A. & Uchida, N. Whole-brain mapping of direct inputs to midbrain dopamine neurons. *Neuron* **74**, 858-873, doi:10.1016/j.neuron.2012.03.017 (2012).
37 Schultz, W. Predictive reward signal of dopamine neurons. *J Neurophysiol* **80**, 1-27 (1998).
38 Grace, A. A. & Bunney, B. S. The control of firing pattern in nigral dopamine neurons: burst firing. *J Neurosci* **4**, 2877-2890 (1984).
39 Grace, A. A. & Bunney, B. S. The control of firing pattern in nigral dopamine neurons: single spike firing. *J Neurosci* **4**, 2866-2876 (1984).
40 Phillips, P. E., Stuber, G. D., Heien, M. L., Wightman, R. M. & Carelli, R. M. Subsecond dopamine release promotes cocaine seeking. *Nature* **422**, 614-618, doi:10.1038/nature01476 (2003).
41 Butini, S. *et al.* Polypharmacology of dopamine receptor ligands. *Prog Neurobiol* **142**, 68-103, doi:10.1016/j.pneurobio.2016.03.011 (2016).
42 Beaulieu, J. M. & Gainetdinov, R. R. The physiology, signaling, and pharmacology of dopamine receptors. *Pharmacol Rev* **63**, 182-217, doi:10.1124/pr.110.002642 (2011).
43 Missale, C., Nash, S. R., Robinson, S. W., Jaber, M. & Caron, M. G. Dopamine receptors: from structure to function. *Physiol Rev* **78**, 189-225 (1998).
44 Mansvelder, H. D., De Rover, M., McGehee, D. S. & Brussaard, A. B. Cholinergic modulation of dopaminergic reward areas: upstream and downstream targets of nicotine addiction. *Eur J Pharmacol* **480**, 117-123 (2003).
45 Di Chiara, G. & Imperato, A. Drugs abused by humans preferentially increase synaptic dopamine concentrations in the mesolimbic system of freely moving rats. *Proc Natl Acad Sci U S A* **85**, 5274-5278 (1988).
46 Laviolette, S. R. & van der Kooy, D. The neurobiology of nicotine addiction: bridging the gap from molecules to behaviour. *Nat Rev Neurosci* **5**, 55-65, doi:10.1038/nrn1298 (2004).
47 Liu, C. L., Gao, M., Jin, G. Z. & Zhen, X. GABA neurons in the ventral tegmental area responding to peripheral sensory input. *PloS one* **7**, e51507, doi:10.1371/journal.pone.0051507 (2012).

48 Steffensen, S. C., Svingos, A. L., Pickel, V. M. & Henriksen, S. J. Electrophysiological characterization of GABAergic neurons in the ventral tegmental area. *The Journal of neuroscience : the official journal of the Society for Neuroscience* **18**, 8003-8015 (1998).

49 Tammimaki, A. *et al.* Impact of human D398N single nucleotide polymorphism on intracellular calcium response mediated by alpha3beta4alpha5 nicotinic acetylcholine receptors. *Neuropharmacology* **63**, 1002-1011, doi:10.1016/j.neuropharm.2012.07.022 (2012).

50 Luetje, C. W. & Patrick, J. Both alpha- and beta-subunits contribute to the agonist sensitivity of neuronal nicotinic acetylcholine receptors. *The Journal of neuroscience : the official journal of the Society for Neuroscience* **11**, 837-845 (1991).

51 Corringer, P. J., Le Novere, N. & Changeux, J. P. Nicotinic receptors at the amino acid level. *Annual review of pharmacology and toxicology* **40**, 431-458, doi:10.1146/annurev.pharmtox.40.1.431 (2000).

52 Gotti, C. & Clementi, F. Neuronal nicotinic receptors: from structure to pathology. *Progress in neurobiology* **74**, 363-396, doi:10.1016/j.pneurobio.2004.09.006 (2004).

53 McGehee, D. S. Molecular diversity of neuronal nicotinic acetylcholine receptors. *Ann N Y Acad Sci* **868**, 565-577 (1999).

54 Albuquerque, E. X., Pereira, E. F., Alkondon, M. & Rogers, S. W. Mammalian nicotinic acetylcholine receptors: from structure to function. *Physiol Rev* **89**, 73-120, doi:10.1152/physrev.00015.2008 (2009).

55 Papke, R. L. Merging old and new perspectives on nicotinic acetylcholine receptors. *Biochemical pharmacology* **89**, 1-11, doi:10.1016/j.bcp.2014.01.029 (2014).

56 Gotti, C. *et al.* Heterogeneity and complexity of native brain nicotinic receptors. *Biochemical pharmacology* **74**, 1102-1111, doi:10.1016/j.bcp.2007.05.023 (2007).

57 Picciotto, M. R. *et al.* Neuronal nicotinic acetylcholine receptor subunit knockout mice: physiological and behavioral phenotypes and possible clinical implications. *Pharmacol Ther* **92**, 89-108 (2001).

58 Jin, X., Bermudez, I. & Steinbach, J. H. The nicotinic alpha5 subunit can replace either an acetylcholine-binding or nonbinding subunit in the alpha4beta2* neuronal nicotinic receptor. *Molecular pharmacology* **85**, 11-17, doi:10.1124/mol.113.089979 (2014).

59 Frahm, S. *et al.* Aversion to nicotine is regulated by the balanced activity of beta4 and alpha5 nicotinic receptor subunits in the medial habenula. *Neuron* **70**, 522-535, doi:10.1016/j.neuron.2011.04.013 (2011).

60 Changeux, J. P. Nicotine addiction and nicotinic receptors: lessons from genetically modified mice. *Nature reviews. Neuroscience* **11**, 389-401, doi:10.1038/nrn2849 (2010).

61 Fowler, C. D., Tuesta, L. & Kenny, P. J. Role of alpha5* nicotinic acetylcholine receptors in the effects of acute and chronic nicotine treatment on brain reward function in mice. *Psychopharmacology (Berl)*, doi:10.1007/s00213-013-3235-1 (2013).

62 Welter, D. *et al.* The NHGRI GWAS Catalog, a curated resource of SNP-trait associations. *Nucleic Acids Res* **42**, D1001-1006, doi:10.1093/nar/gkt1229 (2014).

63 Bush, W. S. & Moore, J. H. Chapter 11: Genome-wide association studies. *PLoS Comput Biol* **8**, e1002822, doi:10.1371/journal.pcbi.1002822 (2012).

64 Slatkin, M. Linkage disequilibrium--understanding the evolutionary past and mapping the medical future. *Nat Rev Genet* **9**, 477-485, doi:10.1038/nrg2361 (2008).

65 Saccone, S. F. *et al.* Cholinergic nicotinic receptor genes implicated in a nicotine dependence association study targeting 348 candidate genes with 3713 SNPs. *Hum Mol Genet* **16**, 36-49, doi:10.1093/hmg/ddl438 (2007).

66 Bierut, L. J. *et al.* Variants in nicotinic receptors and risk for nicotine dependence. *Am J Psychiatry* **165**, 1163-1171, doi:10.1176/appi.ajp.2008.07111711 (2008).

67 Saccone, N. L. *et al.* The CHRNA5-CHRNA3-CHRNB4 nicotinic receptor subunit gene cluster affects risk for nicotine dependence in African-Americans and in European-Americans. *Cancer Res* **69**, 6848-6856, doi:10.1158/0008-5472.CAN-09-0786 (2009).

68 Le Marchand, L. *et al.* Smokers with the CHRNA lung cancer-associated variants are exposed to higher levels of nicotine equivalents and a carcinogenic tobacco-specific nitrosamine. *Cancer Res* **68**, 9137-9140, doi:10.1158/0008-5472.CAN-08-2271 (2008).

69 Morel, C. *et al.* Nicotine consumption is regulated by a human polymorphism in dopamine neurons. *Mol Psychiatry*, doi:10.1038/mp.2013.158 (2013).

70 Sciaccaluga, M. *et al.* Crucial role of nicotinic alpha5 subunit variants for Ca2+ fluxes in ventral midbrain neurons. *FASEB J* **29**, 3389-3398, doi:10.1096/fj.14-268102 (2015).

71 Ramirez-Latorre, J. *et al.* Functional contributions of alpha5 subunit to neuronal acetylcholine receptor channels. *Nature* **380**, 347-351, doi:10.1038/380347a0 (1996).

72 Kuryatov, A. & Lindstrom, J. Expression of functional human alpha6beta2beta3* acetylcholine receptors in Xenopus laevis oocytes achieved through subunit chimeras and concatamers. *Molecular pharmacology* **79**, 126-140, doi:10.1124/mol.110.066159 (2011).

73 Seok, J. *et al.* Genomic responses in mouse models poorly mimic human inflammatory diseases. *Proc Natl Acad Sci U S A* **110**, 3507-3512, doi:10.1073/pnas.1222878110 (2013).

74 Carpenter, R. S. *et al.* Traumatic spinal cord injury in mice with human immune systems. *Exp Neurol* **271**, 432-444, doi:10.1016/j.expneurol.2015.07.011 (2015).

75 Muotri, A. R. The Human Model: Changing Focus on Autism Research. *Biol Psychiatry* **79**, 642-649, doi:10.1016/j.biopsych.2015.03.012 (2016).

76 Fowler, C. D. & Kenny, P. J. Nicotine aversion: Neurobiological mechanisms and relevance to tobacco dependence vulnerability. *Neuropharmacology* **76 Pt B**, 533-544, doi:10.1016/j.neuropharm.2013.09.008 (2014).

77 Sun, W. Dopamine neurons in the ventral tegmental area: drug-induced synaptic plasticity and its role in relapse to drug-seeking behavior. *Current drug abuse reviews* **4**, 270-285 (2011).

78 Noble, D. & Tsien, R. W. The kinetics and rectifier properties of the slow potassium current in cardiac Purkinje fibres. *J Physiol* **195**, 185-214 (1968).

79 Luscher, C. & Slesinger, P. A. Emerging roles for G protein-gated inwardly rectifying potassium (GIRK) channels in health and disease. *Nat Rev Neurosci* **11**, 301-315, doi:10.1038/nrn2834 (2010).

80 Lesage, F. *et al.* Molecular properties of neuronal G-protein-activated inwardly rectifying K+ channels. *J Biol Chem* **270**, 28660-28667 (1995).

81 Jelacic, T. M., Kennedy, M. E., Wickman, K. & Clapham, D. E. Functional and biochemical evidence for G-protein-gated inwardly rectifying K+ (GIRK) channels composed of GIRK2 and GIRK3. *J Biol Chem* **275**, 36211-36216, doi:10.1074/jbc.M007087200 (2000).

82 Velimirovic, B. M., Gordon, E. A., Lim, N. F., Navarro, B. & Clapham, D. E. The K+ channel inward rectifier subunits form a channel similar to neuronal G protein-gated K+ channel. *FEBS Lett* **379**, 31-37 (1996).

83 Slesinger, P. A. *et al.* Functional effects of the mouse weaver mutation on G protein-gated inwardly rectifying K+ channels. *Neuron* **16**, 321-331 (1996).

84 Kofuji, P., Davidson, N. & Lester, H. A. Evidence that neuronal G-protein-gated inwardly rectifying K+ channels are activated by G beta gamma subunits and function as heteromultimers. *Proc Natl Acad Sci U S A* **92**, 6542-6546 (1995).

85 Kuo, A. *et al.* Crystal structure of the potassium channel KirBac1.1 in the closed state. *Science* **300**, 1922-1926, doi:10.1126/science.1085028 (2003).

86 Reuveny, E. *et al.* Activation of the cloned muscarinic potassium channel by G protein beta gamma subunits. *Nature* **370**, 143-146, doi:10.1038/370143a0 (1994).

87 Krapivinsky, G., Krapivinsky, L., Wickman, K. & Clapham, D. E. G beta gamma binds directly to the G protein-gated K+ channel, IKACh. *J Biol Chem* **270**, 29059-29062 (1995).

88 Huang, C. L., Slesinger, P. A., Casey, P. J., Jan, Y. N. & Jan, L. Y. Evidence that direct binding of G beta gamma to the GIRK1 G protein-gated inwardly rectifying K+ channel is important for channel activation. *Neuron* **15**, 1133-1143 (1995).

89 Lacey, M. G., Mercuri, N. B. & North, R. A. Dopamine acts on D2 receptors to increase potassium conductance in neurones of the rat substantia nigra zona compacta. *J Physiol* **392**, 397-416 (1987).

90 Ikeda, K. *et al.* Comparison of the three mouse G-protein-activated K+ (GIRK) channels and functional couplings of the opioid receptors with the GIRK1 channel. *Ann N Y Acad Sci* **801**, 95-109 (1996).

91 Duprat, F. *et al.* Heterologous multimeric assembly is essential for K+ channel activity of neuronal and cardiac G-protein-activated inward rectifiers. *Biochem Biophys Res Commun* **212**, 657-663, doi:10.1006/bbrc.1995.2019 (1995).

92 Blednov, Y. A., Stoffel, M., Alva, H. & Harris, R. A. A pervasive mechanism for analgesia: activation of GIRK2 channels. *Proc Natl Acad Sci U S A* **100**, 277-282, doi:10.1073/pnas.012682399 (2003).

93 Kobayashi, T. *et al.* Ethanol opens G-protein-activated inwardly rectifying K+ channels. *Nat Neurosci* **2**, 1091-1097, doi:10.1038/16019 (1999).

94 Aryal, P., Dvir, H., Choe, S. & Slesinger, P. A. A discrete alcohol pocket involved in GIRK channel activation. *Nat Neurosci* **12**, 988-995, doi:10.1038/nn.2358 (2009).

95 Porjesz, B. *et al.* The utility of neurophysiological markers in the study of alcoholism. *Clin Neurophysiol* **116**, 993-1018, doi:10.1016/j.clinph.2004.12.016 (2005).

96 Lukas, S. E., Mendelson, J. H., Benedikt, R. A. & Jones, B. EEG, physiologic and behavioral effects of ethanol administration. *NIDA Res Monogr* **67**, 209-214 (1986).

97 Klimesch, W. EEG alpha and theta oscillations reflect cognitive and memory performance: a review and analysis. *Brain Res Brain Res Rev* **29**, 169-195 (1999).

98 Edenberg, H. J. & Foroud, T. Genetics of alcoholism. *Handb Clin Neurol* **125**, 561-571, doi:10.1016/B978-0-444-62619-6.00032-X (2014).
99 Crawford, D. C. & Nickerson, D. A. Definition and clinical importance of haplotypes. *Annu Rev Med* **56**, 303-320, doi:10.1146/annurev.med.56.082103.104540 (2005).
100 Yamanaka, S. & Takahashi, K. [Induction of pluripotent stem cells from mouse fibroblast cultures]. *Tanpakushitsu kakusan koso. Protein, nucleic acid, enzyme* **51**, 2346-2351 (2006).
101 Abeliovich, A. & Doege, C. A. Reprogramming therapeutics: iPS cell prospects for neurodegenerative disease. *Neuron* **61**, 337-339, doi:10.1016/j.neuron.2009.01.024 (2009).
102 Wen, Z. *et al.* Synaptic dysregulation in a human iPS cell model of mental disorders. *Nature* **515**, 414-418, doi:10.1038/nature13716 (2014).
103 Bavamian, S. *et al.* Dysregulation of miR-34a links neuronal development to genetic risk factors for bipolar disorder. *Mol Psychiatry* **20**, 573-584, doi:10.1038/mp.2014.176 (2015).
104 Mertens, J. *et al.* Differential responses to lithium in hyperexcitable neurons from patients with bipolar disorder. *Nature* **527**, 95-99, doi:10.1038/nature15526 (2015).
105 Panchision, D. M. Concise Review: Progress and Challenges in Using Human Stem Cells for Biological and Therapeutics Discovery: Neuropsychiatric Disorders. *Stem Cells* **34**, 523-536, doi:10.1002/stem.2295 (2016).
106 Vierbuchen, T. *et al.* Direct conversion of fibroblasts to functional neurons by defined factors. *Nature* **463**, 1035-1041, doi:10.1038/nature08797 (2010).
107 Kriks, S. *et al.* Dopamine neurons derived from human ES cells efficiently engraft in animal models of Parkinson's disease. *Nature* **480**, 547-551, doi:10.1038/nature10648 (2011).
108 Ho, S. M. *et al.* Rapid Ngn2-induction of excitatory neurons from hiPSC-derived neural progenitor cells. *Methods* **101**, 113-124, doi:10.1016/j.ymeth.2015.11.019 (2016).
109 Brennand, K. J. *et al.* Creating Patient-Specific Neural Cells for the In Vitro Study of Brain Disorders. *Stem Cell Reports* **5**, 933-945, doi:10.1016/j.stemcr.2015.10.011 (2015).
110 Marchetto, M. C. *et al.* A model for neural development and treatment of Rett syndrome using human induced pluripotent stem cells. *Cell* **143**, 527-539, doi:10.1016/j.cell.2010.10.016 (2010).
111 Brennand, K. *et al.* Phenotypic differences in hiPSC NPCs derived from patients with schizophrenia. *Mol Psychiatry* **20**, 361-368, doi:10.1038/mp.2014.22 (2015).
112 Nguyen, H. N. *et al.* LRRK2 mutant iPSC-derived DA neurons demonstrate increased susceptibility to oxidative stress. *Cell Stem Cell* **8**, 267-280, doi:10.1016/j.stem.2011.01.013 (2011).
113 Lieberman, R., Kranzler, H. R., Joshi, P., Shin, D. G. & Covault, J. GABRA2 Alcohol Dependence Risk Allele is Associated with Reduced Expression of Chromosome 4p12 GABAA Subunit Genes in Human Neural Cultures. *Alcohol Clin Exp Res* **39**, 1654-1664, doi:10.1111/acer.12807 (2015).
114 Chatterjee, S. *et al.* The alpha5 subunit regulates the expression and function of alpha4*-containing neuronal nicotinic acetylcholine receptors in the ventral-tegmental area. *PLoS One* **8**, e68300, doi:10.1371/journal.pone.0068300 (2013).
115 Kuryatov, A., Berrettini, W. & Lindstrom, J. Acetylcholine receptor (AChR) alpha5 subunit variant associated with risk for nicotine dependence and lung cancer

reduces (alpha4beta2)(2)alpha5 AChR function. *Mol Pharmacol* **79**, 119-125, doi:10.1124/mol.110.066357 (2011).
116 Glaaser, I. W. & Slesinger, P. A. Structural Insights into GIRK Channel Function. *Int Rev Neurobiol* **123**, 117-160, doi:10.1016/bs.irn.2015.05.014 (2015).
117 Heatherton, T. F., Kozlowski, L. T., Frecker, R. C. & Fagerstrom, K. O. The Fagerstrom Test for Nicotine Dependence: a revision of the Fagerstrom Tolerance Questionnaire. *Br J Addict* **86**, 1119-1127 (1991).
118 Takahashi, K. *et al.* Induction of pluripotent stem cells from adult human fibroblasts by defined factors. *Cell* **131**, 861-872, doi:10.1016/j.cell.2007.11.019 (2007).
119 Muller, F. J. *et al.* A bioinformatic assay for pluripotency in human cells. *Nature methods*, doi:10.1038/nmeth.1580 (2011).
120 Rosner, M. H. *et al.* A POU-domain transcription factor in early stem cells and germ cells of the mammalian embryo. *Nature* **345**, 686-692, doi:10.1038/345686a0 (1990).
121 Yuan, H., Corbi, N., Basilico, C. & Dailey, L. Developmental-specific activity of the FGF-4 enhancer requires the synergistic action of Sox2 and Oct-3. *Genes Dev* **9**, 2635-2645 (1995).
122 Rodda, D. J. *et al.* Transcriptional regulation of nanog by OCT4 and SOX2. *J Biol Chem* **280**, 24731-24737, doi:10.1074/jbc.M502573200 (2005).
123 Cooper, S., Pera, M. F., Bennett, W. & Finch, J. T. A novel keratan sulphate proteoglycan from a human embryonal carcinoma cell line. *Biochem J* **286 (Pt 3)**, 959-966 (1992).
124 Chambers, S. M. *et al.* Highly efficient neural conversion of human ES and iPS cells by dual inhibition of SMAD signaling. *Nat Biotechnol* **27**, 275-280, doi:10.1038/nbt.1529 (2009).
125 Zimmerman, L. B., De Jesus-Escobar, J. M. & Harland, R. M. The Spemann organizer signal noggin binds and inactivates bone morphogenetic protein 4. *Cell* **86**, 599-606 (1996).
126 Lim, D. A. *et al.* Noggin antagonizes BMP signaling to create a niche for adult neurogenesis. *Neuron* **28**, 713-726 (2000).
127 Ferreira, A. & Caceres, A. Expression of the class III beta-tubulin isotype in developing neurons in culture. *J Neurosci Res* **32**, 516-529, doi:10.1002/jnr.490320407 (1992).
128 Sulzer, D. *et al.* Dopamine neurons make glutamatergic synapses in vitro. *J Neurosci* **18**, 4588-4602 (1998).
129 Broussard, J. I. Co-transmission of dopamine and glutamate. *J Gen Physiol* **139**, 93-96, doi:10.1085/jgp.201110659 (2012).
130 Stuber, G. D., Hnasko, T. S., Britt, J. P., Edwards, R. H. & Bonci, A. Dopaminergic terminals in the nucleus accumbens but not the dorsal striatum corelease glutamate. *J Neurosci* **30**, 8229-8233, doi:10.1523/JNEUROSCI.1754-10.2010 (2010).
131 Klink, R., de Kerchove d'Exaerde, A., Zoli, M. & Changeux, J. P. Molecular and physiological diversity of nicotinic acetylcholine receptors in the midbrain dopaminergic nuclei. *J Neurosci* **21**, 1452-1463 (2001).
132 Lin, L. *et al.* Spontaneous ATM Gene Reversion in A-T iPSC to Produce an Isogenic Cell Line. *Stem Cell Reports* **5**, 1097-1108, doi:10.1016/j.stemcr.2015.10.010 (2015).

133 Sauvageau, M. *et al.* Multiple knockout mouse models reveal lincRNAs are required for life and brain development. *Elife* **2**, e01749, doi:10.7554/eLife.01749 (2013).
134 Miller, J. D. *et al.* Human iPSC-based modeling of late-onset disease via progerin-induced aging. *Cell Stem Cell* **13**, 691-705, doi:10.1016/j.stem.2013.11.006 (2013).
135 Yan, W., Wu, F., Morser, J. & Wu, Q. Corin, a transmembrane cardiac serine protease, acts as a pro-atrial natriuretic peptide-converting enzyme. *Proc Natl Acad Sci U S A* **97**, 8525-8529, doi:10.1073/pnas.150149097 (2000).
136 Chung, S. *et al.* ES cell-derived renewable and functional midbrain dopaminergic progenitors. *Proc Natl Acad Sci U S A* **108**, 9703-9708, doi:10.1073/pnas.1016443108 (2011).
137 Ferri, A. L. *et al.* Foxa1 and Foxa2 regulate multiple phases of midbrain dopaminergic neuron development in a dosage-dependent manner. *Development* **134**, 2761-2769, doi:10.1242/dev.000141 (2007).
138 Yan, C. H., Levesque, M., Claxton, S., Johnson, R. L. & Ang, S. L. Lmx1a and lmx1b function cooperatively to regulate proliferation, specification, and differentiation of midbrain dopaminergic progenitors. *J Neurosci* **31**, 12413-12425, doi:10.1523/JNEUROSCI.1077-11.2011 (2011).
139 Zetterstrom, R. H. *et al.* Dopamine neuron agenesis in Nurr1-deficient mice. *Science* **276**, 248-250 (1997).
140 Sakurada, K., Ohshima-Sakurada, M., Palmer, T. D. & Gage, F. H. Nurr1, an orphan nuclear receptor, is a transcriptional activator of endogenous tyrosine hydroxylase in neural progenitor cells derived from the adult brain. *Development* **126**, 4017-4026 (1999).
141 Smidt, M. P. *et al.* A homeodomain gene Ptx3 has highly restricted brain expression in mesencephalic dopaminergic neurons. *Proc Natl Acad Sci U S A* **94**, 13305-13310 (1997).
142 Huang da, W., Sherman, B. T. & Lempicki, R. A. Systematic and integrative analysis of large gene lists using DAVID bioinformatics resources. *Nature protocols* **4**, 44-57, doi:10.1038/nprot.2008.211 (2009).
143 Huang da, W., Sherman, B. T. & Lempicki, R. A. Bioinformatics enrichment tools: paths toward the comprehensive functional analysis of large gene lists. *Nucleic Acids Res* **37**, 1-13, doi:10.1093/nar/gkn923 (2009).
144 Grienberger, C. & Konnerth, A. Imaging calcium in neurons. *Neuron* **73**, 862-885, doi:10.1016/j.neuron.2012.02.011 (2012).
145 Pang, Z. P. & Sudhof, T. C. Cell biology of Ca2+-triggered exocytosis. *Current opinion in cell biology* **22**, 496-505, doi:10.1016/j.ceb.2010.05.001 (2010).
146 Russell, M. A., Jarvis, M., Iyer, R. & Feyerabend, C. Relation of nicotine yield of cigarettes to blood nicotine concentrations in smokers. *Br Med J* **280**, 972-976 (1980).
147 Zhang, Y. *et al.* Rapid single-step induction of functional neurons from human pluripotent stem cells. *Neuron* **78**, 785-798, doi:10.1016/j.neuron.2013.05.029 (2013).
148 Yamaguchi, T., Sheen, W. & Morales, M. Glutamatergic neurons are present in the rat ventral tegmental area. *Eur J Neurosci* **25**, 106-118, doi:10.1111/j.1460-9568.2006.05263.x (2007).
149 Thiel, G. Synapsin I, synapsin II, and synaptophysin: marker proteins of synaptic vesicles. *Brain Pathol* **3**, 87-95 (1993).

150 Kuryatov, A., Berrettini, W. & Lindstrom, J. Acetylcholine receptor (AChR) alpha5 subunit variant associated with risk for nicotine dependence and lung cancer reduces (alpha4beta2)alpha5 AChR function. *Mol Pharmacol* **79**, 119-125, doi:10.1124/mol.110.066357 (2011).
151 Doudna, J. A. & Sontheimer, E. J. Methods in Enzymology. The use of CRISPR/Cas9, ZFNs, and TALENs in generating site-specific genome alterations. Preface. *Methods Enzymol* **546**, xix-xx, doi:10.1016/B978-0-12-801185-0.09983-9 (2014).
152 Jinek, M. *et al.* A programmable dual-RNA-guided DNA endonuclease in adaptive bacterial immunity. *Science* **337**, 816-821, doi:10.1126/science.1225829 (2012).
153 Matthews, T. & Boehme, R. Antiviral activity and mechanism of action of ganciclovir. *Rev Infect Dis* **10 Suppl 3**, S490-494 (1988).
154 Mansour, S. L., Thomas, K. R. & Capecchi, M. R. Disruption of the proto-oncogene int-2 in mouse embryo-derived stem cells: a general strategy for targeting mutations to non-selectable genes. *Nature* **336**, 348-352, doi:10.1038/336348a0 (1988).
155 Barnes, W. M. PCR amplification of up to 35-kb DNA with high fidelity and high yield from lambda bacteriophage templates. *Proc Natl Acad Sci U S A* **91**, 2216-2220 (1994).
156 Morel, C. *et al.* Nicotine consumption is regulated by a human polymorphism in dopamine neurons. *Mol Psychiatry* **19**, 930-936, doi:10.1038/mp.2013.158 (2014).
157 Wilhelm, B. T. & Landry, J. R. RNA-Seq-quantitative measurement of expression through massively parallel RNA-sequencing. *Methods* **48**, 249-257, doi:10.1016/j.ymeth.2009.03.016 (2009).
158 Rose, J. E. *et al.* Kinetics of brain nicotine accumulation in dependent and nondependent smokers assessed with PET and cigarettes containing 11C-nicotine. *Proc Natl Acad Sci U S A* **107**, 5190-5195, doi:10.1073/pnas.0909184107 (2010).
159 Marchetto, M. C. & Gage, F. H. Modeling brain disease in a dish: really? *Cell stem cell* **10**, 642-645, doi:10.1016/j.stem.2012.05.008 (2012).
160 Dolmetsch, R. & Geschwind, D. H. The human brain in a dish: the promise of iPSC-derived neurons. *Cell* **145**, 831-834, doi:10.1016/j.cell.2011.05.034 (2011).
161 Lee, G. & Studer, L. Induced pluripotent stem cell technology for the study of human disease. *Nature methods* **7**, 25-27, doi:10.1038/nmeth.f.283 (2010).
162 Hockemeyer, D. & Jaenisch, R. Induced Pluripotent Stem Cells Meet Genome Editing. *Cell Stem Cell* **18**, 573-586, doi:10.1016/j.stem.2016.04.013 (2016).
163 Beevers, J. E., Caffrey, T. M. & Wade-Martins, R. Induced pluripotent stem cell (iPSC)-derived dopaminergic models of Parkinson's disease. *Biochemical Society transactions* **41**, 1503-1508, doi:10.1042/BST20130194 (2013).
164 Jiang, Y. *et al.* Derivation and functional analysis of patient-specific induced pluripotent stem cells as an in vitro model of chronic granulomatous disease. *Stem Cells* **30**, 599-611, doi:10.1002/stem.1053 (2012).
165 Kendler, K. S., Neale, M. C., Heath, A. C., Kessler, R. C. & Eaves, L. J. A twin-family study of alcoholism in women. *Am J Psychiatry* **151**, 707-715, doi:10.1176/ajp.151.5.707 (1994).
166 Noble, D. & Tsien, R. W. Kinetics of slow component of potassium current in cardiac purkinje fibres. *J Physiol* **194**, 31P-32P (1968).

167 Hussein, S. M. *et al.* Copy number variation and selection during reprogramming to pluripotency. *Nature* **471**, 58-62, doi:10.1038/nature09871 (2011).

168 Laurent, L. C. *et al.* Dynamic changes in the copy number of pluripotency and cell proliferation genes in human ESCs and iPSCs during reprogramming and time in culture. *Cell Stem Cell* **8**, 106-118, doi:10.1016/j.stem.2010.12.003 (2011).

169 Shan, Z. Y. *et al.* Continuous passages accelerate the reprogramming of mouse induced pluripotent stem cells. *Cell Reprogram* **16**, 77-83, doi:10.1089/cell.2013.0067 (2014).

170 Zhou, F. C. *et al.* Alcohol alters DNA methylation patterns and inhibits neural stem cell differentiation. *Alcohol Clin Exp Res* **35**, 735-746, doi:10.1111/j.1530-0277.2010.01391.x (2011).

171 Hicks, S. D. & Miller, M. W. Effects of ethanol on transforming growth factor Beta1-dependent and -independent mechanisms of neural stem cell apoptosis. *Exp Neurol* **229**, 372-380, doi:10.1016/j.expneurol.2011.03.003 (2011).

172 Liyanage, V. R., Zachariah, R. M., Davie, J. R. & Rastegar, M. Ethanol deregulates Mecp2/MeCP2 in differentiating neural stem cells via interplay between 5-methylcytosine and 5-hydroxymethylcytosine at the Mecp2 regulatory elements. *Exp Neurol* **265**, 102-117, doi:10.1016/j.expneurol.2015.01.006 (2015).

173 Elkabetz, Y. *et al.* Human ES cell-derived neural rosettes reveal a functionally distinct early neural stem cell stage. *Genes Dev* **22**, 152-165, doi:10.1101/gad.1616208 (2008).

174 Miranda, R. C. MicroRNAs and Fetal Brain Development: Implications for Ethanol Teratology during the Second Trimester Period of Neurogenesis. *Front Genet* **3**, 77, doi:10.3389/fgene.2012.00077 (2012).

175 Lendahl, U., Zimmerman, L. B. & McKay, R. D. CNS stem cells express a new class of intermediate filament protein. *Cell* **60**, 585-595 (1990).

176 Sakakibara, S. *et al.* Mouse-Musashi-1, a neural RNA-binding protein highly enriched in the mammalian CNS stem cell. *Dev Biol* **176**, 230-242 (1996).

177 Sansom, S. N. *et al.* The level of the transcription factor Pax6 is essential for controlling the balance between neural stem cell self-renewal and neurogenesis. *PLoS Genet* **5**, e1000511, doi:10.1371/journal.pgen.1000511 (2009).

178 Favaro, R. *et al.* Hippocampal development and neural stem cell maintenance require Sox2-dependent regulation of Shh. *Nat Neurosci* **12**, 1248-1256, doi:10.1038/nn.2397 (2009).

179 Oni, E. N. & Hart, R. P. Bioinformatic Analysis of DNA Methylation in Neural Progenitor Cell Models of Alcohol Abuse. *Current Pharmacology Reports*, 1-8, doi:10.1007/s40495-016-0065-y (2016).

180 Vangipuram, S. D. & Lyman, W. D. Ethanol affects differentiation-related pathways and suppresses Wnt signaling protein expression in human neural stem cells. *Alcohol Clin Exp Res* **36**, 788-797, doi:10.1111/j.1530-0277.2011.01682.x (2012).

181 Liu, Y., Balaraman, Y., Wang, G., Nephew, K. P. & Zhou, F. C. Alcohol exposure alters DNA methylation profiles in mouse embryos at early neurulation. *Epigenetics* **4**, 500-511 (2009).

182 Jones, A. W. & Sternebring, B. Kinetics of ethanol and methanol in alcoholics during detoxification. *Alcohol Alcohol* **27**, 641-647 (1992).

183 McClintick, J. N. *et al.* Ethanol treatment of lymphoblastoid cell lines from alcoholics and non-alcoholics causes many subtle changes in gene expression. *Alcohol* **48**, 603-610, doi:10.1016/j.alcohol.2014.07.004 (2014).

184 Campbell, J. C., Stipcevic, T., Flores, R. E., Perry, C. & Kippin, T. E. Alcohol exposure inhibits adult neural stem cell proliferation. *Exp Brain Res* **232**, 2775-2784, doi:10.1007/s00221-014-3958-1 (2014).
185 Hansson, A. C. *et al.* Long-term suppression of forebrain neurogenesis and loss of neuronal progenitor cells following prolonged alcohol dependence in rats. *Int J Neuropsychopharmacol* **13**, 583-593, doi:10.1017/S1461145710000246 (2010).
186 Reyahi, A. *et al.* Foxf2 Is Required for Brain Pericyte Differentiation and Development and Maintenance of the Blood-Brain Barrier. *Dev Cell* **34**, 19-32, doi:10.1016/j.devcel.2015.05.008 (2015).
187 Nik, A. M., Reyahi, A., Ponten, F. & Carlsson, P. Foxf2 in intestinal fibroblasts reduces numbers of Lgr5(+) stem cells and adenoma formation by inhibiting Wnt signaling. *Gastroenterology* **144**, 1001-1011, doi:10.1053/j.gastro.2013.01.045 (2013).
188 Oishi, I. *et al.* The receptor tyrosine kinase Ror2 is involved in non-canonical Wnt5a/JNK signalling pathway. *Genes Cells* **8**, 645-654 (2003).
189 Santillano, D. R. *et al.* Ethanol induces cell-cycle activity and reduces stem cell diversity to alter both regenerative capacity and differentiation potential of cerebral cortical neuroepithelial precursors. *BMC Neurosci* **6**, 59, doi:10.1186/1471-2202-6-59 (2005).
190 Xiao, C., Zhang, J., Krnjevic, K. & Ye, J. H. Effects of ethanol on midbrain neurons: role of opioid receptors. *Alcohol Clin Exp Res* **31**, 1106-1113, doi:10.1111/j.1530-0277.2007.00405.x (2007).
191 Zhang, Y., Wang, D., Johnson, A. D., Papp, A. C. & Sadee, W. Allelic expression imbalance of human mu opioid receptor (OPRM1) caused by variant A118G. *J Biol Chem* **280**, 32618-32624, doi:10.1074/jbc.M504942200 (2005).
192 Duan, J. *et al.* Synonymous mutations in the human dopamine receptor D2 (DRD2) affect mRNA stability and synthesis of the receptor. *Hum Mol Genet* **12**, 205-216 (2003).
193 Seo, S., Lim, J. W., Yellajoshyula, D., Chang, L. W. & Kroll, K. L. Neurogenin and NeuroD direct transcriptional targets and their regulatory enhancers. *EMBO J* **26**, 5093-5108, doi:10.1038/sj.emboj.7601923 (2007).
194 Bardy, C. *et al.* Neuronal medium that supports basic synaptic functions and activity of human neurons in vitro. *Proc Natl Acad Sci U S A* **112**, E2725-2734, doi:10.1073/pnas.1504393112 (2015).
195 Isomoto, S. *et al.* A novel ubiquitously distributed isoform of GIRK2 (GIRK2B) enhances GIRK1 expression of the G-protein-gated K+ current in Xenopus oocytes. *Biochem Biophys Res Commun* **218**, 286-291, doi:10.1006/bbrc.1996.0050 (1996).
196 Finley, M., Arrabit, C., Fowler, C., Suen, K. F. & Slesinger, P. A. betaL-betaM loop in the C-terminal domain of G protein-activated inwardly rectifying K(+) channels is important for G(betagamma) subunit activation. *J Physiol* **555**, 643-657, doi:10.1113/jphysiol.2003.056101 (2004).
197 Trapnell, C. *et al.* Differential gene and transcript expression analysis of RNA-seq experiments with TopHat and Cufflinks. *Nat Protoc* **7**, 562-578, doi:10.1038/nprot.2012.016 (2012).
198 Milam, A. H. *et al.* The nuclear receptor NR2E3 plays a role in human retinal photoreceptor differentiation and degeneration. *Proc Natl Acad Sci U S A* **99**, 473-478, doi:10.1073/pnas.022533099 (2002).

199 Bekdash, R. A. & Harrison, N. L. Downregulation of Gabra4 expression during alcohol withdrawal is mediated by specific microRNAs in cultured mouse cortical neurons. *Brain Behav* **5**, e00355, doi:10.1002/brb3.355 (2015).
200 Wu, L., Fan, J. & Belasco, J. G. MicroRNAs direct rapid deadenylation of mRNA. *Proc Natl Acad Sci U S A* **103**, 4034-4039, doi:10.1073/pnas.0510928103 (2006).
201 Agarwal, V., Bell, G. W., Nam, J. W. & Bartel, D. P. Predicting effective microRNA target sites in mammalian mRNAs. *Elife* **4**, doi:10.7554/eLife.05005 (2015).
202 Ignacio, C. *et al.* Alterations in serum microRNA in humans with alcohol use disorders impact cell proliferation and cell death pathways and predict structural and functional changes in brain. *BMC Neurosci* **16**, 55, doi:10.1186/s12868-015-0195-x (2015).
203 Portales-Casamar, E. *et al.* The PAZAR database of gene regulatory information coupled to the ORCA toolkit for the study of regulatory sequences. *Nucleic Acids Res* **37**, D54-60, doi:10.1093/nar/gkn783 (2009).
204 Hsu, S. H., Hsieh-Li, H. M., Huang, H. Y., Huang, P. H. & Li, H. bHLH-zip transcription factor Spz1 mediates mitogen-activated protein kinase cell proliferation, transformation, and tumorigenesis. *Cancer Res* **65**, 4041-4050, doi:10.1158/0008-5472.CAN-04-3658 (2005).
205 Hsu, S. H., Shyu, H. W., Hsieh-Li, H. M. & Li, H. Spz1, a novel bHLH-Zip protein, is specifically expressed in testis. *Mech Dev* **100**, 177-187 (2001).
206 Golub, H. M. *et al.* Chronic Alcohol Exposure is Associated with Decreased Neurogenesis, Aberrant Integration of Newborn Neurons, and Cognitive Dysfunction in Female Mice. *Alcohol Clin Exp Res* **39**, 1967-1977, doi:10.1111/acer.12843 (2015).
207 Hassan, M. A. & Saeij, J. P. Incorporating alternative splicing and mRNA editing into the genetic analysis of complex traits. *Bioessays* **36**, 1032-1040, doi:10.1002/bies.201400079 (2014).
208 Wei, J. *et al.* Characterization of murine Girk2 transcript isoforms: structure and differential expression. *Genomics* **51**, 379-390, doi:10.1006/geno.1998.5369 (1998).
209 Ma, D. *et al.* Diverse trafficking patterns due to multiple traffic motifs in G protein-activated inwardly rectifying potassium channels from brain and heart. *Neuron* **33**, 715-729 (2002).
210 Milovic, S., Steinecker-Frohnwieser, B., Schreibmayer, W. & Weigl, L. G. The sensitivity of G protein-activated K+ channels toward halothane is essentially determined by the C terminus. *J Biol Chem* **279**, 34240-34249, doi:10.1074/jbc.M403448200 (2004).
211 George, A. A. *et al.* Function of human alpha3beta4alpha5 nicotinic acetylcholine receptors is reduced by the alpha5(D398N) variant. *J Biol Chem* **287**, 25151-25162, doi:10.1074/jbc.M112.379339 (2012).
212 Tapia, L., Kuryatov, A. & Lindstrom, J. Ca2+ permeability of the (alpha4)3(beta2)2 stoichiometry greatly exceeds that of (alpha4)2(beta2)3 human acetylcholine receptors. *Mol Pharmacol* **71**, 769-776, doi:10.1124/mol.106.030445 (2007).
213 Dani, J. A. & Harris, R. A. Nicotine addiction and comorbidity with alcohol abuse and mental illness. *Nat Neurosci* **8**, 1465-1470, doi:10.1038/nn1580 (2005).

214 Rose, J. E. *et al.* Psychopharmacological interactions between nicotine and ethanol. *Nicotine Tob Res* **6**, 133-144, doi:10.1080/14622200310001656957 (2004).
215 Owens, J. C. *et al.* Alpha 4 beta 2* nicotinic acetylcholine receptors modulate the effects of ethanol and nicotine on the acoustic startle response. *Alcohol Clin Exp Res* **27**, 1867-1875, doi:10.1097/01.ALC.0000102700.72447.0F (2003).
216 Spanagel, R. *et al.* A systems medicine research approach for studying alcohol addiction. *Addict Biol* **18**, 883-896, doi:10.1111/adb.12109 (2013).
217 Moore, J. C. Generation of human-induced pluripotent stem cells by lentiviral transduction. *Methods Mol Biol* **997**, 35-43, doi:10.1007/978-1-62703-348-0_4 (2013).
218 Dudoit, S., Gentleman, R. C. & Quackenbush, J. Open source software for the analysis of microarray data. *Biotechniques* **Suppl**, 45-51 (2003).